UNIVERSITÀ
DEGLI STUDI
DI PADOVA

UNIVERSITÀ DEGLI STUDI DI PADOVA

Dipartimento di Fisica e Astronomia

Scuola di dottorato in Fisica

XXVI CICLO

TESI DI DOTTORATO

Dynamical and collective properties of active and passive particles in Single File

Direttore della scuola: Prof. Andrea Vitturi

Supervisore: Dott. Matteo Pierno

Co-supervisori: Dott. Fulvio Baldovin,
Prof. Enzo Orlandini

Dottorando: Emanuele Locatelli

Alla mia famiglia

Contents

List of Figures

Riassunto

Il moto di particelle in mezzi irregolari, complessi o affollati è un fenomeno comune, dalla scala microscopica a quella macroscopica. Lo si può incontrare tanto in situazioni comuni, come il traffico, qunato in meccanismi biologici, come la riproduzione e la crescita delle cellule, e in importanti processi chimici e tecnologici, come la catalisi di idrocarburi. In molti casi, il trasporto in mezzi confinati o affollati è guidato da elementi 'attivi', cioè unità che consumano energia per sostenere il loro stato di moto. Fra i diversi sistemi soggetti a confinamento, particolare rilevanza è rivestita dalla diffusione di sfere impenetrabili in un canale così stretto da non permettere il passaggio di più di una particella alla volta, conosciuto come diffusione in Single File. la diffusione in Single File è il meccanismo responsabile del trasporto di ioni attraverso la membrana cellulare, della diffusione in materiali micro e nanoporosi ed è stata osservata in molti altri sistemi naturali ed artificiali.

Scopo di questa tesi è lo studio su scala mesoscopica di particelle passive (diffusive) o attive (auto-propellenti) in condizioni di Single File, con particolare attenzione all'effetto dell'attività sulla dinamica e sulle proprietà delle particelle nel caso siano presenti condizioni al contorno assorbenti. Gran parte del lavoro è stato svolto nello sviluppo di risultati analitici e numerici nel contesto dei Processi Stocastici. Inoltre, mediante tecniche di manipolazione ottica di singola particella in canali microfluidici, abbiamo ottenuto una eccellente confronto fra dati sperimentali e numerici per il processo di svuotamento di un sistema di particelle in condizioni di Single File.

In questa tesi, dopo una breve introduzione ai processi diffusivi fortemente confinati, passeremo in rassegna i lavori più rilevanti della letteratura teorica e speri-

mentale sulla Single File Diffusion, con particolare attenzione ad un formalismo matematico, il *Reflection Principle Method*, che sarà applicato in maniera estensiva nel corso della tesi. Studieremo poi le proprietà di un sistema di particelle diffusive in Single File in presenza di condizioni al contorno assorbenti, concentrandoci sulla *survival probability*, cioè la probabilità di trovare una particella fra gli estremi del sistema al tempo t. Mostreremo come, in condizioni di Single File, abbiamo ottenuto una soluzione analitica per il *processo di svuotamento*, cioè calcoleremo la probabilità che caratterizza la progressiva diminuzione del numero di particelle in presenza di condizioni al contorno assorbenti, e per la survival probability di una particella 'marcata' all'interno della Single File sia in presenza che in assenza di una forza esterna costante. Caratterizzeremo gli andamenti dei tempi caratteristici di sopravvivenza, chiamati Tempi Medi di Primo Passaggio, in funzione della taglia del canale e del numero iniziale di particelle. Indagheremo inoltre numericamente il caso in cui solo la particella centrale del sistema in Single File subisce l'effetto delle condizioni al contorno assorbenti. Osserviamo un decadimento esponenziale della survival probability, come accade nell'usuale moto Browniano, anche in presenza di estremo confinamento. Introdurremo l'attività nella Single File attraverso un modello di particelle Self-Propelled, di cui descriveremo le proprietà in dettaglio. In particolare in questo modello le particelle possono essere o *runners* o *tumblers*, a seconda che la loro traiettoria sia dominata da lunghi tratti rettilinei o da cambi di direzione. In condizioni di Single File, i *runners* tendono a formare aggregati dinamici: questi cluster vengono continuamente formati e distrutti dalle fluttuazioni casuali della forza propulsiva. Per i *tumblers*, le probabilità di sopravvivenza sono ben descritte dalla teoria analitica sviluppata per le particelle passive. Per contro, la formazione di cluster dinamici accresce i comportamenti anomali nei tempi caratteristici di sopravvivenza dei *runners* e ne induce una notevole capacità di opporsi all'azione di un campo esterno.

Parole chiave:
Single File, diffusione sotto confinamento, diffusione anomala, materia attiva, probabilità di sopravvivenza, Fractional Brownian Motion, cluster dinamici, processo di svuotamento, Tempo Medio di Primo Passaggio, microfluidica, trappola ottica, runner, tumbler

Abstract

Particles motion inside complex, irregular or crowded environments is a common phenomenon ranging from microscopic to macroscopic scales. It can be involved in everyday practical problems, like traffic, in fundamental biological mechanisms, like growth and reproduction of cells, and in important industrial or chemical applications, like oil catalysis. In many cases, transport in crowded environments is guided by 'active' elements, i.e. units that consume energy in order to produce motion. Among systems belonging in this class, the diffusion of hard-core particles in a channel so narrow they cannot pass each other, known as Single File Diffusion, has assumed a particular role. Single File Diffusion is responsible for the transport of ions in membrane channels, the diffusion in nano- and micro-porous materials and has been observed in many other natural and artificial systems.

Aim of this thesis is to investigate Single File system of passive (purely diffusive) or active (self propelled) particles, focusing on the effects of the activity on the Single File motion and on the Single File properties in the presence of absorbing boundaries. Most of the work has been carried out developing analytical and numerical tools within the framework of the Stochastic Processes. By using single particle techniques in a microfluidic approach, we obtained an excellent comparison between experimental data and numerical model of particles emptying a Single File channel with open ends.

In this thesis, after a brief introduction in the framework of confined diffusion processes, we will review the most relevant works in the theoretical and experimental literature of Single File Diffusion, with particular attention to an analytical technique, the *Reflection Principle Method*, which will be extensively used in this

thesis. We will investigate the properties of Single File systems of diffusing particles in presence of two absorbing boundaries, with particular interest to the *survival probability*, i.e. the probability to find a particle between the boundaries at time t. We will provide an analytical solution of the *emptying process*, i.e. we calculate the probability characterizing the progressive decrease of the number of particles in the presence of absorbing boundaries, and for the survival probability of a Tagged Particle within the file, either in the presence or in the absence of a constant external force. We also characterize the trend of the characteristic survival times (also called Mean First Passage Times) as function of the system size and of the initial number of particles. We also investigate numerically the case when only the central particle is affected by the absorbing boundaries. We find an exponential decay of the survival probability, as it happens for normal diffusive processes, even in the presence of overcrowding. We will then introduce activity in a Single File system, through a Self-Propelled Particle model, for which we will provide a detailed characterization. In particular, within this model, particles can be either *runners* or *tumblers*, if their motion is dominated by straight runs or by changes of direction, respectively. Under Single File conditions, *runners* tend to form dynamical aggregates: these clusters are continuously formed and disassembled due to random fluctuations of the activity. For *tumblers*, the survival probabilities are still well described by the analytical theory developed for passive diffusing particles. Conversely, the formation of dynamical clusters enhances anomalous behaviours in the characteristic survival times of *runners* and induces a remarkable capacity to overcome the action of an external force.

Keywords:
Single File Diffusion, confined diffusion, anomalous diffusion, active motion, Survival Probability, Fractional Brownian Motion, dynamical clusters, emptying process, Mean First Passage Time, microfluidics, optical trap, runner, tumbler

Introduction

Since its discovery and through the past century, Brownian motion has become a paradigmatic model in science [3]. Characteristic energy scales (k_BT) and length-scales (up to few μm) make it widespread in soft matter Physics and Biology. It proved to be a powerful model in many fields, including ecology and economics, in which diffusion-like equations are extensively used.
However, over time people began to realize that many systems, characterized by strong interactions, traps, confinement or, more recently, self propulsion, cannot be described by simple diffusion models, as they showed drastically different behaviours, generally named *anomalous* diffusion.

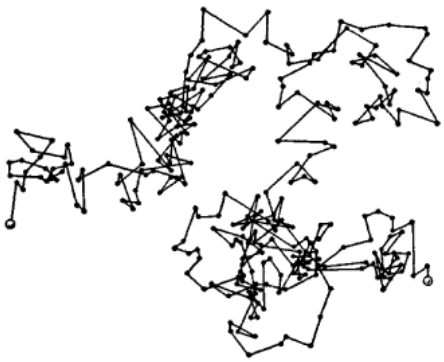

Figure 1: Example of trajectory of a Brownian particle observed by Perrin (from [1]).

Deviations from free Brownian motion have been observed in many cases [4]. A particularly relevant example is the diffusion of particles in restricted or crowded environments. From micro- and nano-porous materials or man-made carbon nanochannels to intracellular transport processes, particles are constricted by boundaries or by obstacles that considerably limit the space available for their motion. Example of confined diffusion can be found in biology, physiology but also in chemical and industrial applications. Diffusion of particles in zeolites [5,6], catalytic reactions in porous media [7], separation techniques of size-dispersed particles on micro- or even nanoscales [8] happen in ex-

Figure 2: a) Lines of cars in heavy traffic (source: Wikipedia). b) Queue in a British post office (font: Daily Mail).

treme confinement conditions. From the biological point of view, DNA translocation [9–11], protein transport in crowded fluids as cytoplasm and nucleoplasm and, in general, many intracellular transport processes are subject to strong spatial constraints [12].

In addition, diffusion in confined environments can involve active motion, i.e. some elements of the system consume energy to obtain propulsion: the continuous input of energy, by definition, drives these systems *out-of-equilibrium*. Active matter has received great attention in the last decade, as it display new physical phenomena, like collective properties [13–15], non-Boltzmann distributions [16], long-range ordering [17] and spontaneous flows [18]. In particular, the properties of active swimmers, also known as *self-propelled particles* (SPP) under spatial constraints have a great relevance from a biological, physiological and medical point of view. Bacterial tendency of accumulation to solid walls was argued [19] to have important consequences on the infection process. Soil functioning is reg-

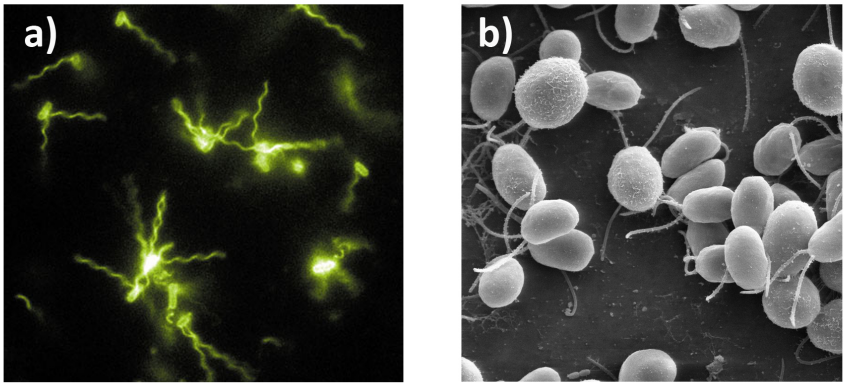

Figure 3: Two examples of Self-Propelled Particles: a) Fluorescent bacteria *E. Coli* (source: Berg Lab) [2]. b) *Chlamydomonas reinhardtii* algae (source: Wikipedia).

ulated by bacteria that typically grow and live in few micrometers size pores; their motility in such extreme environments is interesting also for sterilization and water treatment problems [20].

Finally, particular relevance is covered by the diffusion of hard-core particles in a channel so narrow they cannot pass each other, named Single File Diffusion. As a matter of fact, SFD has a capital importance in chemistry, physics and biology, as it is responsible for the transport of ions in membrane channels [21–24], the diffusion in nano- and microporous materials [5, 25] and has been observed in many other natural and artificial systems [26–34]. Single File systems of active particles can be also found in nature, as they are in general involved into the active processes of protein transport inside cells [12, 35–37].

From a physical point of view, the Single File Diffusion of passive particles is an exactly solvable model and provide a paradigmatic example of anomalous diffusion in crowded *equilibrium* systems. SFD key feature is the preservation of the initial order, that force particles to hinder each other. The displacement of any particle requires the movement of some of the others in the same direction: from this extreme confinement arise strong correlations and a subdiffusive behaviour, where the mean square displacement $\langle x^2(t)\rangle$ scales with $\sqrt{t}$, rather than t [38].

A lot of work has been done in the past years in the theoretical description of the Single File Diffusion, but surprisingly little attention has been devoted to the problem of absorbing boundaries [39–41]. Absorbing boundaries can be used to model diffusion-limited reactions, with application in many real systems. Furthermore, systems of active particles interacting in one dimension have been studied only recently [37], and very little is known about the general features on such Active Single File.

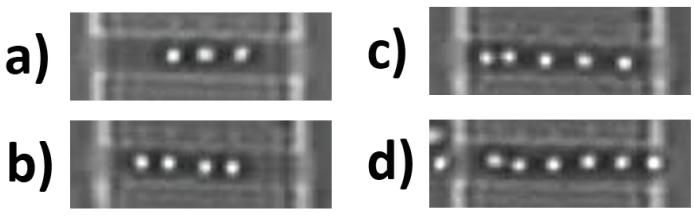

Figure 4: a) - d) Examples of colloidal particles in Single File conditions inside microfluidic channels, a) N=3, b) N=4, c) N=5, d) N=6.

Thesis Outline: Aim of this thesis is to investigate the properties of both diffusive and self propelled particles under Single File conditions in the presence of two absorbing boundaries by providing the exact solution for the emptying process, i.e. the progressive decrease of the number of particles in a region of interest due to the absorbing boundaries, and by comparing theoretical results with numerical and experimental data. In addition, we also focus on the trend of the characteristic emptying times, making extensive use of first-passage statistics concepts, and we will study in details the structural properties of a Single File, putting particular attention on the active case.

In Chapter 1 of this thesis, we will give an overview of the most relevant problems of diffusion in confined or crowded environments. In Chapter 2 we will review the state-of-the-art on Single File Diffusion, from both the theoretical and experimental point of view, focusing on a particular analytical technique, *the Reflection Principle Method*, which will be extensively used throughout the thesis. We will also describe the link between SFD and Fractional Brownian Motion, a stochastic process arised as reference model for anomalous diffusion.
In Chapter 3 we deal with the properties of Single File systems of diffusing particles in presence of two absorbing boundaries, comparing analytical calculations, numerical simulation and experimental results. We will look for the *survival probability*, i.e. the probability to find a particle between the absorbing boundaries at time t. In particular, we will focus on the *emptying process* and on the survival probability of a Tagged Particle within the file: in both cases, an exact analytical solution can be found, even in the presence of a constant external force. We will also study the trend of the characteristic survival times as function of the system size and of the initial number of particles. Finally, we will also study the survival probability when the absorbing boundaries affect only the central particle. We found numerical evidences of an exponential decay of the survival probability; the exponential decay constant is equal to the mean first passage time as it happens for normal diffusive processes, even in overcrowding conditions.
In Chapters 4 and 5 we will introduce activity in our framework, through a Self-Propelled Particle model extensively described in Chapter 4. Within this model, particles can be either *runners* or *tumblers*, if their motion is dominated

by straight runs or by changes of direction, respectively. Under Single File conditions, this distinction leads to profound differences in the collective behaviour of the system and in the dynamical properties. First, passing from one class to the other, a structural transition takes place, characterized by the emergence of aggregates on the *runners*' side, confirmed by the analysis of the radial distribution function. These clusters, held together by active forces acting in contrasting directions should be considered dynamical as, once they are formed, they can be broken without any external action, and then reformed. In the absence of clustering, the theoretical results found for passive diffusive particles are still valid. Conversely, in the other case theory cannot be applied, but we observe that clustering enhances anomalous behaviours in the characteristic survival times and introduces a remarkable capacity to oppose to the action of an external force.
Finally, details of numerical simulations and experimental realizations of SFD systems are reported respectively in Appendix A and B, a short study of spatial correlations in SFD is reported in Appendix C and analytical details on the survival probability of a single Brownian particle con be found in Appendix D.

Chapter 1

Diffusion under confinement

When diffusive transport of small particle takes place in restricted or crowded environments a significant change in the transport properties is always observed. Physicists attention has been addressed, in particular, to the micro- and mesoscopic world, as the cellular biophysics, microbial dynamics and other biological related process take place at these scales. Thanks to last decades advance in microfabrication and single-particle manipulation techniques, biological processes can be mimicked using microfluidic chips and colloids, that provide model systems of controllable environments free from the experimental limitations related to biological matter, like low signal-to-noise ratio and biological hazard. However, effective control of transport properties in artificial micro- and nanostructures requires a deep understanding of the effects induced by a severe confinement: therefore, it is necessary to build a comprehensive theoretical description of these phenomena.

In this Chapter, we will introduce the reader to the theoretical framework of the diffusion of particles under confinement. First, we will recall some basic notions of stochastic processes and we will introduce to *first passage statistics* concepts, which will be extensively used throughout the thesis. We will also briefly mention the three main mechanisms, raised as reference models for anomalous diffusion: Continuous-Time Random Walk (CTRW), Diffusion on a fractal and Fractional Brownian Motion (FBM), pointing out the main differences. Then we will survey the most interesting examples of diffusion under confinement, with particular attention to the intracellular transport mechanisms. We will conclude introducing concepts and methodologies of active matter, paying specific attention to the properties of bacteria and on their behaviour under confinement.

1.1 Basic principles of diffusion

It is well known since centuries that a body immersed in a fluid experience the action of the fluid elements in the surroundings. However, only in the beginning of the 20th century, thanks to the pioneering works of Perrin, scientists discovered that for a sufficiently small particle, typically of μm scale, the action of the fluid elements result in a random trajectory $\vec{x}(t)$ usually called Brownian or diffusive motion [42–45].
Described in terms of statistical mechanics, at a fixed time t, the position of the particle can be described as a *random variable*, X, mathematically defined as

$$X : \Omega \to \mathbb{R} \tag{1.1}$$

where the *sample space* Ω is the space of all distinguishable elementary results of an experiment. In order to characterize a random variable, we introduce the

probability density function $p_X(x)$,

$$p_X(x)dx = \mathbb{P}(x \leq X(\omega) \leq x + dx) \tag{1.2}$$

where $\mathbb{P}$ is the *probability measure* on $\mathcal{F}$, $\mathcal{F}$ being the set of subsets of Ω, $x \in \mathbb{R}$ and $\omega \in \Omega$; $(\Omega, \mathcal{F}, \mathbb{P})$ is usually called *probability space*. Loosely speaking, $p_X(x)$ establishes which numbers are more or less probable as an outcome.
A collection of random variables, parametrized by time, is called *stochastic process*: Brownian motion is one of the most important example. The random nature of the time evolution implies that a different realization, i.e. the set of the outcomes of the random variables of the same experiment, produces a completely different pattern for the observed physical quantities. Thus, it becomes impossible to gain insights on the properties of the system from individual measurements and we are forced to introduce probabilistic and statistical quantities. The first two moments of the random variable, the *average* or mean value

$$\mathbb{E}\{X\} \equiv \langle X \rangle = \int_{-\infty}^{\infty} x\, p_X(x)dx$$

and the *variance*

$$\sigma^2 \equiv \mathbb{E}\{(X - \langle X \rangle)^2\} = \int_{-\infty}^{\infty} (x - \langle X \rangle)^2\, p_X(x)dx$$

provides basic examples of such quantities. Particular relevance in this thesis is assumed by the the Mean Square Displacement (MSD) $\langle (X(t) - X_0)^2 \rangle$, where X_0 is the stochastic process at t=0 and the average is made over many independent realizations. The Mean Square Displacement is a common way to measure the amount of the system 'explored', on average, by the random walk. For a realization of Brownian motion, the MSD is given by

$$\langle x^2(t) - x_0 \rangle = 2\ d\ D\ t$$

where D is called *diffusion coefficient* and represent the explored area per unit time, while d is the dimensionality of the system.
Among the possible different approaches describing Brownian motion, the Langevin equation [46] is one of the most important and will be used as basis for our Self-

Propelled particle model in Chapter 4; we will limit here to the one dimensional case. Langevin equation is essentially Newton's second law for a mesoscopic particle immersed in a fluid

$$m\frac{dv}{dt} = F_e + F_t \qquad v = \frac{dx}{dt}. \tag{1.3}$$

where F_e are the external forces and F_t are the sum of the forces each molecule of the fluid exerts on the particle, decomposed into two contributions:

1. the deterministic damping term (Stokes force) -αv
2. a fluctuating term $f(t)$, which is supposed to have a Gaussian probability distribution function, with zero average, variance σ^2, and *delta-correlated*

$$\langle f(t_1)f(t_2)\rangle = \sigma^2\delta(t_1 - t_2)$$

Under these hypothesis, and for F_e=0, the Langevin equation becomes a stochastic system of differential equations:

$$m\frac{dv}{dt} = -\alpha v + f(t), \qquad v = \frac{dx}{dt}. \tag{1.4}$$

If $\gamma = \alpha/m$ is large enough, $dv/dt \ll 1$ and the *overdamped* limit can be carried out

$$v = \frac{1}{\gamma m}f(t) = \frac{dx}{dt} \tag{1.5}$$

Langevin equation is quite adaptable, as inter-particle or external forces can be added straightforwardly, and can be readily implemented in numerical simulations. Moreover, by standard methods, it is possible to obtain an equivalent description of fluctuations in a Fokker-Planck formalism [47] that provides a deterministic differential equation for the probability distribution function, $p_1(x, t|x_0)$. For Brownian motion in the overdamped limit, it reads

$$\frac{\partial p_1(x,t|x_0)}{\partial t} = D\frac{\partial^2 p_1(x,t|x_0)}{\partial x^2} \tag{1.6}$$

Through Fokker-Planck equation, one can also vary the boundary conditions, which depend on the problem. In this thesis, we have extensively used *absorbing* boundary conditions, i.e. particles are expelled from the system once they reach

the boundary position, limiting to the one dimensional case. In this context, a meaningful quantity is the *survival probability* $S(t|x_0)$, i.e. the probability that a particle, started at $x(0) = x_0$ inside the boundaries, has not been expelled up to time t. If we name the time of the exit event t^*, the survival probability is

$$S(t|x_0) = Prob(t^* > t) \tag{1.7}$$

If terms of the probability distribution function,

$$S(t|x_0) = \int_{b_1}^{b_2} p_1(x, t|x_0) \tag{1.8}$$

where we are assuming a one dimensional system with two absorbing boundaries, placed at $x = b_1$ and $x = b_2$. From $S(t|x_0)$, one can extract the typical timescale associated with the absorption of the particle, called *Mean First Passage Time*, as

$$T_1(x_0) = \int_0^{\infty} S(t|x_0)\ dt \tag{1.9}$$

1.2 Anomalous diffusion and stochastic process

In the years, Brownian motion has proven a powerful toy model in a variety of different fields, from ecology to economics and of course physics, biology and chemistry. However, many systems cannot be described by simple diffusion models, as they show different behaviours. For example, if wall or obstacles are present in the system, the amount of explored space is, on average, drastically reduced and the Mean Square Displacement will behave, in one dimension, as

$$\langle x^2(t) \rangle \propto t^{\alpha} \tag{1.10}$$

where $\alpha < 1$ in this case. Conversely, particle motion could be enhanced rather than decreased and in that case $\alpha > 1$. These processes are generally named *anomalous* diffusion, and particularly *subdiffusion* or *superdiffusion* if $\alpha < 1$ or $\alpha > 1$, respectively.

Despite the term, anomalous processes are ubiquitous and they have gained capital importance in many fields, from Biology to soft and condensed matter Physics [4, 12]. Unfortunately, experimental observations of such behaviours are rather difficult, as interesting time or length-scales are inaccessible. Only in the recent years, thanks to recent technological progresses, scientists have become able to study such processes on an unprecedented nanoscale molecule-by-molecule basis [48–50]. Compared with traditional experiments, single-molecule experiments provide experimental data with more accuracy and higher resolution. Moreover, these single-molecule experiments can capture transient intermediates and detailed dynamics of biological processes by following individual molecules. Finally, in a living cell, many important biological functions are often carried out by single molecules; thus, understanding the behavior of molecules at the individual level is of crucial importance [51].

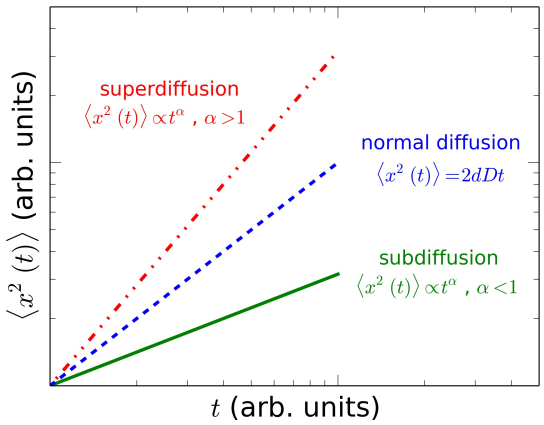

Figure 1.1: Log-Log plot of the Mean Square Displacement as function of time (arbitrary units) for superdiffusion (dashed and dotted line), normal diffusion (dashed line) and subdiffusion (full line).

Parallely, theories of anomalous diffusion and transport of physical particles have experienced a great development. In the following, we will briefly mention the three stochastic processes raised as reference models for anomalous diffusion [12].

1. **CTRW**. Continuous-Time Random Walk models transport processes involving transient immobilization or trapping: a diffusing particle encounters a binding site then it will pause for a while before disassociating and diffusing away [52, 53]. Multiple binding events with a range of rate constants can generate long tails in the waiting time distribution leading to subdiffusive behavior. In addition to having a heavy-tailed waiting time distribution, the CTRW is weakly non-ergodic; the temporal average of a long particle trajectory differs from the ensemble average over many diffusing particles.

2. **Diffusion on a fractal**. Obstructed diffusion (OD) takes place due to

molecular crowding or cytoskeletal networks that impose obstacles around which diffusing molecules have to navigate [54]; also in complex porous structures or heterogeneous media, a tracer particle can face this kind of limitations. If the concentration of obstacles is sufficiently high, then subdiffusive behavior occurs, in which the domain of free diffusion develops a fractal-like structure. At variance with CTRW, Diffusion on a fractal is an ergodic process.

3. **FBM**. Fractional Brownian Motion [55] is used to model the viscoelastic properties of the cytoplasm due to the combined effects of macromolecular crowding and the presence of elastic elements such as nucleic acids and cytoskeletal filaments. As a particle moves through the cytoplasm, the latter "'pushes back"', generating long-time correlations in the particle's trajectory. These memory effects leads to subdiffusive behaviors. FBM is ergodic and its probability density for unconfined subdiffusion is a Gaussian (with a time-dependent diffusivity). A comprehensive treatment of FBM will be given in the Chapter 2.

Determining which type of model best fits experimental data is a nontrivial task, thus ergodicity is often used to help identify the best characterization for anomalous diffusion in living cells.

1.3 Diffusive systems under confinement

In this section, we review some interesting examples of confined diffusion, with particular emphasis on intracellular transport.
A first example is the diffusion water or other small molecules in zeolites [5, 6, 25, 56]. Zeolites are crystalline microporous materials whose composition is very similar to sand, as they are mainly composed of silicons, tetrahedrally surrounded by oxygens. Using these basic building blocks, many kinds of structures can be created with pores and cavities; the different zeolites differ in pore diameter, pore shape and the way these pores are interconnected. Within these cavities move cations, water and/or other molecules.

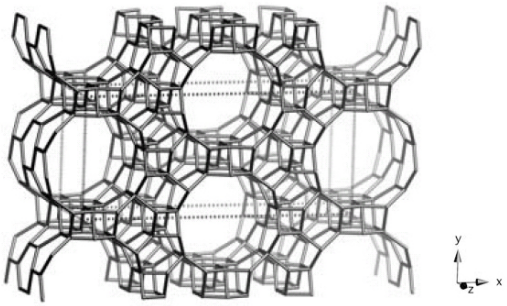

Figure 1.2: AIPO-8 zeolite framework, viewed along [001] (from [56])

Zeolites occur naturally as minerals, and are extensively mined in many parts of the world, finding applications in industry and medicine; among the most important is the use of these materials to catalyze the conversion of crude oil to more useful products like gasoline, kerosine and other smaller hydrocarbons (catalytic cracking). During the catalysis process there is an exchange of ions between the molecules of the cavity walls and the foreign molecules. In order to react, the molecules then have to be transported to the reactive sites inside these pores through diffusion. Often, since pores have a typical size of a few Å, diffusion takes place in Single File conditions, i.e particles are confined in a channel so narrow they cannot pass each other. From an industrial point of view, it is important to be able to predict and describe the mass transfer through the packed-bed reactors used in the chemical industries.

Two other examples comes from polymeric systems. The first is polymer translocation [9–11], a dynamic process in which a polymer pass through a hole whose size is generally much smaller than the average extension of the polymer itself. This is an important biological process related to the migration of DNA and RNA molecules from one region to another of the cell, generally by passing through a narrow pore of the nuclear membrane. Translocation processes may also have practical applications such as the possibility of reading the DNA or RNA sequence by passing it through an artificial nanopore or α-hemolysin channel. It also attracted an intense theoretical debate, as it shows interesting and untrivial anomalous behaviours [57–59].

The second example concerns the dynamic of a tagged monomer (TM) of a polymer in solution [60–62]. While the dynamics of the whole chain is dominated by the motion of its center of mass which follows a normal diffusion, the TM is coupled to the other monomers forming the chain and, at intermediate times, progressively more and more monomers act as constraints on its dynamics, that becomes sub-diffusive. In the long time limit, however, normal diffusion will be recovered. This process is a typical example of sub-diffusion induced by collective

motion of numerous degrees of freedom.

1.3.1 Intracellular diffusive transport

The efficient delivery of proteins and other molecular products to their correct location within a cell is of fundamental importance to normal cellular function and development [63]: its breakdown is a major contributing factor to many degenerative diseases. Intracellular transport is particularly challenging for brain cells, with regards to the efficient trafficking of newly synthesized proteins from the cell body to distant locations on the axon. In healthy neurons, regulation of protein trafficking provides an important mechanism of modifying the strength of synaptic connections between neurons, which is believed to be the cellular substrate of learning and memory [12].

One of the characteristic features of the interior aqueous environment of cells (cytoplasm) and intracellular compartments is that they are crowded with macromolecules and skeletal proteins, which occupy 10%–50% of the volume [65–67]. Cell membranes are also crowded environments containing lipids and various mobile and immobile proteins. One effect of molecular crowding is the increase the effective solute concentration, that leads to an increase of the chemical potential of the solute. Another consequence is that it hinders diffusion; this extreme crowdedness often leads to anomalous diffusion as, for example, for protein diffu-

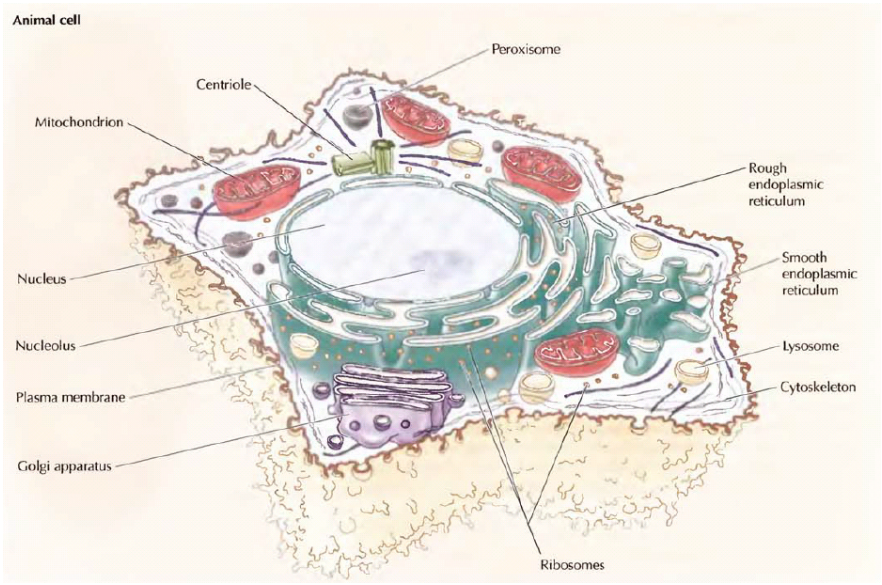

Figure 1.3: Schematical picture showing the structure of an animal cell (from [64])

sion in cytoplasm [54]. As the volume or area fraction of obstacles is increased, also the fragmentation of the available space is increased: many paths taken by a diffusing protein terminate in a dead end and thus do not contribute to diffusive transport. The region of free diffusion develops a fractal-like structure resulting in anomalous diffusion at intermediate times $\langle R^2 \rangle \sim t^\alpha$ and $\alpha < 1$.
Other interesting examples are also given by search processes for protein-DNA binding sites on a DNA chain [68,69], diffusion along spinal dendrites [70] or in the plasma membrane [71, 72] and nuclear transport of kap-cargo complexes [73, 74]. Last but not least, particular importance is covered by diffusion of particles through nanopores [21–24]. Nanopores are highly confining structures with small openings. The biological nanopores are transmembrane channels which control and regulate the ionic or proteic transport in living cells in the presence of electrical-chemical gradients. The ionic channel is a integral protein or an assembly of several protein subunits emebedded in the membrane. These transmembrane proteins form a water-filled channel through which the ion can pass; usually this passages are so narrow that Single File conditions happens. In cells, the slowdown induced by SFD is often overcome by the presence of concentration gradient, which drives the ions in the channel; this process is called *facilitated diffusion*.

1.4 Active matter

The term 'active' refers to the ability of individual units to move by transforming chemical energy, taken from the environment, into kinetic energy [15, 75, 76]. Examples of such systems are mixtures of cell extracts of biofilaments and associated motor proteins [77], the whole cytoskeleton of living cells [78], bacterial suspensions [79], cell layers [80], and terrestrial [81–83], aquatic [84,85] and aerial flocks [86], vibrated granular rods [87–89], colloidal or nanoscale particles propelled through a fluid by catalytic activity at their surface [90,91] and collections of robots [92,93]. The interaction with each other, and with the medium they live in, gives rise to highly correlated collective motion and mechanical stress. Indeed, a distinctive, defining feature of active systems compared to other nonequilibrium systems is the fact that the energy input that drives the system out of equilibrium is local, at the level of each particle, rather than at the system's boundaries as

in a shear flow. This means that random fluctuations in the motion of individual active units are always non negligible; this apparent randomness may have different origins, for example, environmental factors or internal fluctuations due to the intrinsic stochasticity of the processes driving individual motion. Active systems exhibit a wealth of intriguing nonequilibrium properties, including long-range ordering [17] and emergent structures with collective behavior qualitatively different from that of the individual constituents [13–15], non-Boltzmann fluctuation statistics [16], nonequilibrium order-disorder transitions [94, 95], pattern formation on mesoscopic scales [13, 96–98], unusual mechanical and rheological properties [99–104], spontaneous flows and wave propagation and sustained oscillations [13, 18].

Amongst the different systems that belong to this class, bacteria for various reasons become a model system, as they provide a reproducible and reliable experimental system, that display a great variety of the features cited above [105]. Bacteria are unicellular organisms, capable of self reproduction and, in many cases, motility (the biologists' term for self-propulsion). A range of biomechanical mechanisms for motility are shown by different species of bacteria, the simplest of which is the swimming motion of species such as *Escherichia Coli* [106]. Individual *E. Coli* have helical flagella, each of which is forced to rotate by a biochemically powered motor. Because of the chirality of these flagella, their clockwise and anticlockwise motion is inequivalent. One sense of rotation causes the flagella to form a coherent bundle which acts like a (low Reynolds number analogue of a) ship's propeller, resulting in a smooth swimming motion. Initiating the other sense of rotation causes the bundle to separate, with the result that the cell starts to rotate randomly. The canonical motion of *E. Coli* then consists of periods of straight line swimming (called 'runs') interrupted by brief bursts of rotational motion (called 'tumbles'). For *E. Coli*, a typical run lasts about 1 s; to a reasonable approximation the duration of runs is Poisson distributed, so that tumbles can be viewed as random events occurring with a certain event rate α. Tumbles are usually much shorter, of duration $\tau \simeq 0.1$ s, and often treated as instantaneous ($\tau \to 0$). In practice, tumbles may not totally randomize the orientation of the cell body, but for simplicity that assumption is often made, and we adopt it here unless otherwise stated. The swim speed v of *E. Coli* is around 20μm/s, so that under the simplest conditions, i.e. the statistics of the

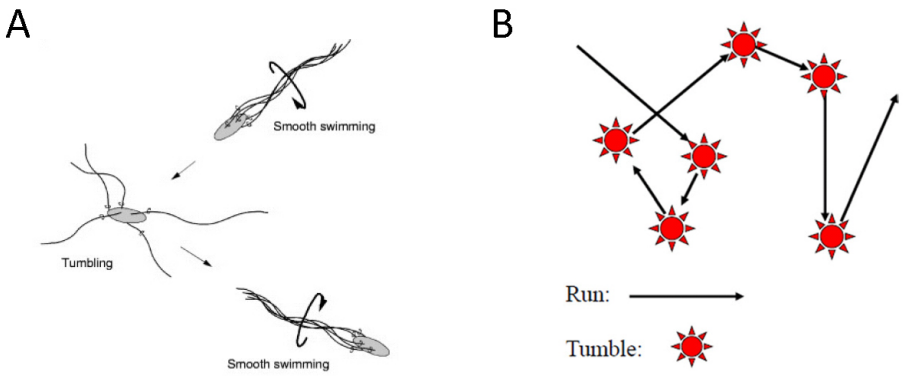

Figure 1.4: A) Pictorical representation of run-and-tumble bacterial motion. B) An unbiased run-and-tumble, on an appropriate scale, is a random walk with an average step size which depend on the run and tumble times (from [105]).

run-and-tumble motion is unbiased by any environmental factors, each bacterium performs a random walk, with an average step length of about 20μm, and about one step per second. The diffusion constant of this stochastic process is readily calculated

$$D_a = \frac{v^2}{\alpha d}$$

where d is the spatial dimensionality and α is the tumble rate. This diffusivity is hundreds of times larger compared to the passive one for colloidal particles of the same size. Brownian motion, however, does still matter: it sets the longest duration possible for a straight run before its direction is randomized by rotational diffusion. The run duration chosen by evolution is usually comparable to, but shorter than, the rotational diffusion time τ_B, so that runs are fairly straight. So, at time and length scales much larger than $1/\alpha$ and v$/\alpha$, respectively, the dynamics just described is equivalent to an unbiased random walk with constant diffusivity D_a.

In the context of confined active processes, we review two distinct topics: intracellular active transport and bacterial motion under confinement.

1.4.1 Intracellular active transport

Two main limitations affect passive diffusion as a mechanism for intracellular transport [12]. First, it can take far too long to travel the long distances necessary to reach targets within a cell, which is particularly acute in the case of the axons and dendrites of neurons. Second, diffusive transport tends to be unbiased, making it difficult to sort resources to specific areas within a cell.

Active intracellular transport can overcome these difficulties so that movement is both faster and direct specific, but does consuming energy. The main type of active intracellular transport involves the molecular motors [107] kinesin and dynein carrying resources along microtubular filament tracks [108]. Microtubules are polarized polymeric filaments with biophysically distinct (+) and (-) ends [109]. On this tracks move molecular motors, proteins that are able to convert stored chemical energy into mechanical work by hydrolyzing ATP molecules. The mechanical work is done by the motors moving in a unidirectional manner along the polar filaments; this polarity determines the preferred direction in which an individual molecular motor moves. Particular motor proteins are associated with specific polar filaments, e.g., kinesins "walk" on microtubules while myosins "walk" on filamentous actin. Physically, a motor protein undergoes a sequence of conformational changes after reacting with one or more ATP molecules, causing it to step forward along the microtubule and providing the energy necessary for the molecular motor to do work in the form of pulling its cargo along the microtubule. Microtubular network is indeed essential in cells, not only for transport properties, but also for its role in the growth, elongation and development of polarity in cells [110–112], for its relevance in viral infection [113], for the emergence of cooperative behaviours [12] and for its capability of targeting and delivering proteins in the correct loca-

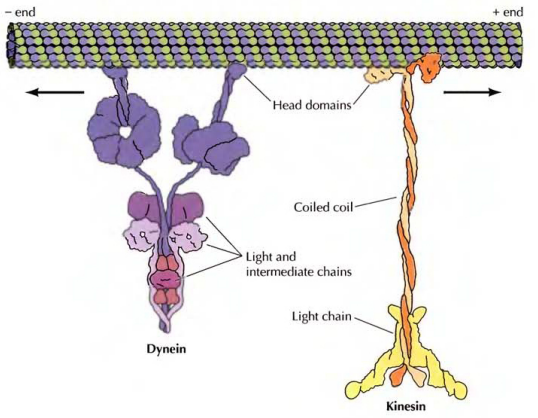

Figure 1.5: Pictorical representation of two types of molecular motors moving along a cellular microtubule (from [64]). Kinesin moves to the right while dynein moves to the left.

tion [36] through a random intermittent search process [114]. Finally, interesting problems in this field are related to active transport on DNA [115] and mRNA translation by ribosome [116].

1.4.2 Microswimmwers under confinement

Bacterial growth and movement in confined spaces is ubiquitous in nature and plays an important role in diverse fields ranging from soil microbiology, water purification, to microbial pathogenesis. The majority of bacteria in soil and bedrock live in pores of size 6 micrometer and smaller. These bacteria constitute a large portion of the Earth's biomass and are essential for the functioning of soil. In order to predict the flux of cells through this microporous substrates one must know the factors controlling bacterial movement in these environments. While much is known of the swimming behavior of bacteria in unrestricted environments the added complication of propulsion through a microporous environment can affect the cell's ability to rotate or maintain an optimal speed, which in turn will alter the rate at which bacteria penetrate a given substrate. This is also an important question for water treatment and purification. Whereas microbiology textbooks consider output from 0.2-μm pore size filters sterile, it has recently been found that numerous bacteria can pass through these membranes and grow thereafter. Moreover, the majority of swimming microorganisms involved in human functions and diseases are found in geometrically confined environments. Spermatozoa in the female reproductive tract swim in constricted domains. Bacteria make their way through host cells and tissues and aggregate in antibiotic-resistant biofilms on surfaces.

A first interesting topic is the accumulation of swimming microorganisms by surfaces [19, 117–119]. Experimental data display a strong enhancement of bacterial density near solid walls, which has been explained by hydrodynamic interactions that result in a reorientation of the swimmers in the direction parallel to the surfaces and an attraction of these aligned cells. However this explanation is still under debate, as a number of simulations suggest that this accumulation can be observed without the presence of hydrodynamics [117–121]. Despite the physical controversy, this effect has already been successfully used in interesting microfluidic applications [14, 122–127].

Another interesting questions concern the minimum size for bacterial propagation through constrictions and what sets the lower limit for the channel width where they can still swim [20]. Three possible physical constraints has been discussed: hydrodynamic drag, constraints to movement of flagella, and adhesion forces. Experimental data shows that only adhesive and friction forces set severe constraints to bacterial motility, while hydrodynamic drag and constraints to flagella does not lead to a complete stalling of bacteria. Penetration in channels smaller than bacterial size, however, is also possible by growth and division for certain type of bacteria, undergoing significant deformations and losing their regular shapes, but still having growth rates that are not significantly different than in unbound medium.

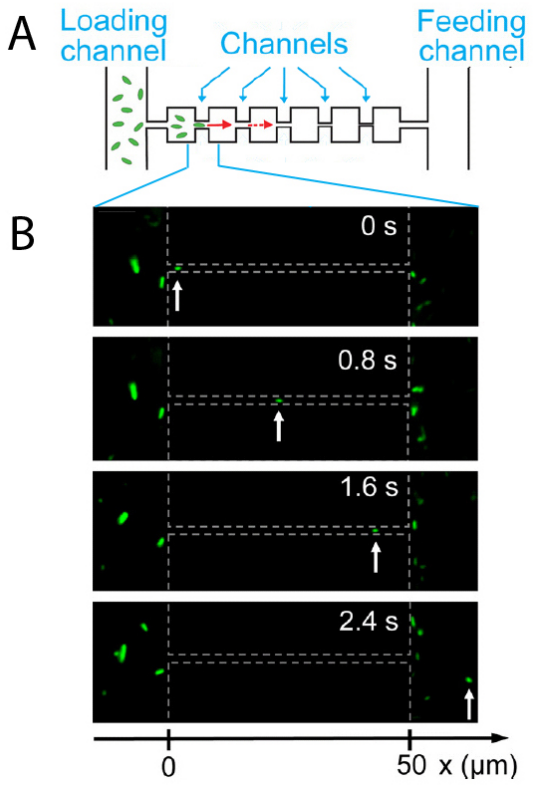

Figure 1.6: (From [20]) A) Schematic of the experimental setup for studying bacterial movement in small constrictions. B) Time-lapse images of an *E. coli* bacterium swimming through a 1.2-μm wide channel and into the chamber area. The arrow points at the swimming bacterium.

Morphogenesis is another highly important theme in both biology and nonequilibrium physics, as the biomechanical interactions arising from the growth and division of individual cells in confined environments are ubiquitous [128]. The structure of bacterial populations is governed by the interplay of many physical and biological factors, ranging from properties of surrounding aqueous media and substrates to cell–cell communication and gene expression in individual cells; this self-organization can lead to significant selective advantages for living organisms. For example, bacteria actively migrate toward surfaces and small enclosed spaces, where they form high-density microcolonies to facilitate quorum sensing. To resist environmental stresses, some species of bacteria form biofilms, which are commonly present in both natural environments (including living tissues,

soils, and aquatic systems) and on synthetic surfaces (such as industrial piping and device implants). An important unexplored consequence of the formation of high-density bacterial colonies is spatial organization caused by the "contact biomechanics" arising from cellular growth and division. At low density, communication among cells occurs mainly through chemotaxis, but as bacteria aggregate and form dense communities, direct biomechanical interaction plays an increasingly strong role in colony organization.
Finally, collective phenomena have also been observed to occur under confinement. Suspension of bacteria confined in a drop self-organizes into a single stable vortex [129] that persists as long as oxygen is available. This pattern is also reminiscent of structures seen in colonies on the surface of agar [130], spontaneously circulating cytoplasmic extracts of algal cells [131, 132], and the rotating interior of fibroblasts on micropatterned surfaces [133].

1.5 Concluding remarks

Summarizing, we have shown several examples of physical systems in which either confinement or crowdedness produce a slowdown of particles dynamics. Biologically, this is a crucial problem, since it mines the efficiency of transport in cells, and has been limited in several ways, in particular through the introduction of active elements and/or one-dimensional tracks (like DNA or microtubules). These processes have typically the goal of transporting a component of a reaction to a specific site, like in the protein-DNA binding site diffusive search: the general properties of this kind of reaction processes in one dimension are not completely understood. We have also reviewed the interesting collective properties that can arise when microorganisms like bacteria or algae experience spatial confinement. Understanding how confinement lead to the emergence of these phenomena is also fundamental to achieve a better understanding of the bacterial behaviour within their own environment.

Chapter 2

Single File Diffusion

In this Chapter we give an overview of the theoretical and experimental literature on the Single File Diffusion. From the theoretical point of view, we will describe the most versatile and powerful techniques used in this framework, with emphasis on the Reflection Principle Method, that will be used in the following Chapters. Then we will briefly define an family of stochastic processes, Fractional Brownian Motion, already introduced in Chapter 1 and we will exploit its connection with SFD. Finally, we will review a series of microfluidic realizations of Single File Diffusion.

2.1 General properties of SFD

We will exploit the general properties of the Single File Diffusion systems by examining the Mean Square Displacement of the central (tagged) particle. In general, for a SFD of N particles we expect a general form of the MSD composed of four different regimes:

(I) a ballistic regime $\langle x^2(t)\rangle \sim t^2$

(II) single-particle diffusive regime $\langle x^2(t)\rangle = 2Dt$

(III) subdiffusive regime $\langle x^2(t)\rangle \sim t^{\frac{1}{2}}$

(IV) collective diffusive regime $\langle x^2(t)\rangle = 2D_N t$, where $D_N \propto \frac{D}{N}$

(I)-(IV) refer to the numbering scheme used in Fig. 2.1. Despite this scheme should be universal, the temporal extension of this four regime is highly affected by the parameters of the system and in certain extreme situations, they can also shrink and disappear or take place at such long times they cannot be observed in a normal simulation or experimental measure.
The ballistic regime takes place at very early times, typically $t < \tau_b = {}^2/_\gamma$, and depends on the friction coefficient of the surrounding fluid; by definition is neglected in the overdamped limit and is generally very difficult to measure experimentally.
After the ballistic regime, a regime of normal diffusion takes place: the MSD has the typical form $< x^2(t) >= 2Dt$, where $D_0 = k_B T/m\gamma$: it is related to the (average) free space between particles and thus its duration depends on the density of the particles. A crossover is expected at $\tau_s \approx 1/\rho^2 D$ [134].
After τ_s, comes the anomalous diffusion regime $< x^2(t) >= Ft^{1/2}$. Since in this regime particles strongly interact and hinder each other, different global quantity of the system affect both its duration and its magnitude. First, the $1/2$ exponent of the subdiffusion is characteristic, and if the size of the system is big enough,

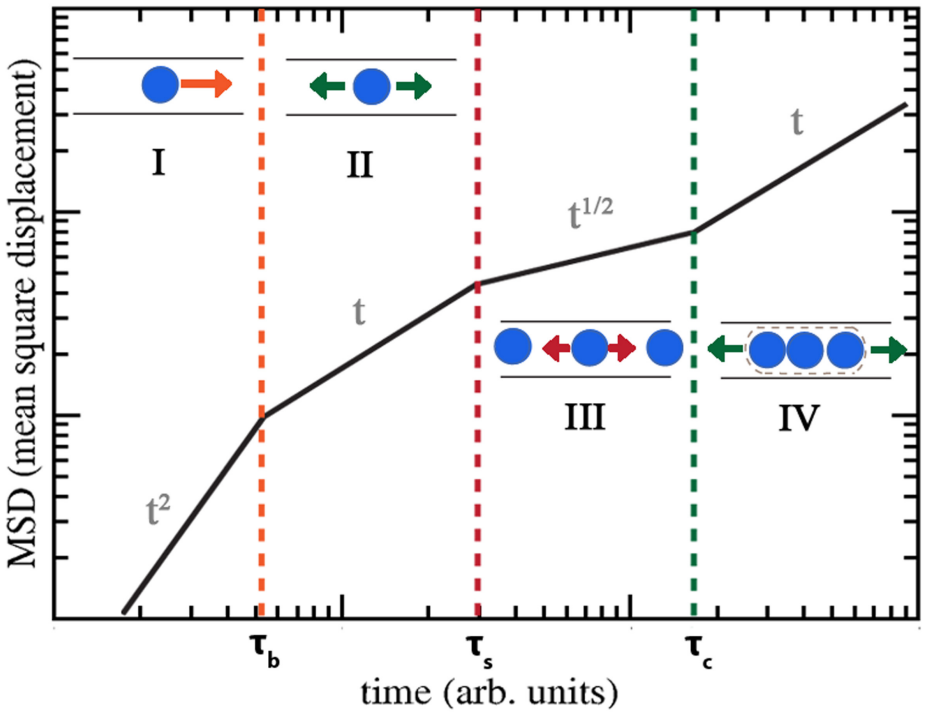

Figure 2.1: Qualitative log-log sketch of the MSD $< (x(t) - x_0)^2 >$ of the central particle for a finite Single File system. The general time dependence of the MSD is a power law $t^{\alpha(t)}$ being $\alpha = 2$ at the beginning of the motion, for $0 < t < \tau_b$ in the ballistic region (I), $\alpha = 1$ for $\tau_b < t < \tau_s$ in the diffusive region (II), $\alpha = 0.5$ for $\tau_s < t < \tau_c$ in the subdiffusive region (III) and again $\alpha = 1$ in the collective diffusive region (IV) obtained in the long time limit $t > \tau_c$.

it not depends on the interaction potential; for small system, however, a slightly bigger exponent is observed, as a finite size effect. The mobility F is as well independent on the details of the interaction potential, as long as the initial order is preserved. The crossover to the next regime happen at $\tau_{coll} = m\gamma N^2 \kappa_T / \pi\rho$ [135], where κ_T is the isothermal compressibility; thus subdiffusion's duration is strongly affected by the number of the particle and the density. The dependence on the number of particles is consistent with the thermodynamic limit, where subdiffusion is the genuine long time regime of the SFD.

Finally, last regime is boundary sensitive, in the sense that the diffusion coefficient is slightly different for different boundary conditions. For periodic boundaries $D_N = D_0/N$ can be obtained analytically [135], while if we consider an initial concentration of particles and natural boundaries $D_N \propto D_0/N$, as entropic effects promote the expansion of the system in the infinite free space available. This regime is called in literature 'collective diffusion' because, as in Rouse model, it is essentially the dynamic of lowest mode of the SF system; this name can be

misleading, as there is no collective motion and velocities are not correlated; instead spatial correlations are established between particles all over the system, as showed in Appendix C.
In all this treatment, initial conditions have deliberately left out, as their influence can be extremely not trivial [136–139]. If we limit at thermal or equispaced initial conditions, such picture for the MSD is valid.

2.2 Theoretical results on Single File Diffusion

From the first pionristic work by Harris [140], that shows the $t^{1/2}$ law of the MSD and the Gaussian nature of the Tagged Particle (TP) probability distribution function, many authors studied the TP dynamic under different conditions [134, 135, 141–148]. Simple arguments to the origin of the $t^{1/2}$ has been presented, using dynamic of vacancies [5], tracer particle density fluctuations [149] or the velocity autocorrelation function [150]; this behaviour has been proved to be rather general, independent on the details of the inter-particle interaction potential, as long as the order is preserved [143]. In the last decade, great importance was given to SF systems with a finite number of particles. Several exact results were found; among them, Kollmann's law [143] is particularly interesting as it provides an universal feature of a SF system, relating the mobility in the $t^{1/2}$ regime to the early time dynamic structure factor.
Between the different exact approaches present in the literature, three of them are particularly interesting as they are quite versatile (they permit to include the presence of external forces, different type of boundary and initial conditions etc..) and elegant: Jepsen line method, harmonization method and reflection principle method. This last one will be treated in detail in a separate section, as it will be used later in all our analytical calculations.
Jepsen line method was named after Jepsen's first derivation [141]; recently, has been recovered [137, 146, 147] as it provided a very powerful and general method. The method consist in a mapping of the interactive system on a non-interacting one through the equivalence of an hard-core collision and the switching of the labels of two identical noninteracting particles. We can recover the correct properties by using an auxiliary variable $\alpha(t)$, the label number of the first particle at the right of a reference line $x(t) = vt$, called the Jepsen line (hence the name);

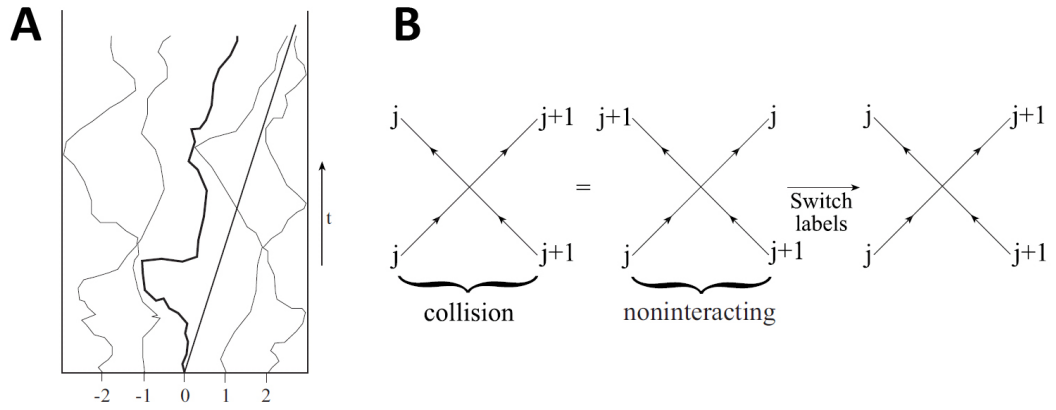

Figure 2.2: (from [147]) A) Schematic motion of Brownian particles in a box, where particles cannot penetrate through each other; each trajectory is restricted by collisions with neighboring particles. The straight line is the Jepsen line. B) In an equivalent noninteracting picture, we allow particles to pass through each other. The paths of a pair of particles experiencing an hard-core collision event can be represented by two noninteracting particles passing through each other and having their label numbers switched.

the Tagged Particle probability distribution function $P(x_T)$ can be obtained using the relation

$$\Pr(x_T < vt) = \int_{-\infty}^{vt} P(x_T) dx_T$$

and, since the event $x_T < vt$ is statistically equivalent to $\alpha \geq 1$

$$\Pr(x_T < vt) = \sum_{\alpha=1}^{N} P_N(\alpha)$$

In contrast to Jepsen line method, harmonization method [134] is very recent. The philosophy behind harmonization is to map the original system to a system consisting of beads interconnected by harmonic springs. In the original system at equilibrium, consider two particles with $N \gg 1$ other particles in between them; they are at an average distance L_{eq} from one another and fluctuations of L around L_{eq} are small. Thus we can expand the extensive free energy of the system $\mathcal{F}(N, L)$ around this minimum, defining a macroscopic spring constant $k_N = \frac{\partial^2 \mathcal{F}(N,L)}{\partial L^2}\big|_{L_{eq}}$. If we now map the system into a chain of harmonic springs with harmonic spring constant κ, we have to require that the total free energies associated with identical displacements from L_{eq} in the two systems must be the same. This implies

$$\kappa = N \frac{\partial^2 \mathcal{F}(N, L)}{\partial L^2}\Big|_{L_{eq}} \tag{2.1}$$

The final step is to replace the interaction potential in the original system with nearest-neighbor spring coupling, under the assumption that there has been time for particles to interact with neighbors $t \gg \tau_{int}$. This mapping is very clever as it uses the slowness of the $t^{1/2}$ regime: a tracer particle in this regime will cross a system of length L in a time of order L^4. This is considerably slower than the relaxation time of the whole system, which scales as L^2. Thus, in the long time limit a tracer particle only sees particles which had sufficient time to reach local thermal equilibrium. That's the reason why equilibrium concept like free energy work so well here. Harmonization has been employed successfully so far to predict MSD and correlations behaviour; it has also been extended to higher dimensions and has been proposed as a framework model for a wide range of physical problems. Unfortunately, it can't provide access to the Tagged Particle probability distribution function.

Several new directions of research emerged in the last year. The effect of an external field acting on all the particles [146] or on the Tagged Particle only [151] has attracted attention since pores induce entropic barriers and are generally inhomogeneous. As already mentioned, initial conditions may have a profound impact on diffusion of the Tagged Particle [136–139] and when an external field is acting on the system, it is important to consider nonuniform initial conditions where the density of particles is determined naturally from Boltzmann's distribution. For example power-law initial conditions induce $< x^2 > \sim t^{\xi}$, with ξ neither 1 nor $1/2$. In some cases the underlying motion is not Brownian, and follows anomalous kinetics [136]. Surprisingly, in all the SFD theoretical literature only a few works were devoted to the study of SFD with absorbing boundary conditions: in [41], authors studied first passage time density of a Tagged Particle in an infinite system while in [39, 40] the long time behaviour of the survival probability of a TP in a SFD in a finite interval was investigated. Absorbing boundaries can be used to model diffusion-limited reactions, with application in many real systems.

2.2.1 Reflection principle method

The Single File Diffusion of passive particle can be studied exactly by using the reflection principle method [145]. The Single File system is characterized by the impossibility of crossing so that the order of the coordinates is strictly preserved during all the dynamical development. This implies that only a section A of the entire configurational space is accessible; this section is determined by the planes $x_i = x_j$, $\forall i, j$. The Single File property can therefore be expressed as the condition that the probability flux through these planes vanishes, i.e., these planes act as reflecting boundaries. As in the case of the usual reflecting boundaries, this condition can be satisfied using the *reflection principle*: if the solution is reflected at the interesting point and added to the original solution, the derivative of the sum normal to this plane vanishes. If the particles act as reflection planes and we have several particles, one has to consider all possible combinations of reflections. Reflection at a plane $x_i = x_j$ simply imply an exchange of the coordinates; the possible combinations of reflections are given by the permutations of all the possible permutation of the N indices

$$P(\mathbf{x}, t|\mathbf{x}^0) = \begin{cases} \sum_{\pi \in P_N} \prod_{k=1}^{N} p(x_{\pi(k)}, t|x_k^0) & \text{if } \mathbf{x} \in A \\ 0 & \text{if } \mathbf{x} \notin A \end{cases} \tag{2.2}$$

As described in [145], the solution is valid only on a particular section of the configurational space, defined by

$$A = \left\{ x_1 < x_2 < \ldots < x_n \right\} \tag{2.3}$$

such that the order is preserved and the Single File condition is guaranteed.
This method has a different approach respect to the 'Jepsen line' method, but it relies on the same principle: each possible collision is taken into account as a switch of the indices of the two non-interacting particles. With the reflection principle method it is possible to transfer the boundary condition problem from the Green function of the entire interacting system to the Green function of the freely diffusing particle. Moreover, we only need the single particle propagator, that means we can exactly reconstruct the full probability of a Single File system in presence of an external force. The main disadvantages of this method are

essentially two: first, the calculation of any average quantity requires a huge amount of numerical power and provides a very difficult task from the analytical point of view. Second, the reflection principle approach is based on two essential ingredients: the particles must be identical and the collisions between them must be elastic, otherwise we could not exchange position and velocities. If one of this condition is not satisfied, the theory is no more valid.

2.3 Fractional Brownian Motion and Single File Diffusion

Since its introduction, fractional Brownian motion (FBM) [55] has proven to be an indispensable tool for stochastic modeling [152]; its applications range from queuing systems [153] to finance [154] to internet traffic [155]. One-dimensional FBM $X_H(t)$ with the Hurst exponent H ($0 < H < 1$) may be viewed as a natural extension of normal Brownian motion. In fact, FBM is a Gaussian process satisfying the criteria that $X_H(0)=0$; for all t and Δt, the increment $X_H(t+\Delta t) - X_H(t)$ is stationary and given by the normal distribution of zero mean and variance $(\Delta t)^{2H}$, so that its probability density function satisfies

$$P\left(X_H(t+\Delta t)|X_H(t)\right) = \frac{1}{\sqrt{2\pi(\Delta t)^{2H}}} \exp\left(-\frac{(X_H(t+\Delta t) - X_H(t))^2}{2(\Delta t)^{2H}}\right)$$

Last, FBM is self similar; indeed, it is often defined as the only Gaussian process with stationary increments that is also self-similar [156]. Thanks to its definition FBM satisfies the expected properties of a generalized Brownian motion, i.e.,

$$\langle X_H^2(t)\rangle = t^{2H}$$

as well as

$$\langle (X_H(t+\Delta t) - X_H(t))^2\rangle = (\Delta t)^{2H}$$

It is immediately inferred from this relations that the covariance of FBM is uniquely given by

$$\langle X_H(t_1)X_H(t_2)\rangle = \frac{1}{2}(|t_1|^{2H} + |t_2|^{2H} - |t_1 - t_2|^{2H})$$

Thus, except for the special case $H = 1/2$ of ordinary BM, the increments of FBM are correlated; in fact, they are negatively (positively) correlated for $0 < H < 1/2$ ($1/2 < H < 1$) and, in turn, gives rise to subdiffusion (superdiffusion). FBM can be expressed in terms of its incremental sequence, i.e., fractional Gaussian noise (FGN) ξ_H(t), such that

$$X_H(t) = \int_0^t \xi_H(t')dt'$$

FBM and FGN have a great relevance in the construction of biophysical models: a key requirement in the construction of these models, in addition to the preference of analytical tractability, is that the model must agree with fundamental physical laws and have a physical foundation. These are provided through its connection to a Fractional (or Generalized) Langevin Equation (FLE) [157]

$$m\frac{dv}{dt} = -\zeta \int_{-\infty}^{t} v(t')K_H(t-t')dt' + \sqrt{2\zeta k_B T}\xi_H(t) \tag{2.4}$$

where, $\xi_H(t)$ is a FGN with memory and $K_H(t) = H(2H-1)|t-t'|^{2H-2}$ is a memory kernel. $K_H(t)$ and $\xi_H(t)$ satisfy the fluctuation–dissipation theorem

$$\langle \xi_H(t)\xi_H(t') \rangle = k_B T \zeta K_H(t-t') \tag{2.5}$$

In an intuitive sense the relationship (2.5) arises because both the friction and the motion of the particle originate from the collision between the particle and its surrounding media. It turns out that the overdamped FLE process fulfills all the criteria of FBM, thus behaving as a subdiffusive FBM of the same anomalous diffusion exponent.

Finally, FBM and SFD can be connected through a Fractional Langevin equation. In fact, from both a phenomenological approach [144] and rigorous calculations [134], a FLE for the tagged (central) particle can be derived. Thus, the dynamic of the Tagged Particle can be described as a FBM of exponent $H = 1/4$, and for this particular kind of FBM we can use SF systems to investigate properties of FBM.

2.4 Experimental realizations of Single File Diffusion

Since its discovery by Hodgdkin and Keynes [21], Single File Diffusion has been observed in very different physical systems [26–32], which can be divided into three different groups, according to their characteristic lengthscale:

1. microscopic scale (channel size: Å- nm)
2. mesoscopic scale (channel size: μm)
3. macroscopic scale (channel size: mm)

The first case is absolutely the most important, as cellular channels and all the biological SF process [12, 21–24, 29], industrial and chemical application of micro- and nanoporous materials [5, 25], medical applications as drug delivery [33], water diffusion in carbon nanotubes [34] etc are characterized precisely by this length-scales. Unfortunately, from an experimental point of view, measures are difficult and, often, result from different studies are still in contradiction.
The third case [31, 32, 158] is quite interesting, also from a more general point of view, as it involves the intriguing idea of a macroscopic realization of Brownian motion. On the other hand, such a system is very delicate and involve lots of technical know-how.
Conversely, colloids motion in microchannels is a genuine Brownian motion, and provide a reliable and long known way to investigate statistical mechanics problems. Experimentally it requires standard equipment and, since time and length-scales in such systems can be easily observed with standard video microscopy, a tracking experiment gives back the trajectories of the observed particles thus providing a direct access to the dynamical relevant information of the system. The first mesoscopic experiment was done by Wei *et al.*: they realized a first well-defined SFD model system by confining polystyrene colloids in a set of circular channels fabricated by photolithography. Colloidal particles were doped with Fe_2O_3 to be paramagnetic; in this way they could tune and control the interaction potential. They observed anomalous behaviours $< \Delta x^2 > \approx Ft^{1/2}$ over two decades of time and confirmed the theoretically predicted Gaussian distribution

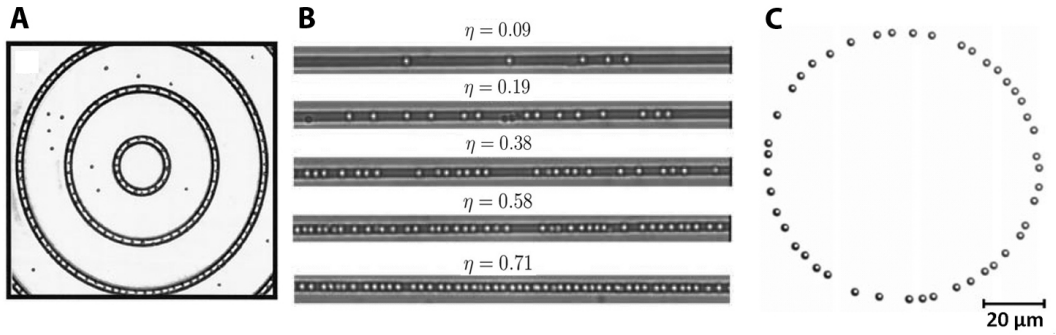

Figure 2.3: Experimental realizations of SFD in microfluidic channels. A) Optical microscope image of three concentric circular channels with colloidal particles confined in them (from [26]). B) Microscope images of silica colloidal spheres in one-dimensional grooves (from [28]). C) Image of colloidal particles trapped by a scanning laser beam to a circular optical trap (from [30]).

of particle displacements

$$x \to \frac{x}{t^{1/4}} \qquad\qquad p(x,t) \to t^{1/4} p(x,t)$$

Later, Lin *et al.* focused on the initial diffusive behaviour using silica colloidal spheres, diffusing into long and narrow polydimethylsiloxane (PDMS) grooves. They found that hydrodynamic interactions play an important role, as the initial diffusion coefficient shows a strong dependence on volume fraction. This was later confirmed to be an hydrodynamic effect by Lutz *et al.* by studying polystyrene particles in optical circular channels, realized by means of a scanning optical tweezers. In the former case, the presence of solid walls imposes strong hydrodynamic boundary conditions; with optical channels this is significantly reduced and only the substrate determines the free diffusion constant. Lutz *et al.* were also able to measure and characterize the subdiffusive behaviour, confirming Kollmann's law.

Chapter 3

Single File Diffusion with absorbing boundaries

First passage statistics deals with the properties of stochastic processes reaching a certain value at a certain time *for the first time*; this value (or set of values) is usually called *absorbing boundary* as it usually marks the death of the process, as it happens in chemical reactions between particles diffusing in a liquid. Often, first passage time is an important dynamic measure that can point out subtleties of underlying anomalous diffusive process [159, 160], and has been applied to attaining to numerous problems, such as diffusion-limited reaction kinetics, polymer cyclization, target search, barrier crossing, polymer translocation, neuron dynamics, self-organized critical models and many others (see [159,160] and references therein).
Surprisingly, among the literature of SFD, very few works were devoted to the study of SF systems with absorbing boundary conditions: in [41], authors studied first passage time density of a Tagged Particle (TP) in a semi-infinite system and its connection to FBM. In [39, 40] the long time behaviour of the survival probability of a TP in a finite interval was investigated, by exploring the possibility of different boundary conditions (one absorbing and one reflecting) and different initial conditions (fixed number of particles or fixed number density).

In this Chapter we report a detailed derivation of the analytical solution to a very similar problem, the emptying process, i.e. the progressive decrease of the number of particles in a region of interest due to the absorbing boundaries, either in the presence or in the absence of an external force. In addition, we present an alternative and exact solution to the problem of the survival probability of a Tagged Particle, limited to the case of two absorbing boundaries and a fixed initial number of particles; moreover, an approximated solution in the presence of an external constant bias was found. The exact solutions to these problems are then validated by comparing them with extensive numerical simulations. In particular, we characterize the exit-side probability, i.e. the probability to fall out of the region of interest from the left boundary or from the right one, and the Mean First Passage Time, which have often a great experimental relevance, by exploiting their trends as function of the most relevant parameters of the system. Finally, we conclude this Chapter with an extensive numerical study on the survival probability of the central particle, in which it is the only particle affected by the absorbing boundaries.

3.1 Emptying process of a non-interacting system

We are interested in the probability of having at least n^* of the initial N non-interacting particles, starting from certain initial conditions $\mathbf{x}^0$ still inside [-$L/2$;$L/2$] at time t, $S_{n^*}(t|\mathbf{x}^0, N, L)$. By definition, this quantity is given by the sum of the probabilities of having n particle still inside at time t, $p_n(t|\mathbf{x}^0, N, L)$

$$S_{n^*}(t|\mathbf{x}^0, N, L) = \sum_{n=n^*}^{N} p_n(t|\mathbf{x}^0, N, L) \tag{3.1}$$

The problem is now to calculate $p_n(t|\mathbf{x}^0, N, L)$. We can define this quantity using the exit times: in fact, if n particles are still inside [-$L/2$;$L/2$], this means that their exit times t^* are bigger than t. On the other hand, N-n particles have already left [-$L/2$;$L/2$] and their exit times are smaller than t. $p_n(t|\mathbf{x}^0, N, L)$ can be thus defined as

$$p_n(t|\mathbf{x}^0, N, L) \equiv P(t_1^*, \dots t_n^* > t, t_{n+1}^*, \dots t_N^* < t|\mathbf{x}^0, N, L) \tag{3.2}$$

since each particle is independent from each other

$$\begin{aligned} p_n(t|\mathbf{x}^0, N, L) = &\int_t^\infty dt_1 - \frac{dS(t_1|x_1^0, L)}{dt_1} \dots \int_t^\infty dt_n - \frac{dS(t_1|x_n^0, L)}{dt_n} \times \\ &\times \int_0^t dt_{n+1} - \frac{dS(t_1|x_{n+1}^0, L)}{dt_{n+1}} \dots \int_0^t dt_N - \frac{dS(t_1|x_N^0, L)}{dt_N} \\ =&S(t|x_1^0, L) \dots S(t|x_n^0, L) \cdot (1 - S(t|x_{n+1}^0, L)) \dots (1 - S(t|x_N^0, L)) \end{aligned}$$

Since particles are independent, we don't know which one exits and which one survives, and we must consider all the possible sequences, i.e all the permutation of the N indices. The temporal order of the exits, however, is irrelevant; thus permutations inside the same set of $N - n$ indices of the exited particles are equivalent, and we have to divide by the number of these permutations. The same holds for the survived ones: thus

$$p_n(t|\mathbf{x}^0, N, L) = \frac{1}{n!}\frac{1}{(N-n)!} \sum_{\pi \in P_N} \prod_{j=0}^{n} S\left(t|x_{\pi(j)}^0, L\right) \prod_{j=n+1}^{N} \left(1 - S\left(t|x_{\pi(j)}^0, L\right)\right) \tag{3.3}$$

Given $p_n(t|\mathbf{x}^0, N, L)$, we can reconstruct $S_{n^*}(t|\mathbf{x}^0, N, L)$ for any n^*.
In the case of random initial conditions, (3.3) simplify to

$$p_n(t|N, L) = \binom{N}{n} S\left(t|L\right)^n \left(1 - S\left(t|L\right)\right)^{N-n} \tag{3.4}$$

because all the survival probabilities are equal, the result is a binomial distribution.
Given $S_{n^*}(t|\mathbf{x}^0, N, L)$, one can obtain interesting quantities as the mean emptying time (MET)

$$T_{n^*}(\mathbf{x}^0, N, L) = \int_0^\infty S_{n^*}(t|\mathbf{x}^0, N, L)dt \tag{3.5}$$

of easy experimental access.

3.2 Emptying process of a Single File Diffusion system

We now consider the emptying process of a Single File of diffusing particles. We face the problem by applying the Reflection Principle Method introduced in section 2.2.1. We start from the calculation of the probability of having all the N particles, started from a set of initial coordinates $\mathbf{x}^0$, inside [-$L/2$;$L/2$] at time t, $p_N(t|\mathbf{x}^0, N, L)$. This is an important quantity, that will be used in the other step of the reconstruction of the emptying process. The Reflection Principle gives us the probability distribution function of a SFD system with absorbing boundaries as permutation of the product of the single particle probability distribution function (see Eq. (2.2)). By definition, $p_N(t|\mathbf{x}^0, N, L)$ is given by

$$p_N(t|\mathbf{x}^0, N, L) = \int_A P(\mathbf{x}, t|\mathbf{x}^0) d\mathbf{x} = \prod_{k=1}^{N} p(x_{\pi(k)}, t|x_k^0) \tag{3.6}$$

inside the available sector A of the configurational space, given by $\{x_1 < x_2 < \ldots < x_N\}$. Notice that the exchange symmetry of the integrand allow us, for each term in the sum over all the possible permutations, to safely come back to $\prod_i p(x_i, t|x_i^0)$ by changing the available sector to

$$\{x_{\pi(1)} < x_{\pi(2)} < \ldots < x_{\pi(N)}\}$$

Figure 3.1 sketches the configurational space for a system of N=3 particles. The available sectors corresponding to three different permutations are enlightened with different colors; the others can be obtained by symmetry. The condition $x_{\pi(1)} < x_{\pi(2)} < x_{\pi(3)}$ imposed by the choice of a certain permutation of the indices automatically exclude all the others. By putting this section together, we actually eliminate the constraints and we integrate on the whole configurational space, giving

$$p_N(t|\mathbf{x}^0, N, L) = \int_C \prod_{k=1}^{N} p(x_k, t|x_k^0)\, d\mathbf{x} \tag{3.7}$$

which is equal to the product of the single particle survival probabilities, as in the non-interacting case. Again, to define $p_n(t|\mathbf{x}^0, N, L)$ we say that n particles

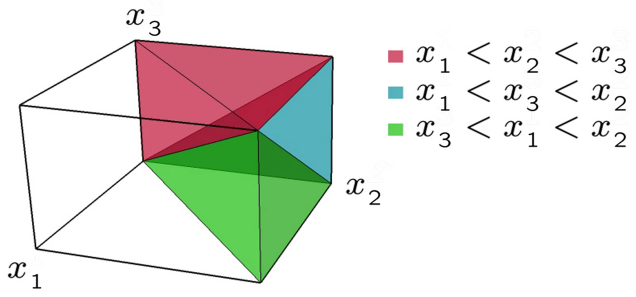

Figure 3.1: Available sectors for different permutations (red $x_1 < x_2 < x_3$, blue $x_1 < x_3 < x_2$, green $x_3 < x_1 < x_2$) of the coordinates in the configurational space for N=3 particles.

have a first passage time larger than t, while for $N-n$ ones the first passage time is smaller than t. Thanks to Eq. (3.7) we thus have

$$\begin{aligned} p_n(t|\mathbf{x}^0, N, L) &= \frac{1}{n!\,(N-n)!} \sum_{\pi \in P_N} \int_t^\infty dt_1 \cdots \int_t^\infty dt_n \\ &\quad \int_0^t dt_{n+1} \cdots \int_0^t dt_N \prod_{k=1}^{N} \left[-\frac{dS(t_k|x^0_{\pi(k)}), L}{dt_k} \right] \\ &= \frac{1}{n!\,(N-n)!} \sum_{\pi \in P_N} \prod_{k=1}^{n} S(t|x^0_{\pi(k)}, L) \prod_{k=n+1}^{N} [1 - S(t|x^0_{\pi(k)}, L)] \end{aligned} \tag{3.8}$$

where the combinatorial factors again arise as a consequence of the particle exchange symmetry, finding again the same result as in the non-interactive case. Notice that, in this case, the mapping is so powerful because we are not doing any average, and we can thus use the symmetry properties of the Reflection Principle Method solution.

We verified the above calculations with Brownian dynamics simulations (see Appendix A for details). We start with two examples of emptying process reconstructions, shown in Fig. 3.2. We distinguish between lattice (left panel) and random (right panel) initial conditions: in the former case, particles are equispaced in the interval [-L_0/2,L_0/2] with $L_0 = N/\rho_0$, ρ_0 being the number density;

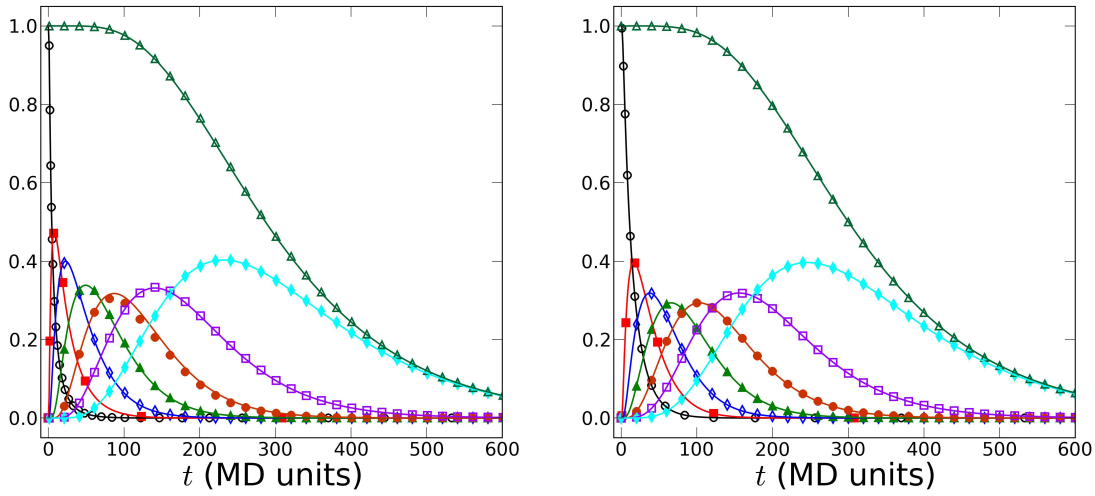

Figure 3.2: Examples of emptying process for Single File systems: $p_n(t|\mathbf{x}^0, N, L)$ (n=0 open circles, n=1 full squares, n=2 open diamonds, n=3 full triangles, n=4 full circles, n=5 open squares, n=6 full diamonds) and $S_1(t|\mathbf{x}^0, N, L)$ (open triangles). In both panels, symbols are data from numerical simulations, while lines are Eq. (3.4) or Eq. (3.1). Left panel: N=7 particles, initially equispaced particles with number density ρ_0=0.5, absorbing boundaries at $L = L_0 + 1$. (MD units). Right panel: N=7 particles, initially distributed with uniform probability in [-L_0,L_0], with number density ρ_0=0.5, absorbing boundaries at $L = L_0$ (MD units).

initial positions are thus given by the formula

$$x_i^0 = -L_0/2 + \frac{iL_0}{N-1}, \qquad i = 0..N-1.$$

We recall that, in order to take into account different initial conditions, we have to choose the correct initial condition for the single particle survival probability. Both panel show that each step of the emptying process is reconstructed correctly and, in particular, the probability of having at least one particle inside the region of interest well reproduces numerical data. Until the end of this Chapter, we will consider only random initial conditions, because usually is very difficult to find or realize equispaced initial conditions in an experimental setup.

The solution we have found is exact and contains all the information about this process; in principle, it is possible to calculate exactly the Mean Emptying time by integrating $S_1(t|N, L)$ over time. As a matter of fact, this remain a formal solution and does not give access at the trends of the MET. Among the parameters of the system, we choose to study, by means of numerical simulations, the dependence on the system size L and on the number of the particle N. These quantities, in an experimental realization, are reliably controlled and varied and hence prone

to be used to test the theoretical predictions.

Results are reported in Fig. 3.3. We start by looking at the dependence of the

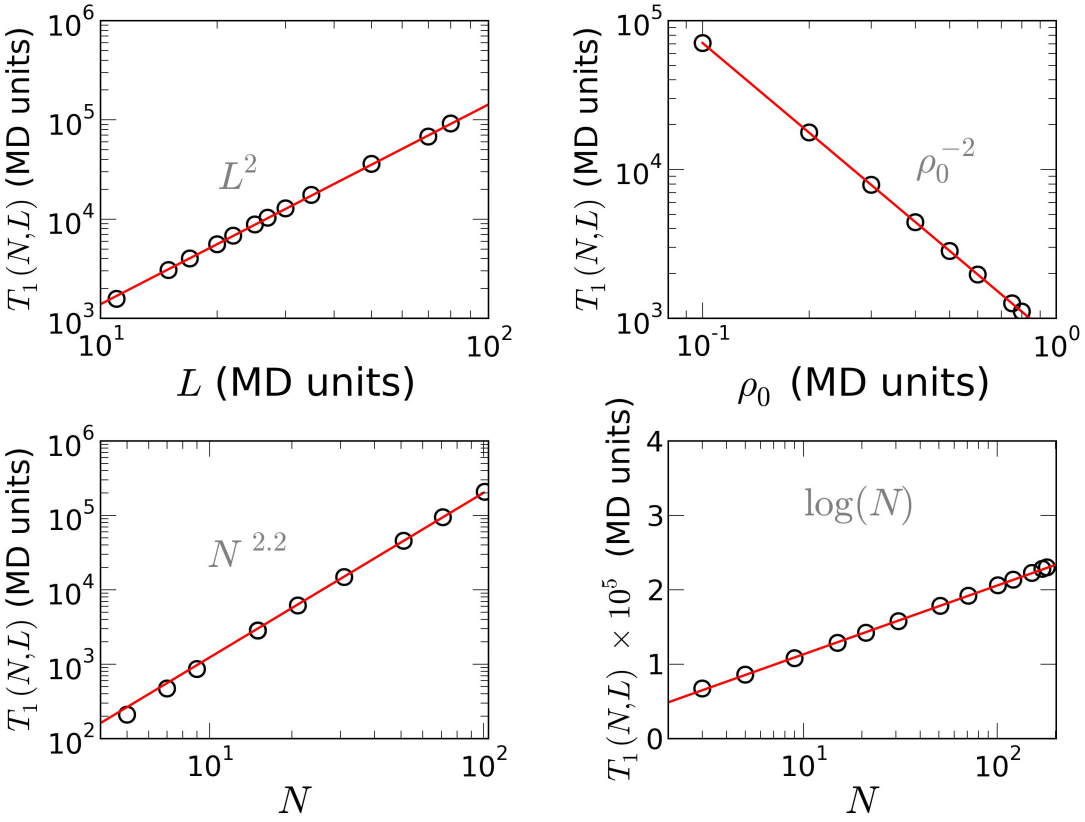

Figure 3.3: Mean Emptying Time for SFD systems. Open circles are data from numerical simulations, lines are the best fit; MD rescaled units are used. Top left panel: Log-log plot of the MET as function of L, N=15 and ρ_0=0.5 fixed; best fit with a power law L^2. Top right panel: Log-log plot of the MET as function of ρ_0, N=15 and $L = L_0$ fixed; best fit with a power law ${\rho_0}^{-2}$. Bottom left panel: Log-log plot of the MET as function of N, ρ_0=0.5 and $L = L_0$ fixed; best fit with a power law, $N^{2.2}$. Bottom Right panel: Semi-log plot of the MET as function of N, L=91 fixed; best fit with a logarithmic function.

MET on L (top left panel of Fig. 3.3). In this case the initial number of the particle is fixed, N=15, as well as the initial density $\rho_0 = 0.5$. The absorbing boundary are changed progressively farther apart, with $L = L_0 + \Delta L$. Data show a clear power-law behaviour as

$$T_1(N, L) \sim L^2 \tag{3.9}$$

reminiscent of the single particle trend; this is consistent with the mapping on a non-interacting system found applying the Reflection Principle.

As a further evidence of this trend, we looked at the MET of a system of N=15 particles with boundary condition fixed at $L = L_0$, varying the system size through the number density $\rho_0 = N/L_0$. Data reported in the top right panel of Fig. 3.3 again show a clear power-law behaviour as

$$T_1(N, L) \sim \rho_0^{-2} \sim L^2 \tag{3.10}$$

that confirm the result of Eq. (3.9).
Then we looked at the trend of $T_1(N, L)$ as function of N, for a system of size $L = L_0$ and fixed density ρ_0=0.5. Also in this case (see bottom left panel of Fig. 3.3) a power-law behaviour

$$T_1(N, L) \sim N^{2.2} \tag{3.11}$$

is observed. This nontrivial trend has to be considered carefully. In fact, by fixing the initial density while the number of particles directly leads to a progressive increase of the system size. A question thus arises: how much of the N^2 behaviour is caused by the increase in the system size?
To answer this question, we fixed the system size L=91 (MD units), and let the number density change with the initial number of particles. Results are reported in the bottom right panel of Fig. 3.3. Surprisingly, the N-dependence is very well reproduced by a logarithmic function, suggesting that nearly all the N^2 dependence observed before was an effect of the progressive increase of the system size. From this analysis emerges that the system size L is the parameter that most influences the Mean Emptying time, since, for a fixed size L, an increase of the number of particles, say from N_1 to N_2, increases MET of the order of $log(N_2/N_1)$.

3.2.1 Emptying process in presence of an external force

We now want to describe how the emptying process in affected by the presence of a constant external force F_e. The idea is to apply again the argument used in the previous section using the survival probability for a single forced Brownian particle as building block for our calculation (see Appendix D for a detailed calculation of this quantity). The application of solution derived above is in principle valid for any value of the external bias F_e. In fact, in the presence of a strong force, particles are dragged on one direction and, substantially, do not interact with each other. In all the other cases, the order is still preserved,

particles are equal and perform elastic collisions: thus the Reflection Principle Method is safely applicable and must lead to the correct result.

We validate this argument again by comparing the analytical findings with

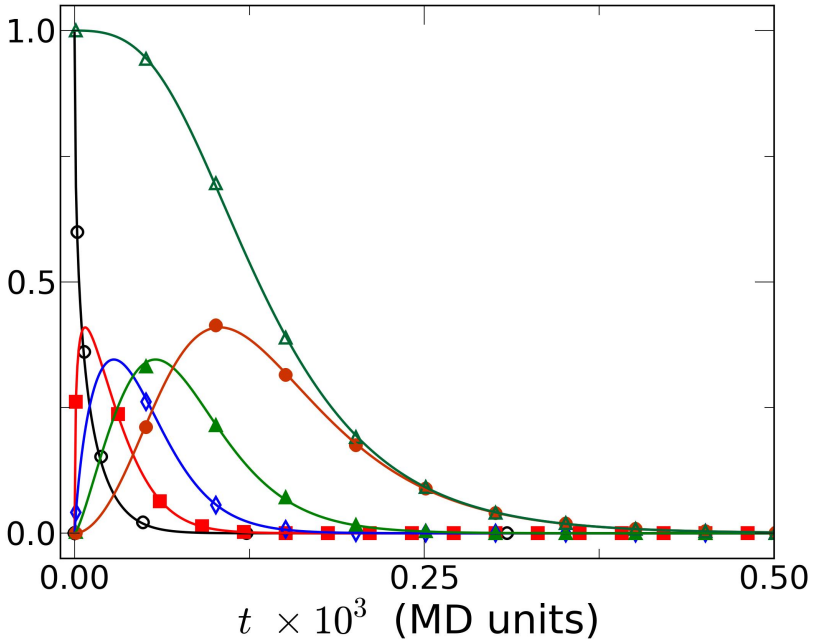

Figure 3.4: Example of emptying process for a Single File system in presence of a constant external force: $p_n(t|\mathbf{x}^0, N, L, F_e)$ (n=0 open circles, n=1 full squares, n=2 open diamonds, n=3 full triangles, n=4 full circles) and $S_1(t|\mathbf{x}^0, N, L, F_e)$ (open triangles). Symbols are data from numerical simulations, lines are Eq. (3.4) or Eq. (3.1) for a system of N=5 particles, initially distributed with uniform probability in [-L_0,L_0], with number density ρ_0=0.5, absorbing boundaries at $L = L_0$ and F_e=0.5 (MD units).

Brownian Dynamics simulations (see Appendix A for details). An example of such comparison is reported in Fig. 3.4. For simplicity, we limit ourselves to random initial conditions. To compute $S_1(t|\mathbf{x}^0, N, L, F_e)$, we have used Eq. (D.29) as building block; as one can see, the theory works nicely also in this case.

Notice that, also in this case, the solution we found is exact but does not give access at the MET trend. In analogy with the previous section we study, by means of numerical simulations, the Mean Emptying Time as function of L, N and F_e. Results are reported in Fig. 3.5. We start by focusing on the effect of the external force on the MET. Top left panel of Fig. 3.5 shows $T_1(N, L, F_e)$, normalized by $T_1(N, L, F_e = 0)$, as a function of F_e. Data show a single-particle like behaviour (shown in the left panel of Fig. D.1), characterized by a power law for $F_e R > k_B T$ as F_e^{-1}, following thus the single particle trend (see Appendix D).

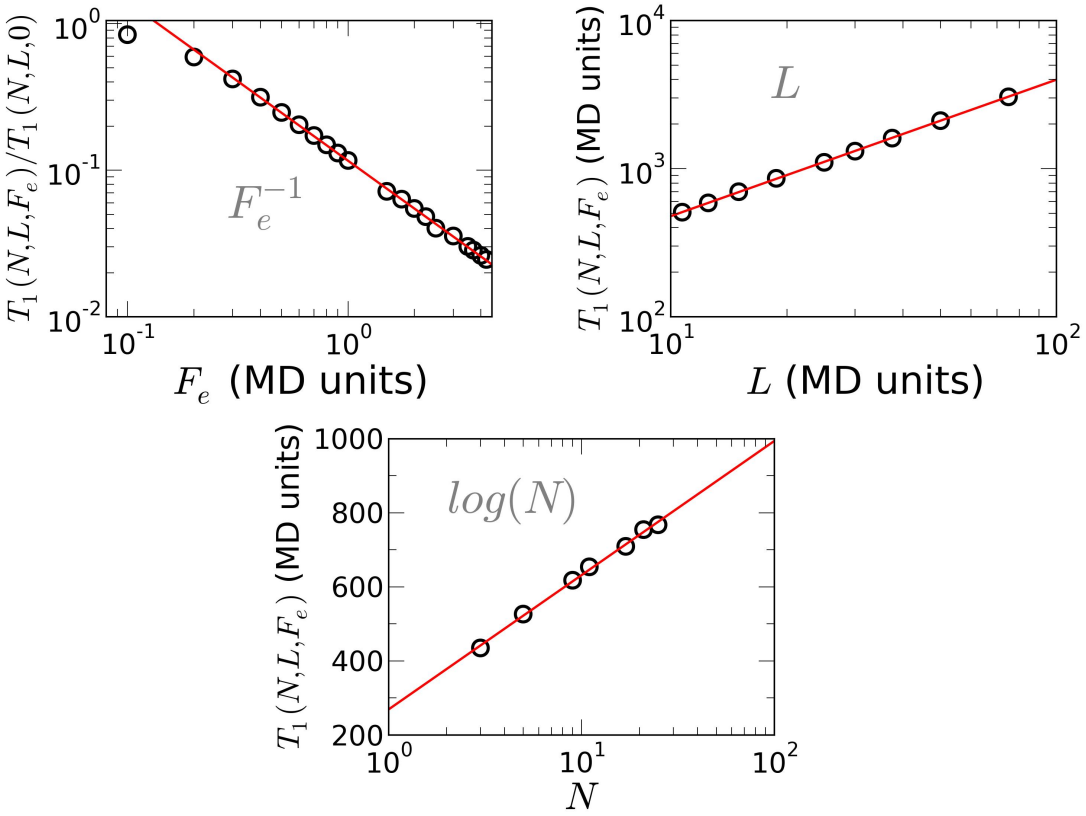

Figure 3.5: Mean Emptying Times for a SFD system in presence of an external force. Top left panel: Log-log plot of the mean emptying time, normalized over $T_1(N, L, F_e = 0)$, as function of F_e, for systems of N=15 particles, number density ρ_0=0.5, absorbing boundaries at $L = L_0$: open circles are data from numerical simulations, the line is the best fit with a power law F_e^{-1}. Top right panel: Log-log plot of the mean emptying time, as function of L, for systems of N=15 particles, number density ρ_0=0.5, F_e=0.5 (MD units): open circles are data from numerical simulations, the line is the best fit with a power law, $L^{0.71}$. Bottom panel: Semi-log plot of the mean emptying time as function of N, for systems with L=15 fixed, F_e=0.5 (MD units): open circles are data from numerical simulations, the line is the best fit with a logarithmic function.

We now look at the L-dependence of the MET, for a system of N=15 particles and F_e=0.5. Data are shown in the top right panel of Fig. 3.5: we observe a linear behaviour, as for the single particle.

Finally, we check the dependence of the MET from the initial number of particles N, for fixed L=15 and F_e=0.5 (MD units). Data are reported in the bottom panel of Fig. 3.5: as in the absence of external forces, also in this case the MET increases only logarithmically for increasing N.

3.3 Survival probability of a Tagged Particle

Another interesting problem that can be tackled within this framework is to focus on a given particle $\bar{x}$ (called *tagged*) and to study its survival probability as the emptying process goes on. We can start from the past section and, in that spirit, reconstruct the survival probability employing $p_n(t|\mathbf{x}^0, N, L, \bar{x} \in [-L/2, L/2])$, i.e. the probability of having exactly n particles inside [-$L/2$,$L/2$] at time t, at the condition that the selected particle is still inside the survival region. This quantity can be obtained with an equilibrium approach by weighting $p_n(t|\mathbf{x}^0, N, L)$ with the probability that, after N-n particles have come out, the selected particle is still inside [-$L/2$,$L/2$]:

$$p_n(t|\mathbf{x}^0, N, L, \bar{x} \in [-L/2, L/2]) = p(N-n|N, \bar{x} \in [-L/2; L/2]) \cdot p_n(t|\mathbf{x}^0, N, L) \tag{3.12}$$

This implies, as in the reconstruction of the emptying process

$$S_{\bar{x}}(t|\mathbf{x}^0, N, L) = \sum_{n=1}^{N} p(N-n|N, \bar{x} \in [-L/2; L/2]) \cdot p_n(t|\mathbf{x}^0, N, L) \tag{3.13}$$

In order to calculate $p(N-n|N, \bar{x} \in [-L/2; L/2])$, we have to take into account the Single File properties of the system, and in particular the exit sequences, i.e. the sequence of the particles' labels, ordered according to their exit times. For a non-interacting system, the set of these sequences would be the whole set of permutations of the labels, since particles can exchange their order and do not have a specific exit rule. In a Single File, however, order must be preserved and this impose a strict constraint on the exit sequences. Having two possible exits, the possible sequences are not trivial, but they can be enumerated by the following rule: a particle can exit if either all the particles to its left or to its right are already out, otherwise the exit is blocked. In Fig. 3.6 all the possible configuration in the case $N = 5$ are shown. The first index must be one of the outer particle (1 or N); then, at each step, follow a bifurcation accounting for the two possible outer indexes. The total number of possible states is 2^{N-1}, as the last index follows from the preceding ones by exclusion. To calculate $p(N-n|N, \bar{x} \in [-L/2; L/2])$ we have just to count the combinations which satisfy the requirement that the selected particle label has not appeared up to $N-n$-th number. Such a calculation

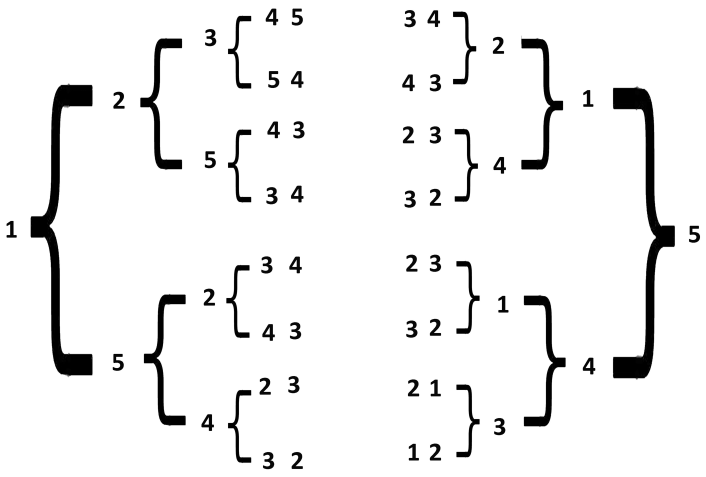

Figure 3.6: Scheme for allowed exit sequences in a Single File system for N =5

is exact and does not depend on any parameter except the particle number N. In the case of equispaced initial conditions, L must be sufficiently large to ensure the validity of Eq. (3.12).

We verified the above calculation with Brownian Dynamics simulations (see Appendix A for details), by focusing on the central particle $\bar{x} = x_c$. As in section 3.2, we start with two examples of survival probability, shown in Fig. 3.7. We distinguish again between equispaced (left panel) and random (right panel) initial conditions. Both panel show that analytical theory matches correctly the numerical data. In the following, we will consider again only random initial conditions, for the same reasons introduced in section 3.2, but also because they provide an equilibrium initial condition, that automatically satisfy the equilibrium assumption underlying Eq. (3.12).

Now we proceed as in section 3.2: also in this case the solution we have found is exact, but does not reveal the trend properties of the MFPT. We thus study the trend of the Mean First Passage Time of the central particle $T_1^{x_c}(N, L)$ numerically, as function of the system size L and of the number of the particle N. In fact,

Results are reported in Fig. 3.8.

We start by looking at the dependence of $T_1^{x_c}(N, L)$ on L (top left panel of Fig. 3.8). As in section 3.2, we have fixed N=13, $\rho_0 = 0.5$, and moved the absorbing boundary progressively farther away, $L = L_0 + \Delta L$. Data show a clear power-law

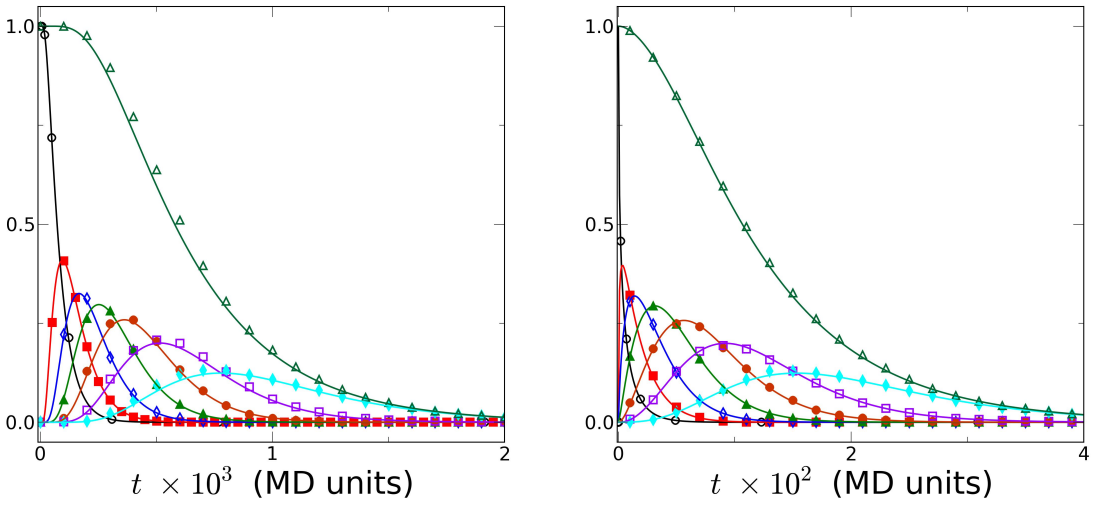

Figure 3.7: Examples of Tagged Particle survival probability: $p_n(t|\mathbf{x}^0, N, L, x_c \in [-L/2, L/2])$ (n=0 open circles, n=1 full squares, n=2 open diamonds, n=3 full triangles, n=4 full circles, n=5 open squares, n=6 full diamonds) and $S_{x_c}(t|\mathbf{x_0}, N, L)$ (open triangles). In both panels, symbols are data from numerical simulations, while lines are Eq. (3.12) or Eq. (3.13). Left panel: N=7 particles, initially equispaced with number density ρ_0=0.5, absorbing boundaries at $L = L_0 + 1$. (MD units). Right panel: N=7 particles, initially distributed with uniform probability in [-L_0/2,L_0/2], with number density ρ_0=0.5, absorbing boundaries at $L = L_0$ (MD units).

behaviour

$$T_1^{x_c}(N, L) \sim L^2 \tag{3.14}$$

as in the case of the emptying process.

As further evidence of this trend, we look at $T_1^{x_c}$ for a system of N=13 particles with boundary condition fixed at $L = L_0$, varying the system size through the number density ρ_0. The results reported in the top right panel of 3.8 show a again a power-law behaviour

$$T_1^{x_c}(N, L) \sim \rho_0^{-2} \sim L^2 \tag{3.15}$$

confirming the result of Eq. (3.14).

Then we looked at the trend of the MFPT as function of N, for a system of size $L = L_0$ and fixed density ρ_0=0.5. The results reported in the bottom left panel of Fig. 3.8 show a power-law behaviour

$$T_1^{x_c}(N, L) \sim N^{2.2} \tag{3.16}$$

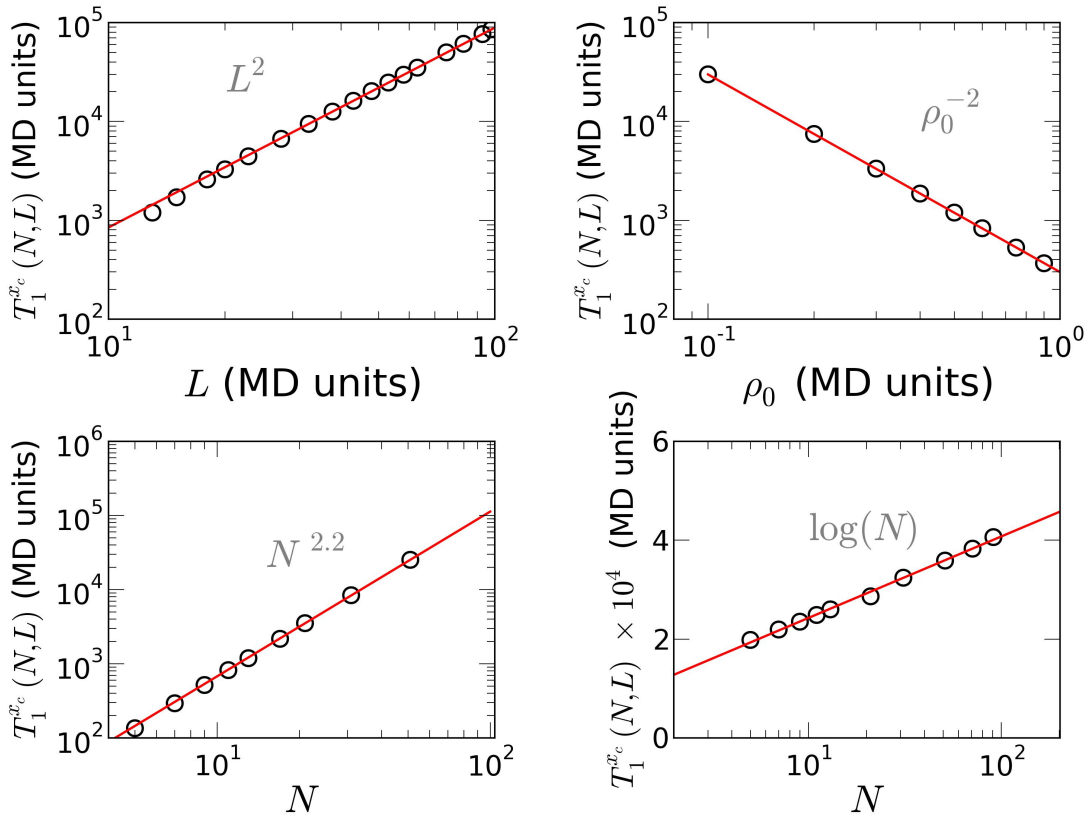

Figure 3.8: Mean First Passage Time of the central particle in SFD systems. Open circles are data from numerical simulations, lines are the best fit; MD rescaled units are used. Top left panel: log-log plot of the MFPT as function of L, N=13 and ρ_0=0.5 fixed; best fit with a power law L^2. Top right panel: log-log plot of the MFPT as function of ρ_0, N=13 and $L = L_0$ fixed; best fit with a power law ${\rho_0}^{-2}$. Bottom left panel: log-log plot of the MFPT as function of N, ρ_0=0.5 and $L = L_0$ fixed; best fit with a power law $N^{2.2}$. Bottom Right panel: log-lin plot of the MFPT as function of N, L=91 fixed; best fit with a logarithmic function.

We then checked again how much of this behaviour is caused by the increase in the system size, by fixing L=91 (MD units). Results are reported in bottom right panel of Fig. 3.8. The dependence on N is again very well reproduced by a logarithmic function. This kind of analysis shows that, although quantitatively different, $T_1(N, L)$ and $T_1^{x_c}(N, L)$ share the same trend with L and N. Essentially, the exit event of any TP takes place during the progressive emptying of the system and thus the characteristic timescales of the former process are dictated by the timescales of the latter.

3.3.1 Survival probability of a Tagged Particle in presence of an external force

In order to reconstruct the survival probability of a Tagged Particle inside a Single File system in the presence of a constant external force, we can adapt the argument used in the unbiased case, by noticing that now the exit sequences are not all equiprobable, but some of them are more likely to occur. For example, if the external force is positive $F_e > 0$, the sequence

$$5 \quad 4 \quad 3 \quad 2 \quad 1 \tag{3.17}$$

is favorite since particles exit by following the direction of the force. Moreover, by making F_e very high, eventually (3.17) becomes the only possible exit sequence. The idea to quantify the effect of the bias is to properly weight each of the old weights $p(N-n|N, \bar{x} \in [-L/2; L/2])$ with a Boltzmann-like factor $\exp(F_e L/2k_B T) = \exp(\Gamma L)$. The choice of this particular factor is dictated by two observations:

1. greater the force, greater is its influence on the exit sequence (in the strong force limit we have only one possible sequence)

2. greater is the system size L, longer the force can act and, thus, greater are its effects

To correctly weight each sequence, we define as a "*correct exit*" the event of a particle exiting at the correct absorbing boundary, i.e. the right one if $F_e > 0$ or the left one if $F_e < 0$; otherwise we have a "*wrong exit*". Within a sequence, we weight a correct exit with a factor $\exp(\Gamma L)$ and a wrong exit with a factor $\exp(-\Gamma L)$. We can uniquely identify them thanks to the Single File condition, as the exit side is determined by the sequence itself. Taking as example, for $F_e > 0$, the temporal sequence of exit events of N=5 particles

$$1 \quad 2 \quad 5 \quad 4 \quad 3$$

where the number refer the particle label. We identify the exit of particles 1 and 2 as wrong exits: in fact, they are obliged to leave the system from the left boundary, as the other is blocked by particle 3,4 and 5. On the other hand the following

two are correct exits, as particles 4 and 5 exit from the right boundary. The last particle is, by definition, alone; the last exit event should not be weighted as the exit side is not uniquely defined, having lost order preservation. If we weight each sequence in this way and than we proceed as in the unbiased case, we obtain the survival probability of a Tagged Particle in a SF in the presence of a constant external force.

We validate these calculations by comparing them with Brownian Dynamics

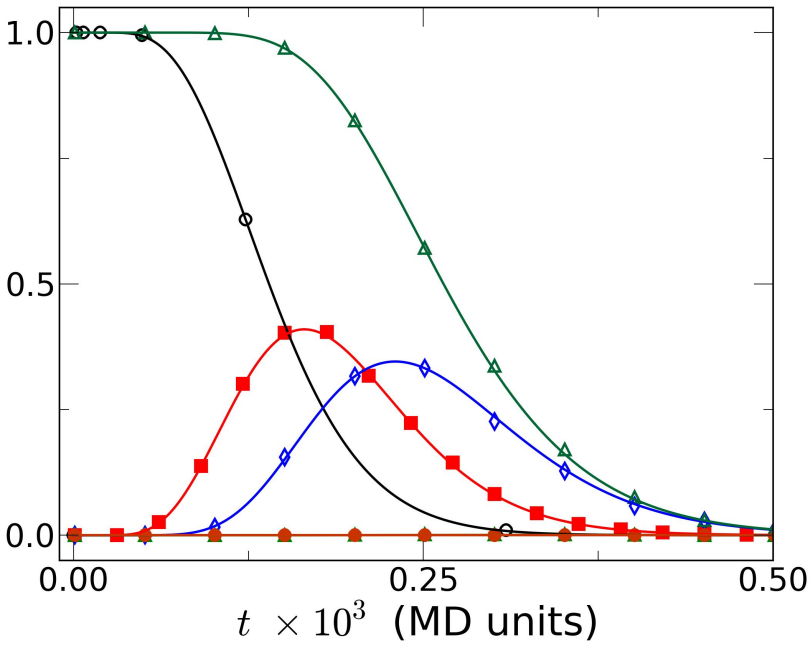

Figure 3.9: Example of Tagged Particle survival probability in presence of an external force: $p_n(t|\mathbf{x}^0, N, L, F_e, x_c \in [-L/2, L/2])$ (n=0 open circles, n=1 full squares, n=2 open diamonds, n=3 full triangles, n=4 full circles) and $S_{x_c}(t|\mathbf{x_0}, N, L, F_e)$ (open triangles). Symbols are data from numerical simulations, while lines are Eq. (3.12) or Eq. (3.13) for a system of N=5 particles, initially distributed with uniform probability in [-L_0/2,L_0/2], with number density ρ_0=0.5, absorbing boundaries at $L = L_0$+20 and F_e=0.5 (MD units).

simulations (see Fig. 3.4). Also in this case, for simplicity, we limit ourselves to random initial conditions. The approximated method we devised works nicely; in particular, the Boltzmann-like weight is able to reproduce the fact that the central particle always exits as third.

Following the previous sections, we study the Mean First Passage Time, as function of L, N and F_e. Results are reported in Fig. 3.10. We start by focusing on the effect of the external force. Top left panel of Fig. 3.10 shows $T_1^{x_c}(N, L, F_e)$, normalized with $T_1^{x_c}(N, L, F_e = 0)$, as a function of F_e. Data, as in the single

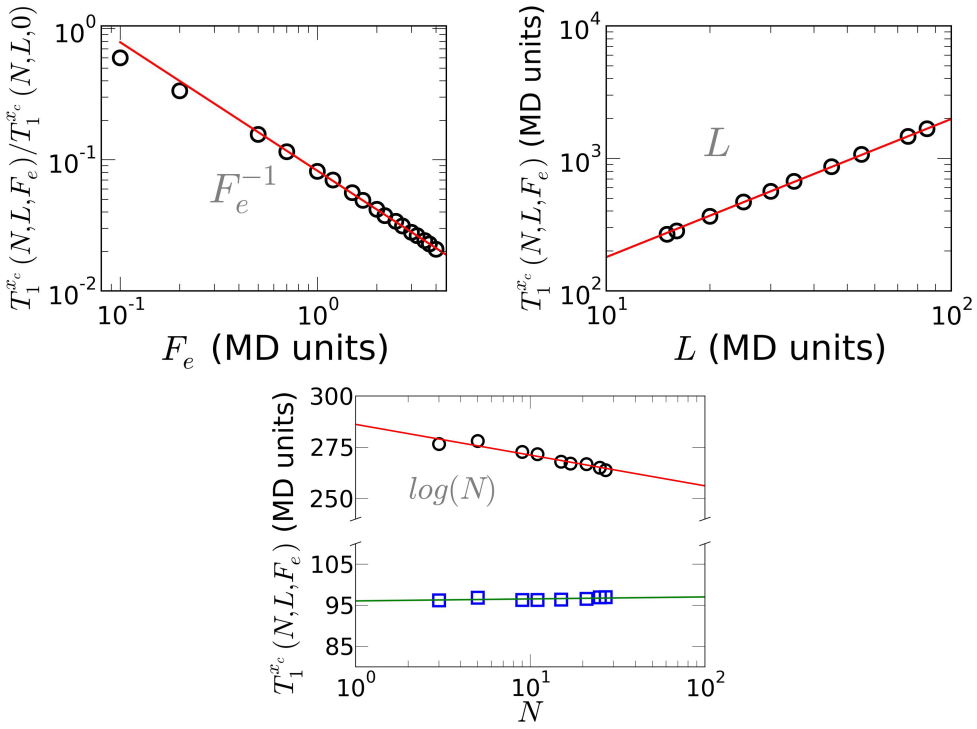

Figure 3.10: Mean First Passage Times for the central particle in SFD, in presence of an external force. Top left panel: Semi-log plot of the MFPT, normalized over $T_1^{x_c}(N, L, F_e = 0)$, as function of F_e, for systems of N=15 particles, number density ρ_0=0.5, absorbing boundaries at $L = L_0$: open circles are data from numerical simulations, line is the best fit with a power law F_e^{-1}. Top right panel: Log-log plot of the MFPT, as function of L, for systems of N=15 particles, number density ρ_0=0.5, F_e=0.5 (MD units): open circles are data from numerical simulations, the line is the best fit with a power law L^1. Bottom panel: Log-log plot of the mean emptying time as function of N, for systems with L=15 fixed, F_e=0.5 (open circles) or F_e=1.5 (blue squares) (MD units): symbols are data from numerical simulations, lines are best fits with a logarithmic function.

particle case, show a power law behaviour as F_e^{-1} for $F_e R > k_B T$ (see Appendix D).

We look now at the dependence of the MET on the system size L, for a system of N=15 particles and F_e=0.5. Data are shown in top right panel of Fig. 3.10: we see again a linear behaviour.

Finally, we check the dependence of the MET from the initial number of particles N, first focusing on the open circles in the bottom panel of Fig. 3.10, referring to L=15 and F_e=0.5 (MD units). As before, data nicely follow a logarithmic function, but in this case, surprisingly, the MFPT decreases for increasing N. This is due to cooperative effects at high densities and intermediate values of F_e:

particles push each other under the action of the external force, contributing to the net movement in one direction. As the channel empties, this effect becomes less and less important; that's why, in the case of the MET, we did not saw it. This is confirmed by the other set of data, L=15 and F_e=1. (open squares), in which we have chosen a greater value of the external force. Now the MFPT shows a fairly constant trend as function of N, because particles are dragged away and do not appreciably interact, thus avoiding cooperative effects.

3.4 Exit-side probabilities

We now want to address to the problem of the exit-side probability in a SFD system, i.e. compute the probability that a given particle will exit on the left or on the right side. To obtain the correct result, we cannot use straightforward calculations, like Eq. (D.31), but we have to look again at the actual exit sequences, as in section 3.3. The general rule is the same: a particle can exit if all the particles on the left or on the right are already exited, otherwise the exit is blocked. We compute the probability by counting for each particle and for each exit the number of occurrences. This has to be applied to all the particles, excepting the last one in each sequence. The last one is a free particle: we must use the hitting probability of a free Brownian particle (D.32), with the appropriate initial condition.

We validated this argument using Brownian Dynamic simulations. Results are reported in Fig. 3.11: left panel shows a comparison between numerical data and the method just described for the left exit-side probability as function of the particle index. As visible, the enumeration of the exit sequences gives the correct result. On the right panel of Fig. 3.11 we show that, apart from finite size effect in very small systems, this quantity is very robust, and it is quite insensitive of initial conditions, system size and, under proper rescaling, initial number of particles.

On the other hand this quantity gives typically too much information: especially from an experimental point of view, an interesting quantity is the fraction of particles on one side

$$\phi = \frac{\sum_k P_L(k)}{N} \tag{3.18}$$

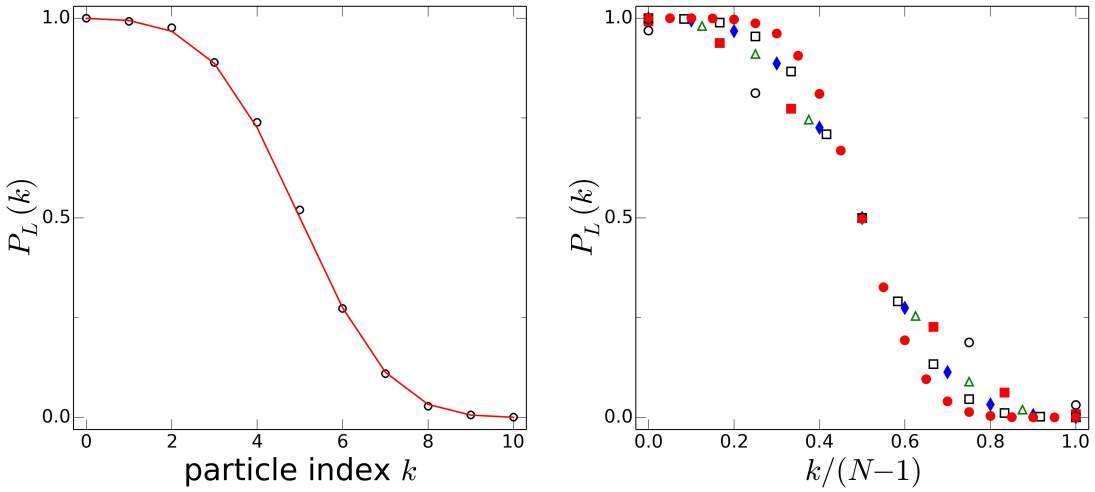

Figure 3.11: Left panel: left exit-side probability as function of the particle index k for a system of N=11 particles. Circles are data from numerical simulations, line is the theoretical reconstruction described in this section. Right panel: left exit-side probability as function of the particle index k, normalized over particle initial number N -1, for systems with different initial particles number: open circles N=5, full squares N=7, open squares N=9, open triangles N=11, full circles N=21.

which is, in the absence of an external force, always equal to $1/2$ for symmetry. If a constant force $F_e > 0$ acts over all the particles this symmetry is broken. We can adapt the previous argument by correctly weighting each sequence, as in section 3.3.1. We have to exclude again the *N-1*-th particle because the exit side is not uniquely defined. The last particle will be a free forced Brownian particle, started from x_0. Thus, the hitting probability will be given by Eq. (D.33), with the appropriate initial condition.

We validate the above argument with Brownian Dynamic simulations; results are reported in Fig. 3.12. Now, the interesting quantity is given by the unbalance between the fraction of particles exiting on the two sides

$$J_{LR} = \frac{\sum_k P_R(k) - \sum_k P_L(k)}{N} \tag{3.19}$$

or, equivalently, by the fraction of 'upstreaming' particles

$$\phi_{F_e} = 1 - J_{LR} = 2\frac{\sum_k P_L(k)}{N} = 2\frac{\langle N_{F_e} \rangle}{N} \tag{3.20}$$

where $< N_{F_e} >$ is the average number of particles exiting on the left. For particles whose transport properties are dominated by F_e, $\phi_{F_e} \simeq 0$, whereas for particles

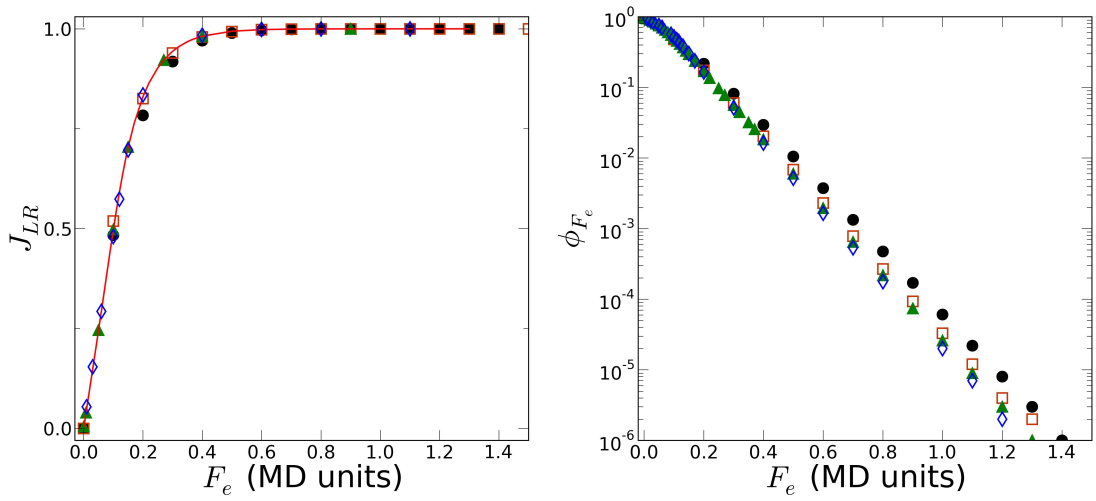

Figure 3.12: Left panel: total flux of particles to the right end as function of the external force F_e, for different values of initial particles number: full circles N=5, open squares N=9, full triangles N=11, open diamonds N=13; line is the theoretical reconstruction described in this section. Right panel: fraction of upstreaming particles as function of F_e, for different values of initial particles number (symbols as in left panel).

less influenced by the external force, $\phi_{F_e} \simeq 1$. The left side of Fig. 3.12 shows J_{LR} as function of F_e for a fixed value of the system size L and different values of N: data are very well reproduced by our method and clearly show that the unbalance is independent on N. On the right panel, ϕ_{F_e} reveal an exponential behaviour as function of F_e, i.e. the fraction of 'upstreamers' decreases exponentially almost independently from the initial particles number N.

3.5 Real *vs* point particles

All the result we have reported so far, refer to the case of a SFD of point particles. We also tried to extend the results derived above to object with a characteristic size σ, in our case the diameter, interacting through a truncated shifted Lennard-Jones potential (see Appendix A). In order to take into account the excluded volume during the calculation of the single-particle survival probability $S(t|x^0)$, we have to reduce the survival region by subtracting $N\sigma/2$ from each end

$$L^* = L - N\sigma/2$$

and, for initial positions on a lattice, rescale initial positions as

$$L_0^* = L_0 - (N-1)\sigma/2$$

before integrating $p(x,t|x_0)$. The rescaled probability density is

$$p(x_i,t|x_0) = \frac{2}{(b_2-b_1-N\sigma)}\sum_{n=1}^{\infty}\sin\left(\frac{n\pi(x-b_1-N\sigma/2)}{b_2-b_1-N\sigma}\right) \sin\left(\frac{n\pi(x_{i,0}^*-b_1-N\sigma/2)}{b_2-b_1-N\sigma}\right)e^{-\frac{D_t n^2\pi^2 t}{(b_2-b_1-N\sigma)^2}} \quad (3.21)$$

where $x_{i,0}^*$ are the new initial positions, obtained by rescaling the initial box and applying the corresponding rules for the rescaled lengths

$$x_{i,0}^* = -L_0^*/2 + \frac{L_0^* i}{N-1} = x_{i,0} - (i - \frac{N-1}{2})\sigma \quad (3.22)$$

With this scaling, the spatial integral becomes

$$\int_{b_1+N\sigma/2}^{b_2-N\sigma/2}\sin\left(\frac{n\pi(x-b_1-N\sigma/2)}{b_2-b_1-N\sigma}\right) = \frac{b_2-b_1-N\sigma}{n\pi}(1-cos(n\pi))$$

which leads to

$$S(t|x_{i,0}) = \frac{4}{\pi}\sum_{n=0}^{\infty}\frac{\sin\left(\frac{(2n+1)\pi(x_{i,0}^*-b_1-N\sigma/2)}{b_2-b_1-N\sigma}\right)e^{-\frac{D_t(2n+1)^2\pi^2 t}{(b_2-b_1-N\sigma)^2}}}{(2n+1)} \quad (3.23)$$

The total probability for a SFD is again given by

$$S_N(t|N,L,\mathbf{x}_0) = \prod_{i=1}^{N} S(t|L-N\sigma,x_{i,0}) \quad (3.24)$$

Unfortunately this first step is also the last in which this rescaling works. Probably, to proceed into the reconstruction of the emptying process, we must take into account some details of the interaction between particles.
However, we validated the above rescaling with Brownian Dynamics simulations, described in details in Appendix A. Figure 3.13 report several examples of comparison between numerical data and Eq. (3.24), limited to equispaced initial conditions, for different values of N (top left panel), ρ_0 (top right panel) and L

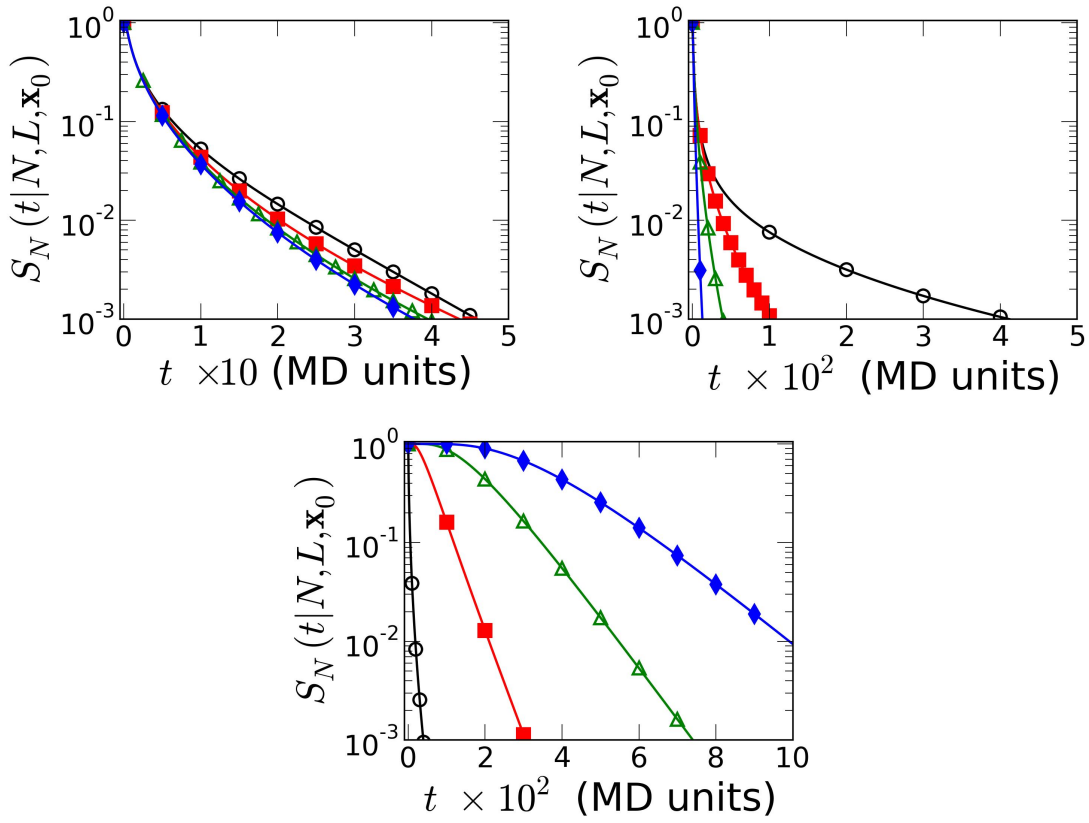

Figure 3.13: $S_N(t|N,L,\mathbf{x}_0)$ for SF systems of particles with a characteristic diameter σ=1; MD units are used. In each panel, symbols are data from numerical simulations, lines are Eq. (3.24); initial condition are equispaced in [-L_0/2,L_0/2] and scaled using Eq. (3.22). Top left panel: initial density ρ_0=0.5, absorbing boundaries at $L = L_0 + 2\sigma$ and different initial number of particles: open circles N=5, full squares N=9, open triangles N=11, full diamonds N=21. Top right panel: N=15 particles, absorbing boundaries at $L = L_0 + 2\sigma$ and different values of the initial density ρ_0: open circles ρ_0=0.1, full squares ρ_0=0.3, open triangles ρ_0=0.5, full diamonds ρ_0=0.75. Bottom panel: N=15, initial density ρ_0=0.5 and different positions of the absorbing boundaries: open circles L=16σ, full squares L=20σ, open triangles L=25σ, full diamonds L=30σ.

(bottom panel). In each case the analytical solution Eq. (3.24) very well reproduces numerical data.

3.6 Emptying process of colloids in microfluidic channels

We show in this section an experimental measurement of the survival probability of N=3 colloidal particles confined in microfluidic sub-micrometric channels, carrying out a comparison between numerical simulations and experimental data. Although the measure is conceptually simple, the realization of the SF conditions and the accurate control of the initial conditions are extremely challenging tasks. Details of the experimental setup, sample preparation and acquisition procedures can be found in Appendix B and in [161, 162].

Briefly, the chip is a polydimethylsiloxane (PDMS) chamber, made of two reservoirs separated by a PDMS barrier and connected via a set of eight central sub-micrometric channels (length 5 μm), plus two lateral channels (width 100 μm, height 16 μm) to facilitate hydrostatic pressure equilibration between the reservoirs. The whole system is filled with a 500 nm polystyrene particles suspension, dispersed in a 5 mM KCl water solution. The potassium chloride is needed for screening electrostatic interactions and ensure hard sphere interactions between the particles. A snapshot of the system is visible in Fig. 3.14. Holographic optical tweezers [162] are used to move particles inside the channels: once a sufficient number of colloids (from 3 to 6) is trapped inside the channel, particles are

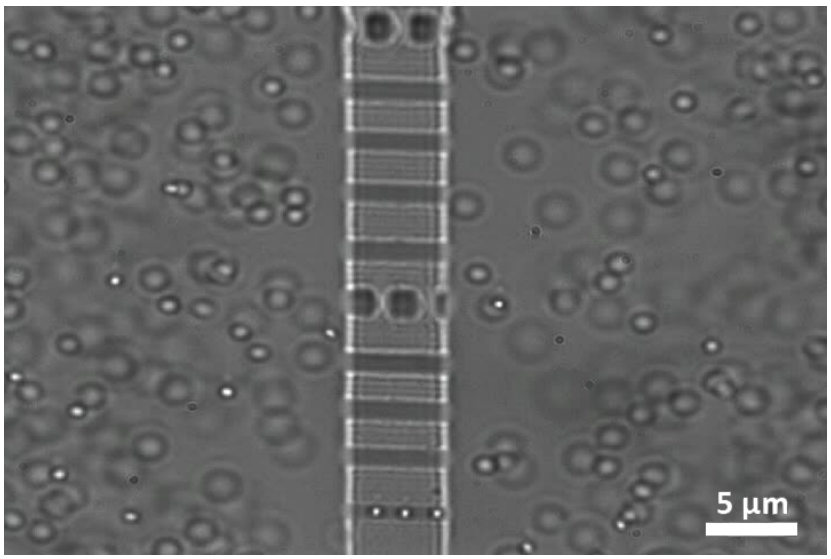

Figure 3.14: Snapshot of the PDMS sub-micrometric channels.

released and start to diffuse. We record the trajectories of the particles in the eight SF channels within the field of view of a a 100x oil immersion objective (UPLSAPO, Olympus) using a CCD camera (The Imaging Source DMK31BF03), until the last particle leave the channel. Nearly 250 different realizations have been recorded. To reconstruct the trajectories of the diffusive particles, a custom-made IDL (Interactive Data Language) program [163] has been used (see Appendix B for details). An example of the recorded trajectories is reported in Fig. 3.15

We are interested in the emptying times τ, i.e. the smaller time at which the

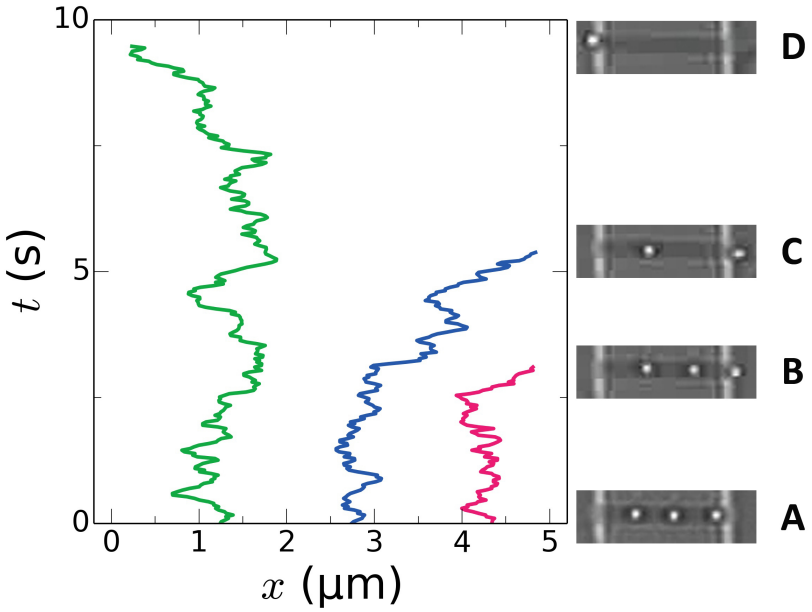

Figure 3.15: Trajectories of the 3 colloidal particles inside the channel at the initial time, extracted from experimental images using IDL tracking routines [163]. As example of the tracking success, we report A: Initial configuration. B-C-D: Exit events of the three particles. Notice that both the exit sides and the particle positions are correctly reconstructed.

channel is completely empty, to compute the survival probability as

$$S(t|L) = \mathrm{Prob}\Big\{\tau > t|L\Big\} \tag{3.25}$$

i.e. we want the probability that the channel is not empty at time t. In order to compare numerical and experimental data, we need to discuss some experimental subtleties. First, the eight sub-micrometric channels have slightly different widths. Though particles are always in Single File, the interactions with the walls are each time different and particles diffusion coefficient change in a non-

trivial way. Thus, to compare the different data sets, we have to rescale the emptying times properly.

Second, between the two macroscopic reservoirs the hydrostatic pressure (acting in our case from left to right) persist for several days after the sample has been sealed, due to the filling procedure. Measurements have been carried out before the equilibration time; thus a preliminary check on the presence of this bias has been done. From the analyzed trajectories, we computed, for each channel, the exit-side probability. Under the assumption that the effect of the bias is the same for each channel, the resulting fraction of particles exiting on the left side is $\phi_{F_e} \simeq 0.56$. By looking at Fig. 3.12, we estimated an equivalent external force $F_e = 0.09$ (MD units).

Finally, to perform a comparison between numerical and experimental data, we

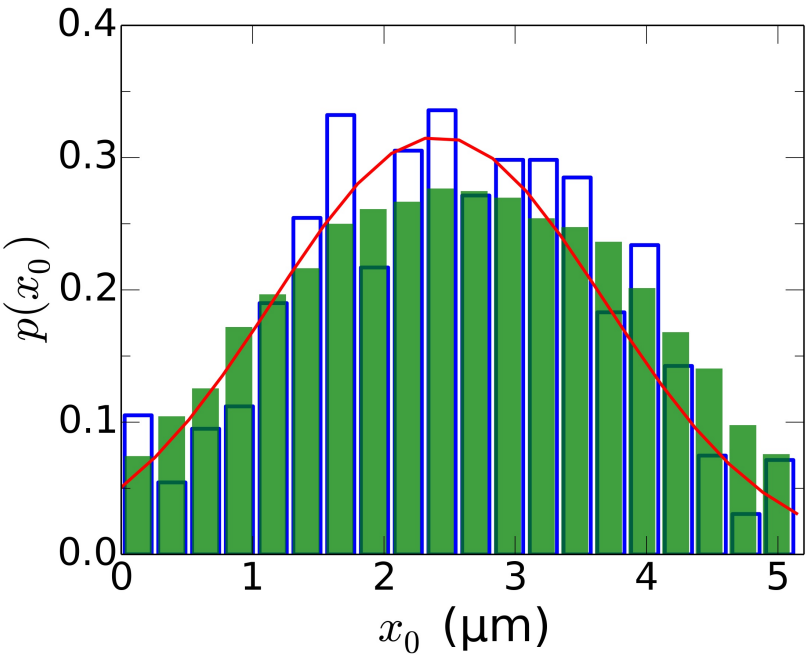

Figure 3.16: Distribution of the initial position of the particles inside the channel: empty bars refer to experimental data, line is a Gaussian fit, full bars refer to numerical data, obtained through a specific Monte Carlo scheme described in the text.

checked the distribution of the initial conditions over all the different data sets. The result is reported in Fig. 3.16: empty bars refer to experimental data. It is definitely evident that particles are not uniformly distributed along the channel, at variance with what happens in numerical simulations. The distribution shown in Fig. 3.16 rather reproduced by a Gaussian, peaked in the center of the channel

with a standard deviation $\sigma \approx L/4$ (red line in Fig. 3.16); outside of the channel, the distribution drop to zero. To perform a reliable comparison between numerical and experimental data, we have to reproduce this initial distribution in our Brownian Dynamics simulations: this mapping can be obtained using a Monte Carlo scheme, in which we draw initial positions from a Gaussian distribution with the same features of the one measured from experimental data, ensuring at the same time the excluded volume and rejecting any condition outside of the boundaries. The corresponding distribution is also reported in Fig. 3.16 (filled bars).

As anticipated, to compare data from different channels with numerical simu-

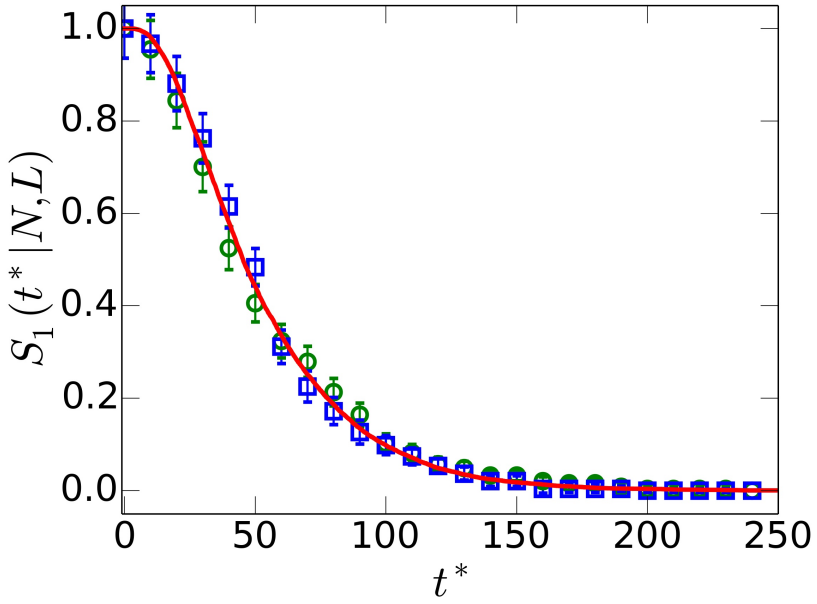

Figure 3.17: Emptying process of N=3 particles in a L=5 μm channel as function of rescaled time t^*, $t^* = D_k\, t/R^2$ (open circles and line), $t^* = T_1{}^{(num)}\, t/T_1^k$ (open squares). Symbols refer to experimental data, line refer to numerical data.

lations, we need to rescale the emptying times properly. We found two possible ways to achieve this goal. The first way is to perform the following rescalement

$$t \to t' = \frac{D_k\, t}{R^2} \tag{3.26}$$

where D_k is the diffusion coefficient of a single colloidal particle in the channel k. Notice that t' is adimensional: thus the comparison with numerical data is straightforward. The diffusion coefficient, for each channel, can be extracted by

measuring the Mean Square Displacement of a single Brownian particle. From each set of data, we isolated the time window in which the last particle is alone. The estimated diffusion coefficients are in the range 0.07-0.25 μm^2, smaller than the theoretical diffusion coefficient for a 500 nm colloid, D=0.35 μm^2. Due to limited statistics these estimates are quite rough; thus an alternative method was devised.

The second method works as follow: first, we compute the numerical Mean Emptying Time, ${T_1}^{(num)}$, using the adimensional variable $t' = {D}_{(num)}\, t/{R^2}_{(num)}$. Then, for each data set, we compute the Mean Emptying Time T_1^k, in seconds, and we then rescale time as

$$t \to t'' = \frac{{T_1}^{(num)}}{T_1^k}\, t \tag{3.27}$$

obtaining again an adimensional quantity, as ${T_1}^{(num)}$ is adimensional. This method is more reliable, because ${T_1}^{(num)}$ can be calculated with very high accuracy, as the limit is set only by the machine precision, and a good estimate of T_1^k can be obtained also from a limited set of data.

Results are reported in Fig. 3.17: circles refer to the first rescalement procedure, squares to the second, while the line are numerical data, realized employing the Lennard-Jones potential (see Appendix A). We see that both give compatible results; moreover, we also see that numerical data superimpose on the experimental points remarkably well.

Following the same procedure and using the same data, we also reconstructed the survival probability of the central particle. Results are reported in Fig. 3.18. Even in this case, we still appreciate that the two rescalement methods (circles for Eq. 3.26, squares for Eq. 3.27) give compatible results; numerical simulations (full line) are in quite good agreement with the experimental data. These data are a strong proof that a simple description in terms of diffusing particles with hard-core interaction is sufficient to account for the emptying process of a system of colloids in Single File, without taking into account hydrodynamic interactions explicitly. The consistent variation of the diffusion coefficient observed in channels of different width can be effectively ascribed to hydrodynamic interactions with the PDMS walls, but once this has been taken into account, hydrodynamic interactions are no further needed.

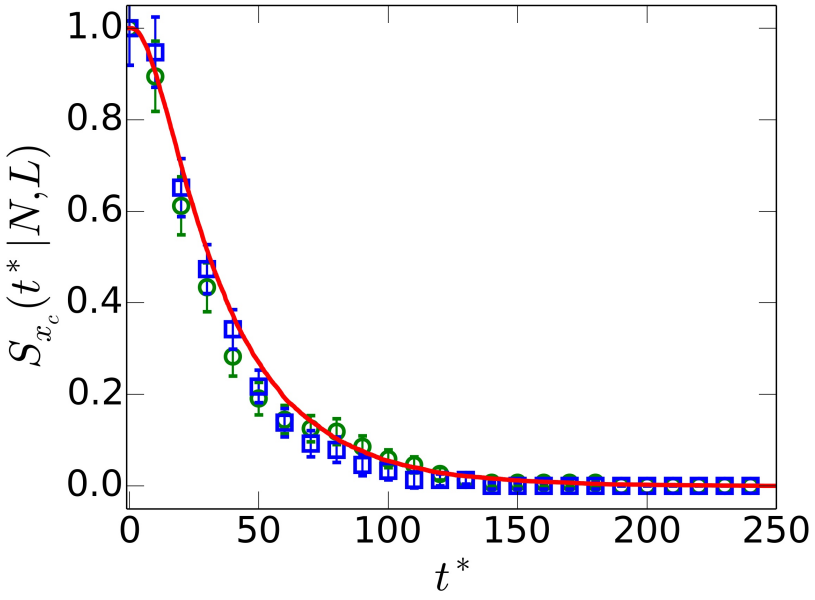

Figure 3.18: Survival probability of the central particle in SF system of N=3 particles in a L=5 μm channel as function of rescaled time t^*, $t^* = D_k\, t/R^2$ (open circles and line), $t^* = T_1{}^{(num)}\, t/T_1^k$ (open squares). Symbols refer to experimental data, line refer to numerical data.

Finally, we remark that the limited number of particle observed, N=3, is due essentially to fabrication limits. In fact, as mentioned, channels were 5 μm long, thus N=3 particles of 500 nm already occupy 1/3 of the channel. We succeeded to insert up to five or six particles inside a channel but, at that point, the channel was completely full and the outermost particles were immediately expelled; thus, we limited to a smaller initial number.

3.7 Survival probability of the central particle

We now arrive to the last SFD survival problem faced in this Chapter. We want to investigate the survival probability of the central particle when the other particles are not affected by the presence of the two absorbing boundaries. This is a much harder problem compared to the emptying process, because in this case particles are not really identical and the Reflection Principle cannot be used safely. This problem is related to the survival probability of a FBM of exponent H=1/4. This kind of problem has been studied recently in [41] in the case of a semi-infinite interval and an absorbing boundary; they found that the first passage time density (and hence the survival probability) has a power-law tail in the

long time limit.

We performed extensive Brownian Dynamics simulations of Lennard-Jones particles with characteristic diameter σ, to gain insight on the effect of the different SFD regimes on the survival probability. Referring to Fig. 2.1 in Chapter 2, the

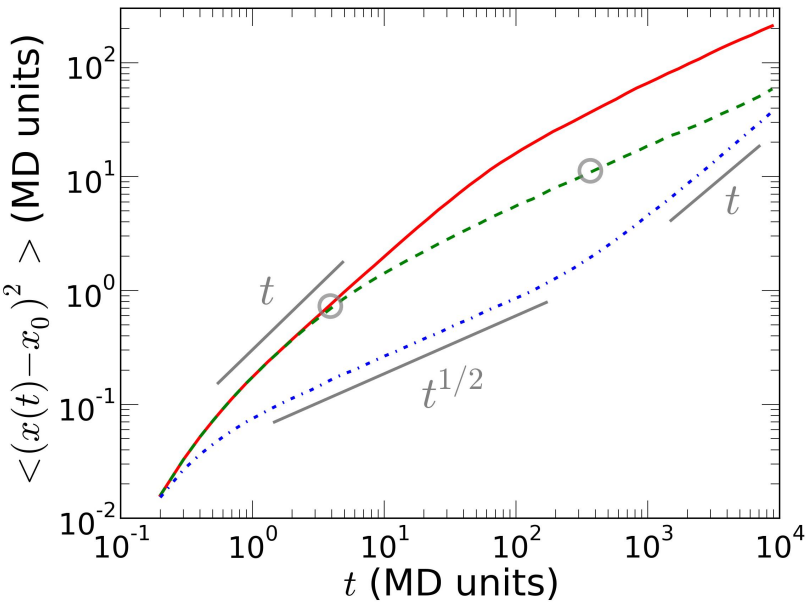

Figure 3.19: Log-log plot of the MSD for the central particle in a Single File system of N=75 particles for different values of initial density: ρ_0=0.1 (solid line), ρ_0=0.3 (dashed line), ρ_0=0.75 (dotted and dashed line). The two circles represent the MFPTs associated with two different choices of L: $L = 2\sigma$ corresponding to $T_1 \sim 4$ and $L = 10\sigma$ corresponding to $T_1 \sim 360\sigma$ (MD units). The corresponding survival probabilities are reported in Fig. 3.20.

typical time evolution of the MSD of a SFD system is composed by an initial diffusion, followed by a subdiffusive regime, after which normal diffusion comes back in finite systems. The anomalous regime, $\langle x^2 \rangle \sim t^{1/2}$ is very slow compared to the others; it is reasonable to expect that $S(t|x_0)$ should present the signature of the onset of this slowdown, for example through a crossover from an exponential behaviour, typical of normal diffusion, to a power law. In order to associate a given curve to a SFD regime, we choose the position of the boundary conditions at [-L/2,L/2] and we measure the survival probability, fixing x_0=0. From this curves, we calculate the MFPT $T_1(L)$ and, by looking at the MSD, we identify the regime as the one containing the MFPT.

Examples of MSD obtained from simulations for SFD systems of N=75 particles are reported in Fig. 3.19: by changing the value of L and the density ρ_0, we can

access to all the regimes. In particular, the two open circles refer to the MFPT of $L = 2\sigma$ and $L = 10\sigma$; the corresponding survival probabilities are reported in Fig. 3.20. The natural logarithm of the measured survival probabilities are

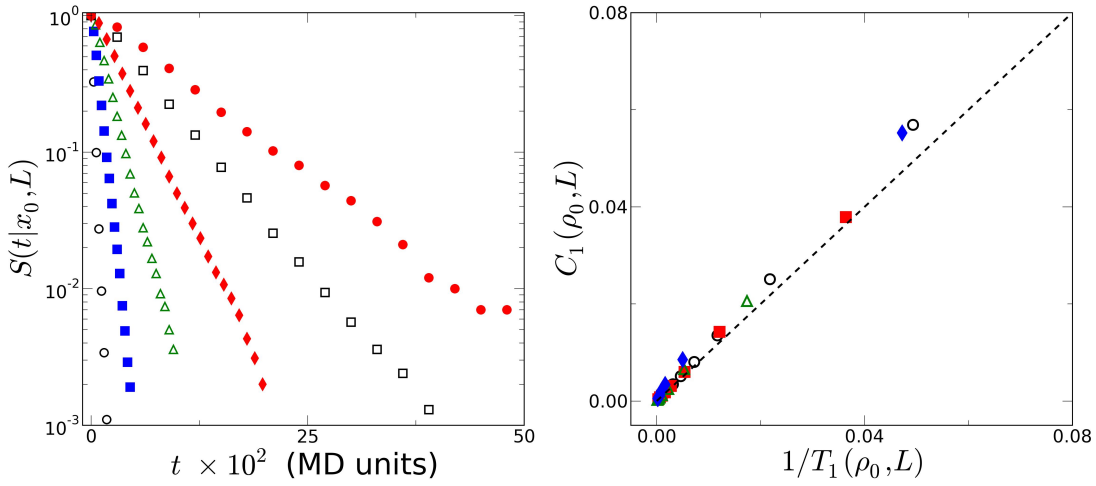

Figure 3.20: Left panel: Survival probability for N=75 particles with an initial density $\rho_0 = 0.3$ (semi-log scale), for different positions of the absorbing boundaries at [-L/2,L/2]: $L = 2\sigma$ open circles, $L = 4\sigma$ full squares, $L = 6\sigma$ open triangles, $L = 8\sigma$ full diamonds, $L = 10\sigma$ open squares, $L = 12\sigma$ full circles. MD rescaled units are used. Data refer to regimes II and III of Fig. 2.1. Particularly, the MFPTs of $L = 2\sigma$ (open circles) and $L = 10\sigma$ (open squares) correspond to the two open circles reported in Fig. 3.19. Right panel: survival probability decay constant as a function of the inverse of the mean first passage time, for different initial densities: $\rho_0 = 0.1$ (open circles), $\rho_0 = 0.3$ (full squares), $\rho_0 = 0.5$ (open triangles), $\rho_0 = 0.75$ (filled diamonds). The dashed line is the expected trend $C = 1/T_1(x_0)$ with no fitting parameters.

reported in the left panel of Fig. 3.20, for different values of L and for a initial density $\rho_0 = 0.3$. L is taken in such a way the Tagged Particle is can be in the diffusive or in the subdiffusive regime. The linear trend of the plots evidences the exponential nature of $S(t|x_0)$, even in the subdiffusive region. To support this evidence, we look for

$$S(t|x_0) \approx e^{-C(L,x_0)t} \approx e^{-t/T_1(L,x_0)} \tag{3.28}$$

as in the case of usual Brownian case, as it is a feature of the exponential function only. In the right panel of Fig. 3.20, we report, for different initial densities, the decay constant C of $S(t|x_0)$, obtained through interpolation, as a function of the inverse of the mean first passage time, measured directly from the trajectories. For all the different densities, the points follow the dashed line $C = 1/T_1(x_0)$, thus providing a strong evidence that a survival probability of the form (3.28)

holds even in the anomalous region.

3.8 Concluding remarks

Summarizing, we have studied the dynamical properties of Single File Diffusion systems of point-like particles in presence of absorbing boundaries. We have introduced the concept of emptying process, i.e. a generalized survival probability for a system of N particles, and we have found the exact solution to this problem for a SFD system using the Reflection Principle method, in the presence or in the absence of a constant external force. Notice that it can be further extended, introducing a generic external force, as long as particles are identical, collisions are elastic and we are able to provide the single particle survival probability. We have also found a solution for the survival probability of a Tagged Particle (TP) within the File, by selecting and counting the exit sequences. This solution is based on the (equilibrium) assumption that all the possible sequences are equiprobable and is exact for uniform initial conditions, as it is the equilibrium distribution for a SF finite system. We also adapted this method to calculate the survival probability in the presence of an external constant force. In this last case a generalization is not straightforward, and remains an interesting open theoretical problem, as colloids in extended holographic traps or even ions in cellular membrane channels are subject to non-constant forces.
In every case, we also exploited the trends of the Mean Emptying Times and of the Mean First Passage Times as function of the system size L, the initial number of particles N and the external force F_e, in order to gain practical insights useful in experiments or, possibly, applications of these concepts. Notice that both the MET and the MFPT have the same trend with L and F_e as the single particle MFPT, as SFD is exactly mapped on a N-particle non interacting system. Interestingly, if the system size is fixed, the MFPT as function of N only grows logarithmically, with the exception of the MFPT of the central particle in presence of small external forces, when we observe a decrease of this quantity due, probably, to crowding effects. Moreover, following the same argument used in the TP survival probability, we have calculated the Single File exit-side probabilities; in the presence of an external force, the fraction of particles moving against F_e decreases exponentially with F_e, almost independently from N.

We have also began to study theoretically the emptying process of a Single File system of particles with characteristic size σ, trying to renormalize the results valid for point-like particles to take into account excluded volume. Although our theoretical analysis has been stopped after the first reconstruction step, by comparing numerical simulations with experimental data of diffusing colloids in microfluidic channels we have found that an essential SFD model, neglecting hydrodynamic interactions between particles, is able to reproduce experimental data. The key parameters to control are initial conditions, excluded volume and external forces. In any case, the emptying process for particles of size σ remains another very interesting open theoretical problem, and will be extremely useful for a direct comparison between theory and experiments.
Finally, under the hypothesis that the central particle is the only particle that can be absorbed at the boundaries, the numerical study of the survival probability shows that $S(t)$ decay exponentially in time, as as it happens for Brownian motion, even when it has entered the subdiffusive region and thus its motion is hindered by the other particles. The comparison between the exponential decay constant and the mean first passage time is a quite strong proof supporting this result; it would be suitable to check these findings experimentally.

With this Chapter we conclude our study on the properties of Single File systems of diffusive particles. From now on, we will populate our Single File systems with self-propelled particles, modeled within the formalism of stochastic processes, neglecting the hydrodynamic details of the propulsion.

Chapter 4

Self-propelled particle model

Microswimmers self-propulsion or molecular motors activity are complex processes that often involve numerous degrees of freedom. To understand the physics of this systems and the collective properties displayed when interactions among particles are present, a suitable microscopic description is required [164–167]. Self-propelled particles (SPP) represent a versatile and tractable microscopic realization of active systems. Although these have been originally introduces as simplified agent-based models of flocks of birds and shoals of fish [15], they can also act as realistic models for less complex systems, such as polar protein filaments (e.g., F actin) in gliding motility assays on surfaces decorated with molecular motors (e.g., myosin) [13], suspensions of swimming microorganisms [168], colloidal or nanoscale particles propelled through a fluid by catalytic activity at their surface [90, 91] or even layers of vibrated granular rods [169].

In this Chapter, after a small introduction on the SPP literature, we will present a model for an Active Brownian Particle in one dimension. We will introduce an extension of the original model [170], we will define two adimensional numbers, the Péclet number Pe and the Tumbling number Tu and we will study some properties of the model, the velocity distribution function, the mean square displacement and the survival probability. Finally, we will derive a relation between Pe and Tu that defines two class of swimmers, *runners* and *tumblers*, characterized by straight motion or changes of direction, respectively.

4.1 Microscopic description of active matter

Usually, a self-propelled particle is described by a position variable $\mathbf{x}$ and an orientation variable, the angular coordinate θ in 1D-2D, or (θ, ϕ) in 3D. It also has an individual self-propulsion velocity of magnitude v, pointing in a direction specified by the orientation variable. This velocity can be expressed through an adimensional quantity, the Péclet number [171] $\mathrm{Pe} = v\sigma/D_t$, where σ is a characteristic lengthscale and D_t is the diffusive coefficient of a passive particle of the same size of the swimmer. We can divide the different models of SPP in three groups: hydrodynamic models, velocity-dependent friction and 'energy depot' models, Vicsek-like and Active Brownian Particles (ABP).
Velocity-dependent friction and energy depot models [172] are Langevin-based models in which self propulsion is introduced through a nontrivial friction coefficient $\gamma(r, v)$ that can depend on velocity and eventually on position. $\gamma(r, v)$ is given by a phenomenological function of $|v|$ in the former case or, in the latter, through a (phenomenological) evolution equation for the energy consumption of the swimmer.
Vicsek-like [15] or ABP [172] are very simple models based on Langevin equations for position, in which self propulsion is introduced as a constant force or

velocity acting on the particle in the direction given by the orientational variable. These model explicitly consider the evolution of the orientation θ as a stochastic process of some kind (Brownian motion, CTRW, explicit run-and-tumble etc).

Finally, the hydrodynamic description of SPP is based on a Navier-Stokes equation such that the flow field generated by flagellar motion (or self propulsion in general) can be reproduced [174, 175]. Based on their hydrodynamic behaviour, two class of SPP can be defined: *pushers* and *pullers*, descriptive of many flagellated bacteria and algae, respectively. The flow field generated is sketched in fig. 4.1. Alongside them, a third class are *squirmers*, that moves by direct manipulation of the velocity field on its surface; ciliated microorganisms often belong to this class. Such an approach can also be extended to the study of active liquid crystals [176].

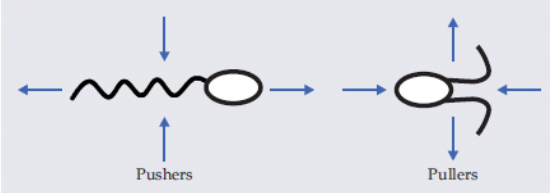

Figure 4.1: (From [173]) Schematic representation of the hydrodynamics of pushers and pullers microswimmers. Pushers, repel fluid in the swimming direction and draw in fluid in the lateral directions. Pullers swim flagella first and create the opposite flow field. (Both of the swimmers sketched here move from left to right.)

4.2 Active particle model

In order to introduce activity in a SF system, we have chosen a model for an (overdamped) Active Brownian particle (ABP) in one dimension [170]

$$\begin{cases} \dot{x} = (k_B T)^{-1} D_t \left[F_a \cos\left(\theta(t)\right) + F_e \right] + \xi_t(t) \\ \dot{\theta} = \xi_r(t) \end{cases} \tag{4.1}$$

where F_a is the constant self-propulsion force, pointing in a direction subject to a (overdamped) rotational Brownian motion; F_e is an eventual external force contribution, also considered as constant. $\xi_t(t)$ and $\xi_r(t)$ are, respectively, the Gaussian white noise random force and torque, each satisfying the fluctuation-dissipation theorem; F_a is related to the velocity of the self-propelled object by

$$F_a = v_{ac} m \gamma_t$$

In the original model [170], the rotational diffusion satisfy the Stokes-Einstein relation $D_r = \frac{k_B T}{8\pi\eta R^3}$; thus D_t and D_r are related by

$$\frac{D_t}{D_r} = \frac{4}{3}R^2 \tag{4.2}$$

thus, rotational and translational characteristic times,$\tau_r = 1/2D_r$ and $\tau_t = R^2/2D_t$ respectively, scaled the same way

$$\tau_t \propto \tau_r \propto \frac{\eta R^3}{k_B T} \tag{4.3}$$

To adapt the model to our specific needs, we drop the constraint (4.2); the rotational diffusion coefficient D_r becomes a new free parameter. The equations of motion (4.1) remain valid and $\xi_r(t)$ still satisfy the fluctuation-dissipation theorem

$$\langle \xi_r(t)\xi_r(t')\rangle = \sqrt{2D_r}\delta(t-t')$$

Although this is not a great change in the structure of the model, we will see that the actual consequences are interesting.

Finally, we define two dimensionless parameters that will be useful in the next sections to describe the properties of the system. The first one is the Péclet number, already mentioned in the previous section; the relation with the active force is given by

$$F_a = \frac{k_B T \mathrm{Pe}}{R}$$

The other dimensionless quantity we introduce is

$$\mathrm{Tu} = \frac{\tau_t}{\tau_r} = \frac{R^2 D_r}{D_t} \tag{4.4}$$

called the *'tumbling number'*. When Tu$\gg 1$ the particle changes its direction very frequently (*tumbler*) compared to the typical time it takes to diffuse over lengthscales of the order of R. Conversely, if Tu $\lesssim 1$ the particle tends to keep its direction (*runner*) because the rotation is slow, compared to the typical diffusive time.

This parameter suggest that we can effectively mimic "run-and-tumble" motion, the typical locomotion of bacteria, by setting a value of D_r such that the correlation timescale of the rotational diffusion is equal to the typical run timescale

τ_{run}

$$\tau_{run} = \frac{1}{2Dr}$$

Obviously, this is not sufficient to reproduce the details of run-and-tumble; we simply want to extend the model to processes in which the orientational change is ruled by some internal mechanism. Anyhow, on a certain timescales, we believed that such a coarse-grained approach can share the same properties of more complex propulsion mechanisms.

4.3 Model properties

4.3.1 Velocity probability distribution function

It is possible to calculate analytically the stationary probability distribution function for the velocity. We consider the velocity equation in the overdamped limit, at first excluding the thermal bath noise

$$v(t) = \frac{F_a}{\gamma_t}\cos(\theta)$$

In this case v is a function of the random variable θ and so

$$P_\theta(v) = \int d\theta P(\theta, t)\delta\left(v - F_a\cos(\theta)\right)$$

$P(\theta, t)$ is the probability distribution function of a freely diffusive particle on a circle, i.e. the probability distribution function of the diffusion process with periodic boundary conditions

$$\begin{cases} \frac{\partial P(\theta,t)}{\partial t} = D_r \frac{\partial^2 P(\theta,t)}{\partial \theta^2} \\ P(-\pi, t) = P(\pi, t) \\ \lim P(\theta, t) \underset{t\to 0}{\to} \delta(\theta - \theta_0) \end{cases} \tag{4.5}$$

The solution is given by

$$P(\theta, t) = \frac{1}{2\pi} + \frac{1}{\pi}\sum_{n=1}^{\infty}\left[\cos(nx_0)\cos(nx) + \sin(nx_0)\sin(nx)\right]e^{-D_r n^2 t} \tag{4.6}$$

In the long time limit, the distribution becomes uniform on the interval $[-\pi, \pi]$, $P(\theta) = 1/2\pi$. Using the property of the δ function

$$\delta(g(x)) = \frac{\delta(x - x_0)}{|g'(x_0)|}$$

we obtain

$$\begin{aligned} P_\theta(v) &= \int d\theta \frac{1}{2\pi} \frac{\delta\left(\theta - \arccos(v\gamma_t/F_a)\right)}{F_a \sin\left(\arccos(v\gamma_t/F_a)\right)} \\ &= \frac{1}{2\pi\, F_a} \frac{1}{\sqrt{1 - v\gamma_t/F_a}} \end{aligned} \tag{4.7}$$

If we now add the effect of the thermal bath,

$$v(t) = \frac{F_a}{\gamma_t}\cos(\theta) + \xi_t(t)$$

the solution is given by the convolution of the probability distribution functions of the two random variables

$$\begin{aligned} P(v) &= \int_{-\infty}^{\infty} P_\theta(v') P_\xi(v - v') dv' \\ &= \int_{-\infty}^{\infty} dv' \int_0^{2\pi} d\theta \frac{1}{2\pi} \delta\left(v' - \frac{F_a}{\gamma_t}\cos(\theta)\right) \frac{1}{\sqrt{2\pi\sigma^2}} e^{-\frac{(v-v')^2}{2\sigma^2}} \\ &= \int_0^{2\pi} d\theta \frac{1}{2\pi} \frac{1}{\sqrt{2\pi\sigma^2}} e^{-\frac{(v - F_a/\gamma_t \cos(\theta))^2}{2\sigma^2}} \end{aligned} \tag{4.8}$$

where $\sigma = m/k_B T$.

We verified the above calculations by Brownian Dynamics simulations. As left panel of Fig. 4.2 shows, Eq. (4.8) reproduces correctly the velocity probability distribution function measured from simulation. From the right panel of Fig. 4.2, one can also see that the result is independent from the chosen value of D_r, as long as the overdamped assumption on the angular dynamics is justified. Notice that the distribution is symmetric and, for high Pe, markedly non-Gaussian, showing the presence of two bumps at high velocities, slightly below $v_a = \mathrm{Pe}D/R$. This is a 1D feature, in the sense that it is the distribution of a single component of the velocity; being in 1D, the velocity component in the direction of the channel longitudinal axis is the only one available.

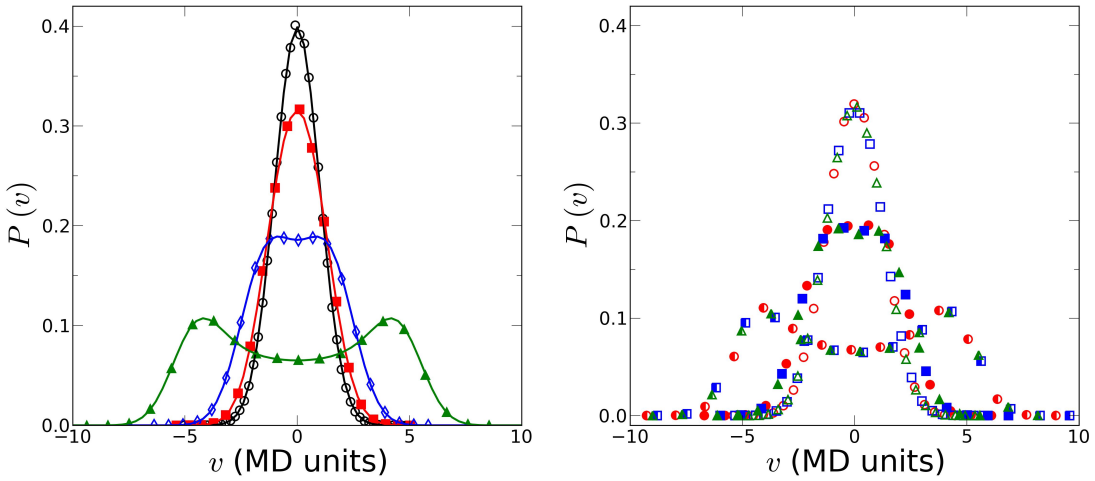

Figure 4.2: Left panel: stationary probability distribution function $P(v)$ measured from simulations (symbols), for Tu=0.75 and different values of the Péclet number: Pe=0 open circles, Pe=50 full squares, Pe=100 open diamonds, Pe=250 full triangles. Lines are given by Eq. (4.8). Right panel: stationary probability distribution function $P(v)$ measured from simulations for different values of Tu (Tu=200 circles, Tu=20 squares, Tu=2.5 diamonds, Tu=0.75 triangles) and different values of Pe (Pe=50 open symbols, Pe=100 full symbols, Pe=250 half-filled symbols).

4.3.2 Active particle Mean Square Displacement

In the overdamped limit, we can also calculate the average position and the mean square displacement of the particle in the absence of external forces. We start from

$$\begin{cases} \dot{x} = \frac{1}{m\gamma_t} F_a \cos(\theta) + \xi_t(t) \\ \dot{\theta} = \xi_r(t) \end{cases} \tag{4.9}$$

The angular process is a Brownian motion on a circle: it mean square displacement is given by

$$\langle (\theta - \theta_0)^2 \rangle = 2D_r t$$

The angular probability distribution function is, in principle, given by (4.6). However, since it is coupled to the other equation through a periodic function, we can try to use the pdf of the open boundary condition case

$$P(\theta, t) = \frac{1}{\sqrt{4\pi D_r t}} e^{-\frac{(\theta-\theta_0)^2}{4D_r t}}$$

First we can formally solve the equation for the position as

$$x(t) = \frac{1}{m\gamma_t}\left[F_a \int_0^t \cos(\theta(s))ds + \int_0^t \xi_t(s)ds\right]$$

Then, the average displacement from the initial position can be calculated by

$$\langle x(t) - x_0\rangle = \frac{1}{m\gamma_t} F_a \int_0^t \langle\cos\theta(s)\rangle ds$$

The average of $\cos\theta$ is simply

$$\langle\cos\theta(t)\rangle = \int_{-\infty}^{\infty} d\theta\cos(\theta)P(\theta,t) = \cos(\theta_0)e^{-D_r t}$$

from which follows

$$\langle x(t) - x_0\rangle = \frac{F_a}{D_r}\cos(\theta_0)\left[1 - e^{-D_r t}\right]$$

For the mean square displacement, we have to go through the following expression

$$\begin{aligned}\langle(x(t) - x_0)^2\rangle = \frac{1}{(m\gamma_t)^2}\Big[F_a^2 \int_0^t dt_1 \int_0^t dt_2 \langle\cos\theta_1\cos\theta_2\rangle + \\ + 2F_a \int_0^t dt_1 \int_0^t dt_2 \langle\xi_{t,1}\cos\theta_2\rangle + \int_0^t dt_1 \int_0^t dt_2 \langle\xi_{t,1}\xi_{t,2}\rangle\Big] \quad (4.10)\end{aligned}$$

The most difficult part is given by $\langle\cos\theta_1\cos\theta_2\rangle$, which, by definition, is given by

$$\langle\cos\theta_1\cos\theta_2\rangle_{t_1>t_2} = \int d\theta_1 \int d\theta_2 \cos\theta_1\cos\theta_2 G(\theta_1,\theta_2,t_1-t_2)P(\theta_2,t_2)|_{t_1>t_2}$$

where

$$G(\theta_1,\theta_2,t_1-t_2) = \frac{1}{\sqrt{4\pi D_r(t_1-t_2)}}\exp\left(-\frac{(\theta_1-\theta_2)^2}{4D_r(t_1-t_2)}\right)$$

is a two point probability density function. This yields

$$\langle\cos(\theta_1)\cos(\theta_2)\rangle_{t_1>t_2} = \frac{1}{2}e^{-D_r(t_1-t_2)}\left[1 + \cos(2\theta_0)e^{-4D_r t_2}\right]$$

The expression for $\langle \cos(\theta_1)\cos(\theta_2)\rangle_{t_2>t_1}$ is obtained in the same way by exchanging t_1 and t_2. Putting this together one obtains

$$\langle (x(t)-x_0)^2\rangle = 2D_t t + \frac{F_a^2}{(m\gamma)^2}\frac{1}{D_r^2}\left[D_r t + e^{-D_r t} - 1 + \frac{\cos(2\theta_0)}{12}\left(e^{-4D_r t} + 3 - 4e^{-D_r t}\right)\right] \tag{4.11}$$

This result can be expressed in a more elegant way by using the two dimensionless parameters Pe and Tu

$$\langle (x(t)-x_0)^2\rangle = 2Dt + \frac{\mathrm{Pe}^2 R^2}{\mathrm{Tu}^2}\left[D_r t + e^{-D_r t} - 1 + \frac{\cos(2\theta_0)}{12}\left(e^{-4D_r t} + 3 - 4e^{-D_r t}\right)\right] \tag{4.12}$$

It is interesting to see that:

- For very small times $D_r t << 1$ only the first term survives: the system experience free diffusion before the onset of the activity.

- At a certain time τ_s, second order terms becomes relevant: the expression for the MSD becomes

$$\langle (x(t)-x_0)^2\rangle = 2D_t t + \frac{1}{2}\frac{\mathrm{Pe}^2 R^2}{\mathrm{Tu}^2} D_r^2 \left(1+\cos(2\theta_0)\right) t^2$$

  and we see the onset of a t^2 region.

- If $\theta_0 = \pi/2$, the second order terms in the expansion disappears and the term of order t^3 becomes relevant

$$\langle (x(t)-x_0)^2\rangle = 2D_t t + \frac{\mathrm{Pe}^2 R^2}{\mathrm{Tu}^2}(D_r t)^3$$

- In the long time limit $D_r t >> 1$ ($\tau_{D_r} = \frac{4\pi^2}{2D_r}$), only the linear term matters and a new "active" diffusive regime comes into place

$$\langle (x(t)-x_0)^2\rangle = 2D_t t + \frac{\mathrm{Pe}^2 R^2}{\mathrm{Tu}^2} D_r t = 2D_t\left(1 + \frac{\mathrm{Pe}^2}{\mathrm{Tu}}\right) t$$

  with an "active" diffusion coefficient given by

$$D_a = D_t + \frac{1}{2}\frac{\mathrm{Pe}^2 D_t}{\mathrm{Tu}} \tag{4.13}$$

Remarkably, we would have found the same diffusion coefficient by considering a run-and-tumble motion with characteristic tumble rate $\alpha = 2D_r$. As already mentioned in section 1.4, run-and-tumble motion, in the long time limit, is equivalent to a random walk with a diffusion coefficient

$$D_a = \frac{v_a^2}{\alpha}$$

where v_{ac} is the velocity of the bacteria during a run and α is the tumble rate. Taking $\alpha = \tau_r^{-1} = 2D_r$ we have

$$\frac{v_a^2}{\alpha} = \frac{\mathrm{Pe}^2 D_t}{2\mathrm{Tu}}$$

Adding for completeness the contribution of the heath bath we obtain

$$D_a = D_t + \frac{\mathrm{Pe}^2 D_t}{2\mathrm{Tu}}$$

which is exactly our active diffusion coefficient. Notice also that D_a, in analogy with usual Brownian motion, define a new timescale

$$\tau_a = \frac{R^2}{D_a} \tag{4.14}$$

τ_a is the typical timescale of the self-propelled motion.

Since experimentally it would be difficult to always set the initial direction of the active force at the same value θ_0, it is convenient to relax the condition $\theta(0) = \theta_0$ and draw out the initial angle from a uniform distribution on $[-\pi, \pi]$. In order to calculate the correct mean square displacement, we start from Eq. (4.12) and average over $[-\pi, \pi]$ (or $[0, \pi/2]$ for symmetry). Hence

$$\langle \cos(2\theta_0) \rangle = \int_0^{\pi/2} \cos(2\theta_0) \frac{1}{2\pi} d\theta_0 = 0$$

and that the mean square displacement becomes

$$\langle (x(t) - x_0)^2 \rangle = 2D_t t + \frac{\mathrm{Pe}^2 R^2}{\mathrm{Tu}^2} \left[D_r t + e^{-D_r t} - 1 \right] \tag{4.15}$$

In this case, only a superdiffusive t^2 regime is possible. The superdiffusive timescale τ_s can be evaluated simply by imposing the equality between first and second order contributions of the MSD, giving

$$\tau_s = \frac{2R^2}{\mathrm{Pe}^2 D_t \cos^2\theta_0}$$

In the case $\theta_0 = \pi/2$, one must equate first and third order terms, obtaining

$$\tau_s = \sqrt{\frac{3R^2}{\mathrm{Pe}^2 D_t D_r}}$$

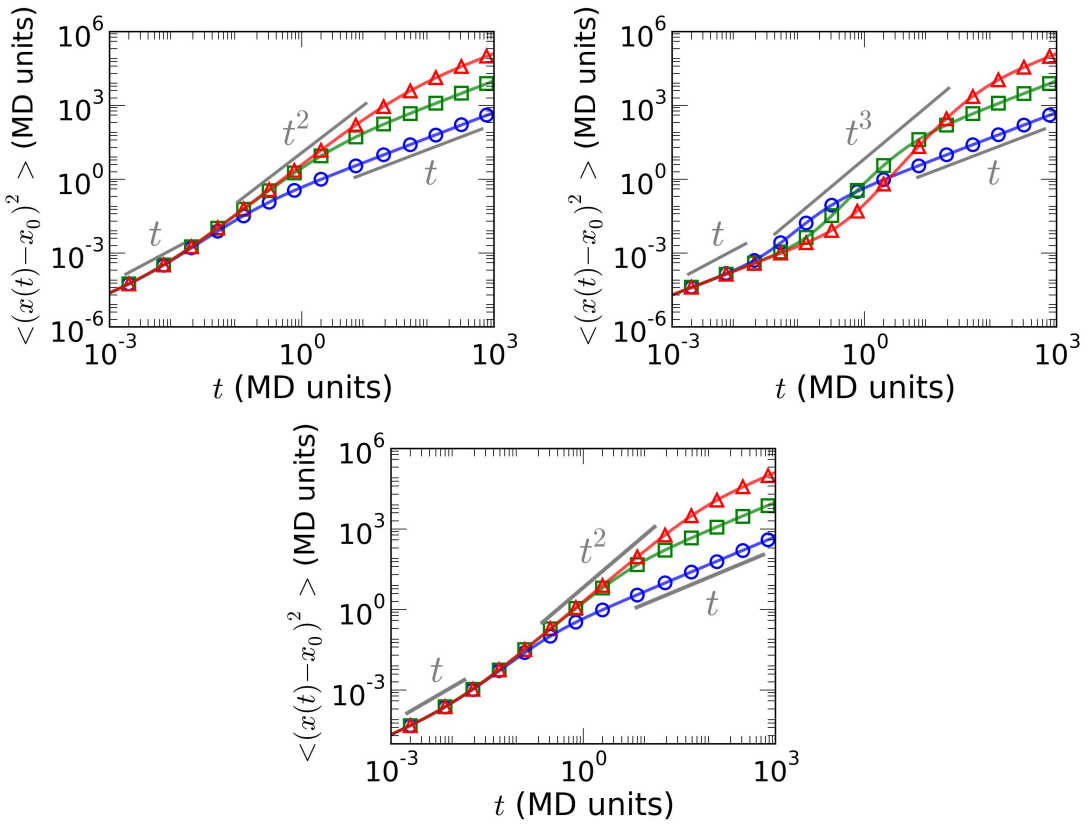

Figure 4.3: Log-log plots of the mean square displacement of a single active particle for Pe=100 and different values of the tumbling number (circles Tu=200, squares Tu=10, triangles Tu=0.75). Symbols are data from numerical simulations, lines are Eq. (4.12) in the two top panels and Eq. (4.15) in the bottom panel. Top left panel: θ_0=0. Top right panel: θ_0=$\pi/2$. Bottom panel: θ_0 uniformly distributed over [-π, π].

Finally, in the case of a random angular initial condition, one obtains

$$\tau_s = \frac{4R^2}{\mathrm{Pe}^2 D_t}$$

We verified the above calculations by Brownian Dynamics simulations (see Appendix A for details). Figure 4.3 show a good agreement between numerical simulations and equations (4.12) or (4.15).

4.3.3 Scaling of the Mean Square Displacement

It can be useful to find a way to rescale the mean square displacement for different values of the parameters of the model to collapse the data on a single curve. In the passive case this is very simple because

$$\langle (x(t) - x_0)^2 \rangle = 2Dt$$

and a simple rescale as $t \to Dt$ gives the correct result. In the case of active particles, several timescales are unveiled: one imposed by the rotational process τ_r, one superdiffusive timescale τ_s at intermediate times and one associated with the long time diffusion, τ_a. We can still try to find such a rescaling by looking at the MSD analytical expression (4.12). First, notice that we cannot rescale MSDs with different θ_0. Notice also that, when the activity becomes important, the contribution of the translational diffusion is irrelevant and there is only one single characteristic timescale, $\tau_r = 1/2D_r$. In the opposite limit, under a certain value of Pe, the thermal background takes over and we set back to a passive particle. To estimate this value we can impose that the superdiffusive timescale τ_s has to be bigger than the rotational time τ_r. From this we get

$$\begin{aligned}
&\mathrm{Pe} \leq \sqrt{\frac{2\mathrm{Tu}}{2cos^2\theta_0}} && \theta_0 \neq \pi/2 \\
&\mathrm{Pe} \leq \sqrt{\frac{3\mathrm{Tu}}{2}} && \theta_0 = \pi/2 \\
&\mathrm{Pe} \leq \sqrt{8\mathrm{Tu}} && \theta_0 \,\text{random}
\end{aligned}$$

We found the following rescaling:

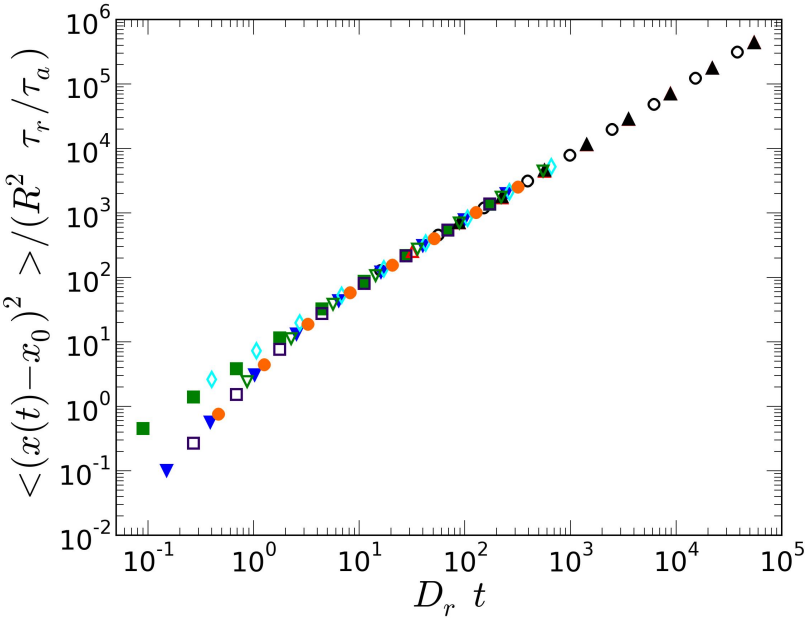

Figure 4.4: Rescaled mean square displacement of a single active particle with θ_0 uniformly distributed over [-π, π], for different values of Péclet and tumbling numbers: open circles Pe=10 Tu=200, full squares Pe=1 Tu=0.75, open upward triangles Pe=100 Tu=200, full downward triangles Pe=10 Tu=0.75 , open diamonds Pe=10 Tu=1.67, full circles Pe=100 Tu=1.67, open squares Pe=100 Tu=0.75, full upward triangles Pe=1 Tu=200, open downward triangles Pe=10 Tu=1.67.

$$t \to D_r t \qquad \langle (x(t)-x_0)^2 \rangle \to \frac{\langle (x(t)-x_0)^2 \rangle}{\left(\frac{1}{\mathrm{Tu}} + \frac{1}{2}\frac{\mathrm{Pe}^2}{\mathrm{Tu}^2}\right)} \tag{4.16}$$

Figure 4.4 show this rescalement for random initial angles and different choices of the parameters. Obviously, (quasi-)passive particles cannot be rescaled correctly at intermediate times, while the scaling is correct in the long time limit. However, the mean square displacements of particles with very different Tu collapse remarkably well onto on a single curve.

4.3.4 Survival Probability

We finally give some examples of the survival probability $S(t|x^0, L)$, i.e. the probability that a particle started at x^0 has remained inside a certain region of interest of size L until time t, for a single ABP obeying the equations of motion described above in the presence of two absorbing boundary condition at [-$L/2$,$L/2$]. The analytical solution of this problem is not available yet and we limit ourselves to provide examples of this quantity, since they will be used in the

following Chapters. Left panel of Fig. 4.5 show several survival probabilities for a

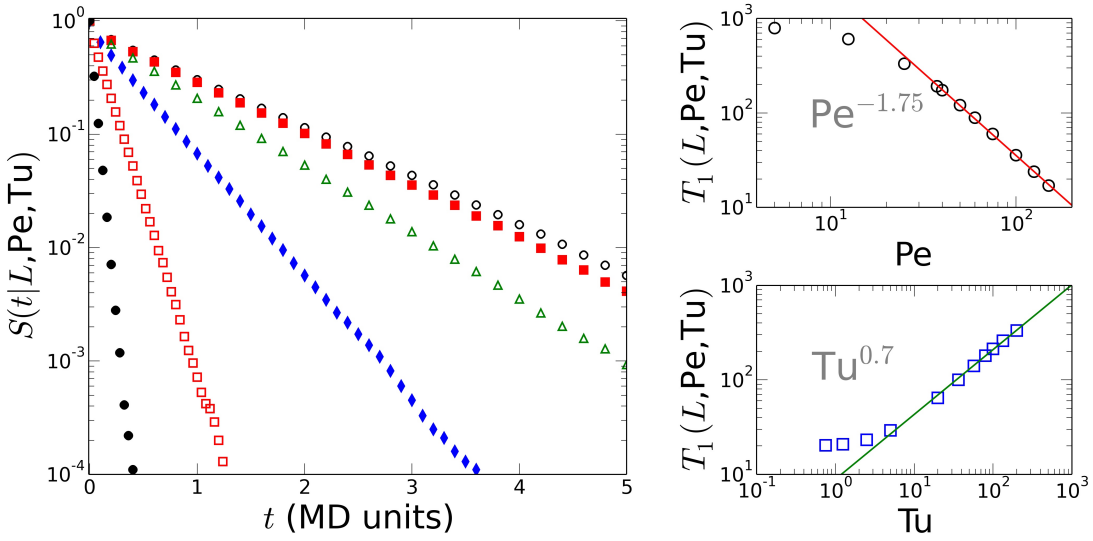

Figure 4.5: Left panel: Survival probabilities of a single ABP with two absorbing boundaries at L=10 (MD units), Tu=200 and different values of the Péclet number: open circles Pe=0, full squares Pe=5, open triangles Pe=12.5, full diamonds Pe=25, open squares Pe=50, full circles Pe=100. Top right panels: MFPT as function of Pe, L=10 (MD units), Tu=200 fixed. Symbols are data from numerical simulations, line is a best fit with a power law $\mathrm{Pe}^{-1.75}$. Bottom right panels: MFPT as function of Tu, L=10 (MD units), Tu=25 fixed. Symbols are data from numerical simulations, line is a best fit with a power law $\mathrm{Tu}^{0.7}$.

single ABP at fixed Tu=200, L=10 (MD units) and different values of the Péclet number. The curves reported are clearly exponential, as in the passive case. In the two right panels, we have reported the Mean First Passage Time

$$T_1(x^0, L) = \int_0^\infty dt S(t|x^0, L)$$

as function of Pe (top, L=10 and Tu=200 fixed) and Tu (bottom, L=10 and Pe=25 fixed). In the top panel, we first notice a region in which $T_1(L,\mathrm{Pe},\mathrm{Tu})$ is fairly constant; this corresponds to the quasi-passive particle condition introduced in the previous section; then, it monotonically decreases as a power law $\mathrm{Pe}^{-1.75}$. In the bottom panel, again we first notice a region in which $T_1(L,\mathrm{Pe},\mathrm{Tu})$ is fairly constant, corresponding to particles that do not satisfy the condition $T_1(L,\mathrm{Pe},\mathrm{Tu}) > \tau_r$, i.e. the angular coordinate is not completely decorrelated from its initial value; notice that this condition was satisfied in the top panel. Then, it monotonically increases as a power law $\mathrm{Tu}^{0.69}$. These exponents seems to rule out the possibility of a straightforward description of this model in terms of an

effective temperature; in fact, an effective temperature should be readable from the active diffusive coefficient $D_a = k_B T_{eff}/m\gamma$, that should lead to Pe $^{-2}$ and Tu $^{-1}$.

Finally, we also checked the dependence on the MFPT on the system size L,

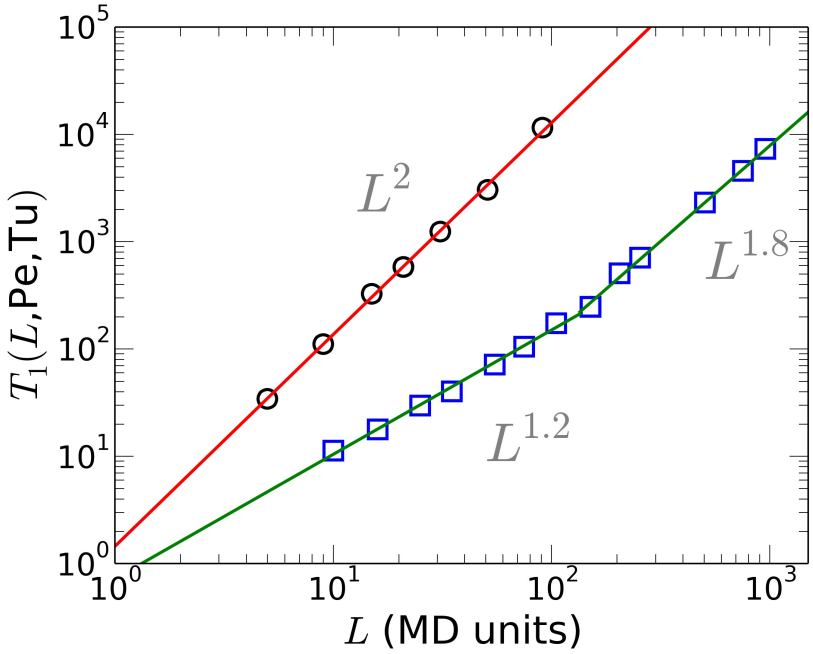

Figure 4.6: MFPT of a single active particle, as function of L, open circles Pe=100, Tu=200, open squares Pe=100, Tu=0.75. Symbols are data from numerical simulations, lines are best fits with a power law L^2 for open circles, $L^{1.2}$ and $L^{1.8}$ for open squares at low and high values of L, respectively.

for Pe=100 and two different values of Tu. As visible in Fig. 4.6, for Tu=200 we observe a single trend, $T_1(L,\mathrm{Pe},\mathrm{Tu}) \propto L^2$, as for a passive particle. In the other case, Tu=0.75, we observe two trends, with distinct power-law behaviours: at low values of L, the MFPT grows as $L^{1.2}$, while in the other limit grows as $L^{1.8}$. The reason for these anomalous trends resides in the condition $T_1(L,\mathrm{Pe},\mathrm{Tu}) > \tau_r$ mentioned above. A particle with Tu=200 has a very small decorrelation time, much smaller than every MFPT considered in our simulation; we are thus automatically in the active diffusive region and the trend is the one of a diffusing particle. On the other hand, a particle with Tu=0.75 has a long decorrelation time, longer or comparable to the MFPTs measured in the low-L region. The exponent is not exactly unitary because for $\theta \approx \pi/2$ the active force vanishes and the particle is practically passive; therefore, thanks again to the long decorrelation time, very long residence times can happen. If the system is big enough and

the MFPT becomes comparable to $\tau_R = 4\pi^2/2D_r$, the particle enter the active diffusive region; again, the growth is not exactly quadratic because, again thanks to the long decorrelation time, it is possible to have very long straight runs, that lead to abnormally short residence times.

4.3.5 Running *vs* tumbling: a transition line

The influence of the reorientational process on the translational dynamics depends on the typical timescale of the rotation but also on the magnitude of the active force involved. Intuitively, if reorientations are very frequent a typical trajectory will be more tangled with respect to the ones in which reorientations are less frequent. On the other hand, if we increase the propulsion force, even for frequent reorientations, a particle will cover longer and longer distances within the same time interval and thus fairly straight runs will appear in the trajectory.
This argument can be made more quantitative way by looking at the typical timescales of rotational and translational motion, τ_r and τ_a respectively. If $\tau_r < \tau_a$ the direction of motion has already changed while a fraction of the particle radius has been covered; in the other case the swimmer has to cover a long distance (compared to its radius) before a sensible change in the orientation has taken place. Equating this two timescales leads to a relation between the Péclet and the tumbling numbers:

$$\mathrm{Pe} = \mathrm{Tu}\sqrt{2\left(1 - \frac{1}{\mathrm{Tu}}\right)} \tag{4.17}$$

The condition above is visible in Fig. 4.7 This relation defines a curve that divides the plane Tu-Pe in two regions: the *tumbling* region below the curve, where reorientations (tumbles) are more frequent and a *running* region, above the curve, where long runs are prevalent. In Fig. 4.7 we have reported several examples of real microswimmers, by computing their corresponding values of Pe and Tu from experimental data, in order to contextualize this transition line. It is interesting to notice that almost the totality of microswimmers falls in the running region [177–181]; only a particular *E. Coli* mutant, which has been created with the inability to perform runs (*tumbler* mutant) falls in the tumbling one [179].
Also artificial microswimmers, such as catalytic Janus colloids [182], can be placed in this diagram. Janus colloids self-propulsion find its origin in phoretic effects of various kind (diffusiophoresis, thermophoresis, electrophoresis, chemophoresis),

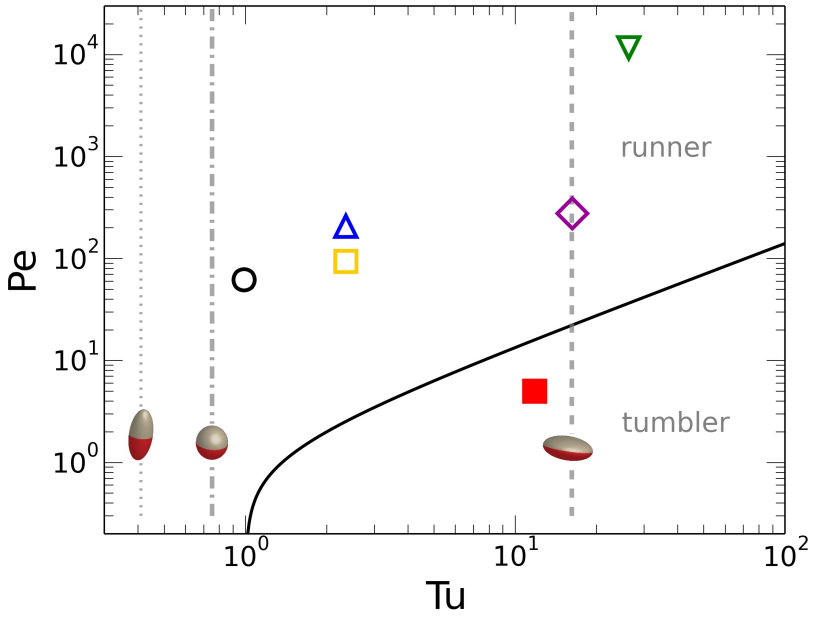

Figure 4.7: Transition line 4.17 in the plane Tu-Pe (log-log scale); points and dashed lines are the values of Tu and Pe for real systems. Symbols of different color refer to different microorganisms: (from left to right) full black diamond for *V. Alginolyticus* [177], open blue circle for *P. Putida* [178], full yellow square for wild type and full red square for tumbler type *E. Coli* [179], open violet pentagon for *R. Spheroides* [180], full green triangle for *C. Reinhardtii* [181]. Vertical gray lines refer to Janus microswimmers with different ratios between symmetry axis a and equatorial axis b: (from left to right) dotted for a/b=2(prolate spheroids), dashed and dotted for a/b=1 (spheres), dashed for a/b=0.2 (oblate spheroids). For these kind of particles, Tu is fixed, while Pe can be tuned varying, for example, H_2O_2 concentration [182].

but they do not have an internal reorientational mechanism; they thus are subject to thermal rotational diffusion. For a given shape Tu is fixed and propulsion can be varied changing some external parameter. Figure 4.7 shows three examples of particles of different shapes: a prolate spheroid, a sphere and an oblate spheroid. Their tumbling number depends on the ratio between the symmetry axis a and the equatorial axis b and become greater if a/b is very small, thus for oblate spheroid or disk-like particles.

An equivalent and intuitive way to describe the picture we have just given is through the definition of two kind of *persistence*: a *time persistence*, measured by the rotational decorrelation time and a *spatial persistence*, measured by the distance traveled before the decorrelation time. Temporal persistence is related to the rotational process only, and is a partial indicator of the dynamic state of the swimmer. On the contrary, spatial persistence include the effect of the propulsive force and is, thus, a good indicator: a low spatial persistence particle

will reside in the tumbling region, while a high spatial persistence particle will fall into the running region. In this latter case, the term *persistence* derives from the fact that, for increasing values of this quantity, we have increasing displacements in a fairly straight direction. In the other case, the term comes from the analogy between an observable trajectory of this kind of SPPs and a polymer. For any kind of polymer we can calculate the *persistence length* l_p, as a measure of the "stiffness" of the polymer itself. The definition is

$$\langle \mathbf{r}_i \mathbf{r}_j \rangle \simeq exp(-s/l_p) \tag{4.18}$$

where r_i and r_j are vectors tangent to the polymer and $s = |i-j|b$ is the contour distance between the two monomers along the chain (b is the bond length). The scalar product of the two tangent vectors define an angle, ϕ; we can rewrite (4.18) as

$$\langle \cos(\phi_{i,j}) \rangle \simeq e^{-s/l_p} \tag{4.19}$$

For our trajectory, s is a time coordinate; since particles in our model have an intrinsic angular variable, for sufficiently high values of Pe, this simplifies to

$$\langle \cos(\theta) \rangle \simeq e^{-2\,D_r t} \tag{4.20}$$

thus relating the temporal persistence to the rotational diffusion constant and to the rotational timescale.

Chapter 5

Active particles in Single File

In this Chapter, we study the behaviour of Active Brownian Particles (ABP) under Single File conditions, or Active Single File (ASF); the ABP model used has been extensively treated in Chapter 4. Each particle in the system is active, and they are all identical. As anticipated in Chapter 4, within the framework of this model we can distinguish between *runners* and *tumblers*, whose dynamics is dominated by straight runs or tumbles, respectively. We will show in the following sections that this distinction under SF conditions leads to crucial differences in the dynamical behaviour of the system. First, passing from one class to the other, a transition takes place, characterized by the emergence of aggregates of *runners*. Collisions are the starting point of these clusters, and, for *runners*, they look alike inelastic collisions, while they remain elastic for *tumblers*. In order to verify the existence of this dynamical transition, we tested the validity of the Reflection Principle through the emptying process, finding again a strong distinction between *runners* and *tumblers*. We then proceed in the study of the dynamical properties of an Active Single File in presence of absorbing boundaries by using the same techniques introduced in Chapter 3 for passive particles, we calculate the survival probability of a Tagged Particle in the absence of an external force. Moreover, in the spirit of Chapter 3, we numerically study the exit probabilities and the trends of the MET and of the MFPT as function of the system size L and of the number of particles N, for both *runners* and *tumblers*. Also this analysis reveals profound differences between the two class of swimmers.

5.1 Clustering transition

As anticipated in the introduction, we start by studying the clustering transition, that find its origin in the different dynamical properties of the two classes of swimmers. Since *Runners* tend to maintain the direction of their motion, after a collision they stick together, creating a 'nucleation point' for bigger structures. These are held together by the action of the propulsion of their elementary constituent. On the contrary, after a collision *tumblers* detach from each other almost immediately and, thus they do not tend to aggregate.
We studied the aggregation phenomenon by looking at the radial distribution function in one dimension:

$$\rho G_2(x) = \frac{1}{N}\langle \sum_{i \neq j} \delta\left(x - (x_i - x_j)\right)\rangle \tag{5.1}$$

that describes how density varies as a function of the distance between each pair of particles. Variations in the density reveal structural properties of the system and allow us to find the presence of aggregates. To investigate this quantity, we realized Brownian Dynamics numerical simulations using periodic boundary conditions and the Lennard-Jones type potential (see Appendix A for details); we

fixed the number of particles N=21, the number density ρ=0.5 and varied both the tumbling and the Péclet numbers.

The left panel of Fig. 5.1, show two examples of radial distribution function,

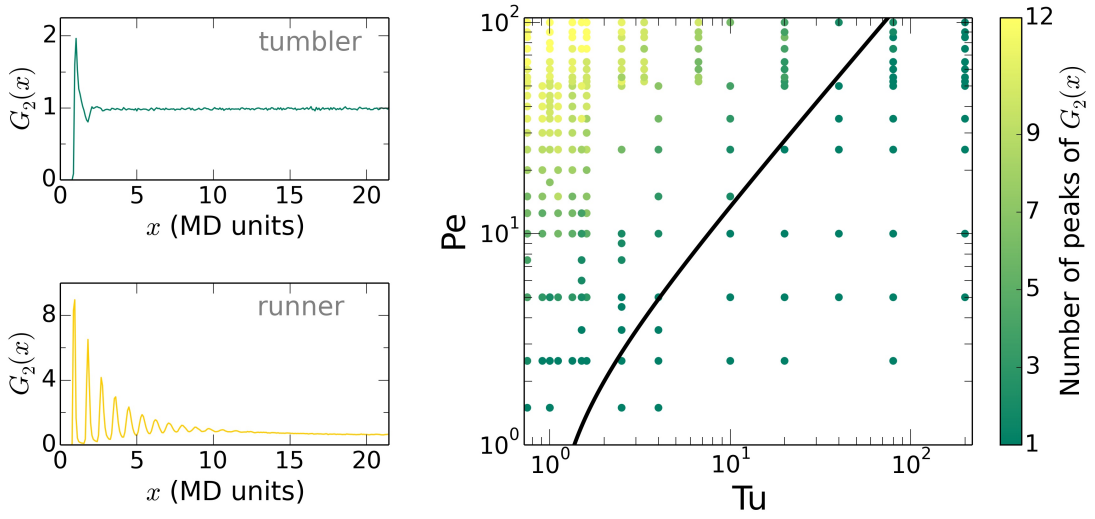

Figure 5.1: Left panel: examples of radial distribution function $G_2(x)$ for a Single File system of N=21 particles with number density ρ=0.5 and periodic boundary conditions in a box [-L/2,L/2] of size $L = N\sigma/\rho$. Top left panel: *tumblers* Tu=200, Pe=100; bottom left panel: *runners* Tu=0.75, Pe=100. Right panel: scatter plot of the number of peaks of $G_2(x)$ as function of Pe and Tu for ASF systems, with the same N, ρ and boundary conditions as the examples in the left panel; the black line is Eq. (4.17).

for *tumblers* in the top panel (Pe= 100, Tu=200), for *runners* in the bottom one (Pe= 100, Tu=0.75). As visible, the structure function is completely different in the two cases: $G_2(x)$ for a system of *tumblers* presents only one peak, while for a system of *runners* several peaks are observed, exactly one particle diameter from each other. These peaks reveal the formation of aggregated structures of particles, with different sizes. Notice that these are dynamical clusters, as there is no real attraction between the swimmers; when the propulsions cease to have opposite directions, particles detach causing the progressive dismantling or even the abrupt breakdown of the aggregate.

To verify that cluster formation is a characteristic feature of an active Single File of *runners*, we measured the number of peaks of $G_2(x)$, which sets the maximum cluster size. We plot the number of peaks as a function of the Péclet number and of the Tumbling number. Data from numerical simulations are reported in the right panel of Fig. 5.1 as a scatter plot. From these raw data, we can already argue the trend of the quantity we are observing: under the line Eq. (4.17),

the radial distribution function present a single peak. In the running region, the number of peaks increases for increasing Pe or decreasing Tu.

To have a better picture of the effect, we look at the level curves of the number of

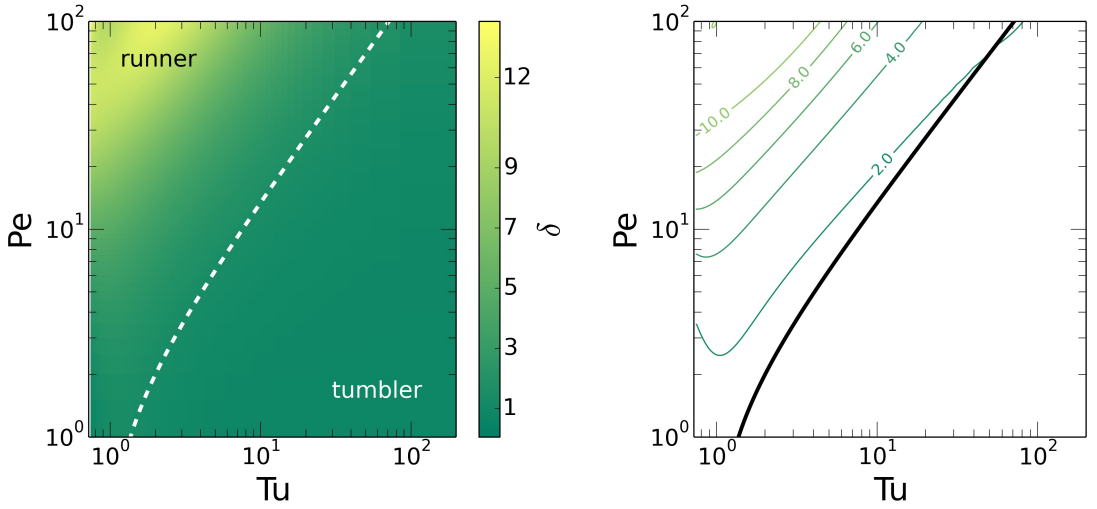

Figure 5.2: Left panel: Color plot of the number of peaks of $G_2(x)$ as function of Pe and Tu; white dashed line is Eq. (4.17). Right panel: level curves of the number of peaks of $G_2(x)$ as function of Pe and Tu; black line is Eq. (4.17). In both panels, N, ρ and boundary conditions are the same as in Fig. 5.1

peaks as a function of Pe and Tu. We performed a bivariate spline approximation on the data shown in Fig. 5.1 and we computed its level curves; we limited ourselves to 0<Pe<100 and 0.75<Tu<200 in order to have a better result in our fitting process. The results are reported in Fig. 5.2: the spline representation is the left Fig. of the panel, the level curves are in the right panel. From both plots one can see that, effectively, the relation (4.17) set a transition line between the *tumblers* region and the *runners* region, the last being characterized by the formation of clusters.

5.2 Dynamical transition

Results obtained in the previous section show that the interplay between rotation and translation can lead to drastic effects, such as aggregation without an attractive potential. These behaviours can be mapped into a change of the collisional properties of the particles, from elastic to inelastic. Generally speaking, a collision between two particles is elastic if the duration of the pair interaction is much smaller than the characteristic timescale of the particles translational dynamics,

namely,

$$\tau_{int} \ll \tau_{transl}$$

In the case of passive Brownian particles, we identify τ_{transl} with the diffusional timescale τ_D. Within our ABP model, the motion is ruled by the action of the self-propulsion, regulated by the angular dynamics. This means that the characteristic timescale of the translational dynamics must be referred to the active motion while the interaction time is set by the timescale of the rotational Brownian motion: consequently

$$\tau_{int} = \tau_r = \frac{1}{2D_r} \qquad \tau_{transl} = \tau_a = \frac{R^2}{2D_a}$$

Since the condition for the elastic collision is given by

$$\tau_r \ll \tau_a$$

we find that Eq. 4.17 should also set a transition line between elastic and inelastic interaction regions. As already mentioned, in the tumbling region the rotational decorrelation time is sufficiently small that, after a collision, the direction of the active force has already changed and, typically, particles detach from each other. Conversely, *runners* maintain their direction of motion and tend to stick together as in an inelastic collision.

To validate this argument, we tested the validity of the Reflection Principle Method through the emptying process. We remind that the Reflection Principle works nicely only in the case of elastic collisions. Hence, we expected a to find a good result in the tumbling region and a non negligible error for *runners*. Left panels of Fig. 5.3 show two examples of emptying probability 1-$S_1(t|N, L)$, for *tumblers* (Pe=100, Tu=200, top panel), for *runners* (Pe=100, Tu=0.75, bottom panel). Symbols refer to numerical data, while lines are obtained from Eq. (3.1); details on the theoretical reconstruction of the emptying process for ASF system can be found in next section. For *tumblers*, the theoretical prediction matches data perfectly, while for *runners* the analytical prediction gives a relevant underestimation of the emptying time. Notice that this is caused by the presence of aggregates. Being formed by contrasting forces, these clusters are, typically, very slow, and the bigger they get, the slower they move. Thus, in terms of emptying

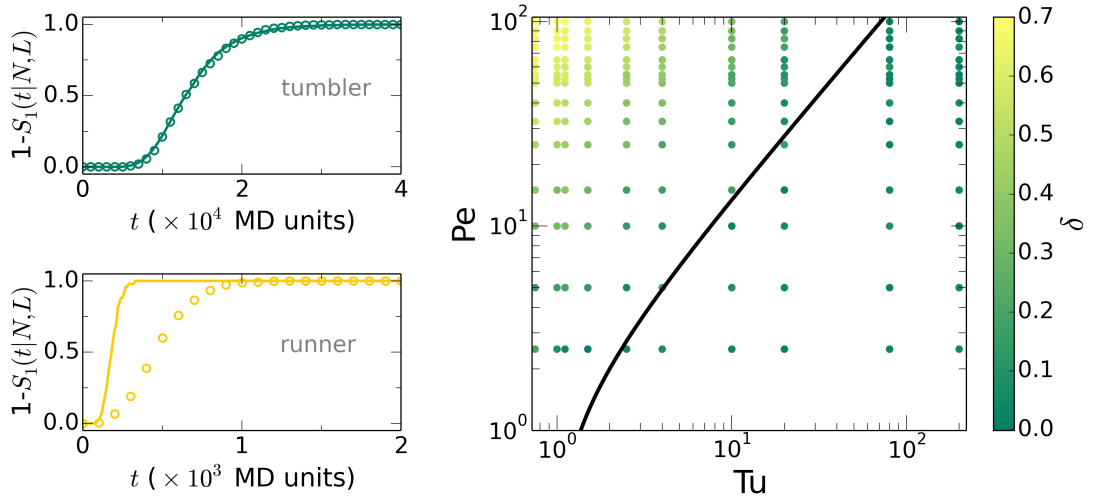

Figure 5.3: Left panels: examples of emptying curves for ASF systems of N=21 particles, with number density ρ=0.5 and absorbing boundary conditions at [-L/2,L/2] $L = L_0$+10; symbols refer to data from numerical simulations, lines are Eq. (3.1). Top left panel: *tumblers* Tu=200, Pe=100; bottom left panel: *runners* Tu=0.75, Pe=100. Right panel: scatter plot of δ, the MET relative difference between simulations and the analytical prediction, as function of Pe and Tu for ASF systems, with the same N and ρ as the examples in the left panel; the black line is Eq. (4.17).

time, the formation of clusters is a disadvantage for *runners*. On the other end, we will see in the next section that Mean Emptying Times for systems of *runners* are still much smaller than for *tumblers* at the same Péclet number.

In order to measure the discrepancy between theoretical predictions and simulations, we looked at the relative error between the numerical and the theoretical Mean Emptying Times

$$\delta = \frac{T_1^{(num)} - T_1^{(theo)}}{T_1^{(num)}} \tag{5.2}$$

We collected data from simulations of active Single File systems of N=21 particles, initial density ρ_0=0.5 and absorbing boundaries at $L = L_0$+10 for different values of Pe and Tu. Data from numerical simulations are reported in the right panel of Fig. 5.3. From raw data, the theory seems to work well below the line defined by (4.17). However as one approaches this condition and beyond, the relative error gets bigger and bigger.

In order to have a more quantitative information, we looked for level curves of δ as function of Pe and Tu. As in the previous section, we first performed a bivariate spline approximation on the data shown in Fig. 5.3 and then we computed its level curves; we limited again to 0<Pe<100 and 0.75<Tu<200 in

order to have a better result in our fitting process. Results are reported in left and

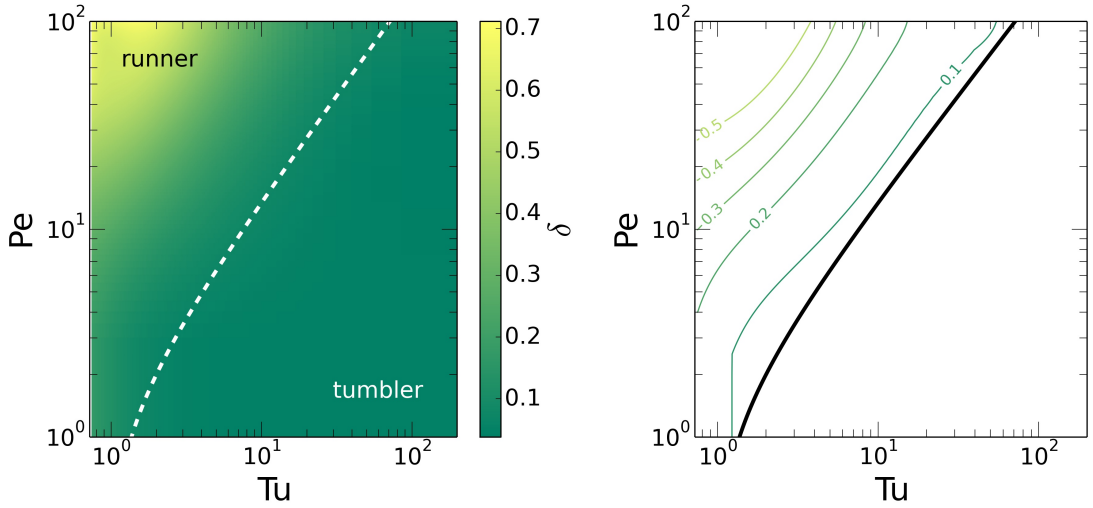

Figure 5.4: Left panel: color plot of δ as function of Pe and Tu; the dashed line is Eq. (4.17). Right panel: level curves of δ as function of Pe and Tu for ASF systems; the black line is Eq. (4.17). In both panels, N and ρ are the same as in Fig. 5.3.

right panels of Fig. 5.4. Both quantitatively support the trend observed in Fig. 5.3, i.e. δ increases while going far above the reference line (4.17). This confirms that, for *tumblers'*, the Reflection Principle Method works well suggesting that collisions are elastic, while for *runners*, the tendency to maintain the direction of motion leads to cluster formation, affecting the collisional properties and deeply modifying the emptying dynamics of the system.

5.3 Emptying process of Active Single File systems

We now report a more detailed study on the emptying process for Active Single File systems. We start by detailing the reconstruction of the emptying probability for *tumblers*. The procedure follow the one of section 3.2, where now $S(t|L)$ is the survival probability of a single SPP. As anticipated in section 4.3.4, the analytical form of $S(t|L)$ for the SPP model is not available; as basis for our calculations, we used numerical data obtained from dedicated Brownian Dynamics simulations, limited to the case of random initial conditions on both spatial and angular coordinates. An example of such comparison is reported in Fig. 5.5:

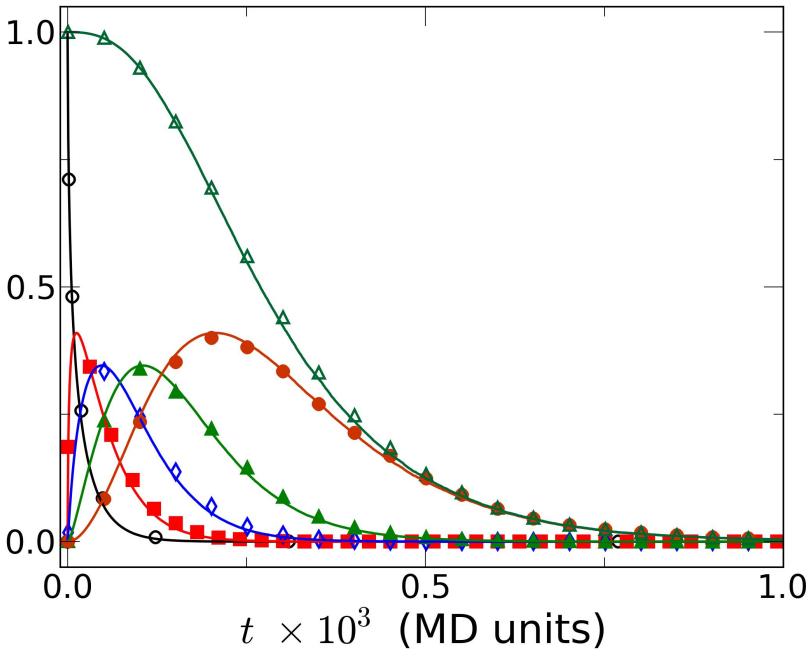

Figure 5.5: Example of emptying process for *tumblers* SPPs: $p_n(t|N, L, \mathrm{Pe}, \mathrm{Tu})$ (n=0 open circles, n=1 full squares, n=2 open diamonds, n=3 full triangles, n=4 full circles) and $S_1(t|N, L, \mathrm{Pe}, \mathrm{Tu})$ (open triangles) for a system of N=5 particles, initially distributed with uniform probability in [-L_0/2,L_0/2], with number density ρ_0=0.5, absorbing boundaries at $L = L_0$, Pe=100, Tu=200 (MD units). Symbols are data from numerical simulations, while lines are Eq. (3.4) or Eq. (3.1).

the theoretical lines are in a very well agreement with numerical data. This is a demonstration of the robustness of the Reflection Principle Method; its validity being based on the relevance of the order preservation on the dynamics of the system, is even satisfied in the presence of self-propulsion.

Besides the validation of the analytical method, we used Brownian Dynamics simulations to explore the behaviour of these systems in the Tu-Pe plane. Results are reported in Fig. 5.6. Surprisingly, Eq. (4.17) marks again a division between high-MET particles (*tumblers*) and low-MET particles (*runners*). Notice that a high Péclet number is not the only condition to satisfy for a fast emptying process: for example in the upper right corner (*tumblers* of high Pe), METs are of the same magnitude as in the lower left corner (*runners* of low Pe).

As anticipated, in the spirit of Chapter 3, we study the dependence of the MET on L and N. In Chapter 4.3.4, we referred to the MFPT of a single ABP as $T_1(L, \mathrm{Pe}, \mathrm{Tu})$; in the following we will drop the explicit dependence on Pe and Tu for simplicity, as Pe=100 will be fixed and, to enlighten the differences be-

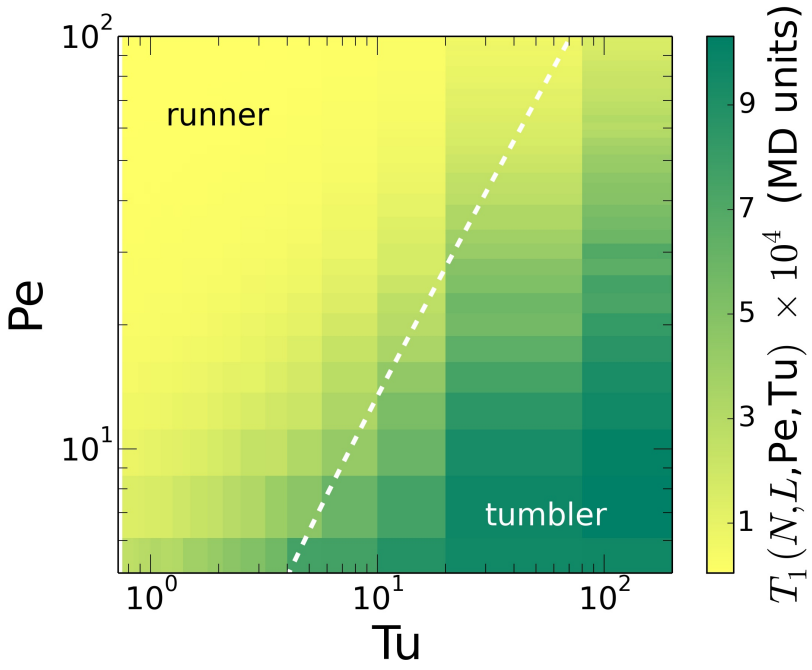

Figure 5.6: Mean Emptying Times as function of Pe and Tu, measured from numerical simulations of ASF systems, N=21, $L = L_0 + 10$, ρ_0=0.5. White dashed line is Eq. (4.17).

tween the two species of swimmers, we will choose two representative values of Tu, Tu=200 for *tumblers* and Tu=0.75 for *runners*. We carried out the same measurements performed in section 3.2 and reported the results in Fig. 5.7. We focus on the substantial differences between *tumblers* and *runners*. In all cases, Mean Emptying Times for *runners* are much smaller than for *tumblers*, coherently with Fig. 5.6. Moreover, *tumblers* scale exactly as passive particles and, as function of L, as a single *tumbler* (see Fig. 4.6); on the contrary, *runners* show always anomalous trends. For example, we observe that, as function of L, their trend is governed by an exponent whose value is smaller with respect to the one observed for a single *runner*.

Finally, as function of N, the MET of a system of *runners* will increase faster with respect to *tumblers* (as $N^{0.67}$). By increasing the number of swimmers, we enhance cluster formation: bigger and slower aggregates will form, that will remain safely inside the channel until an appropriate fluctuation of the self-propelled directions will drag the particles out of the cluster.

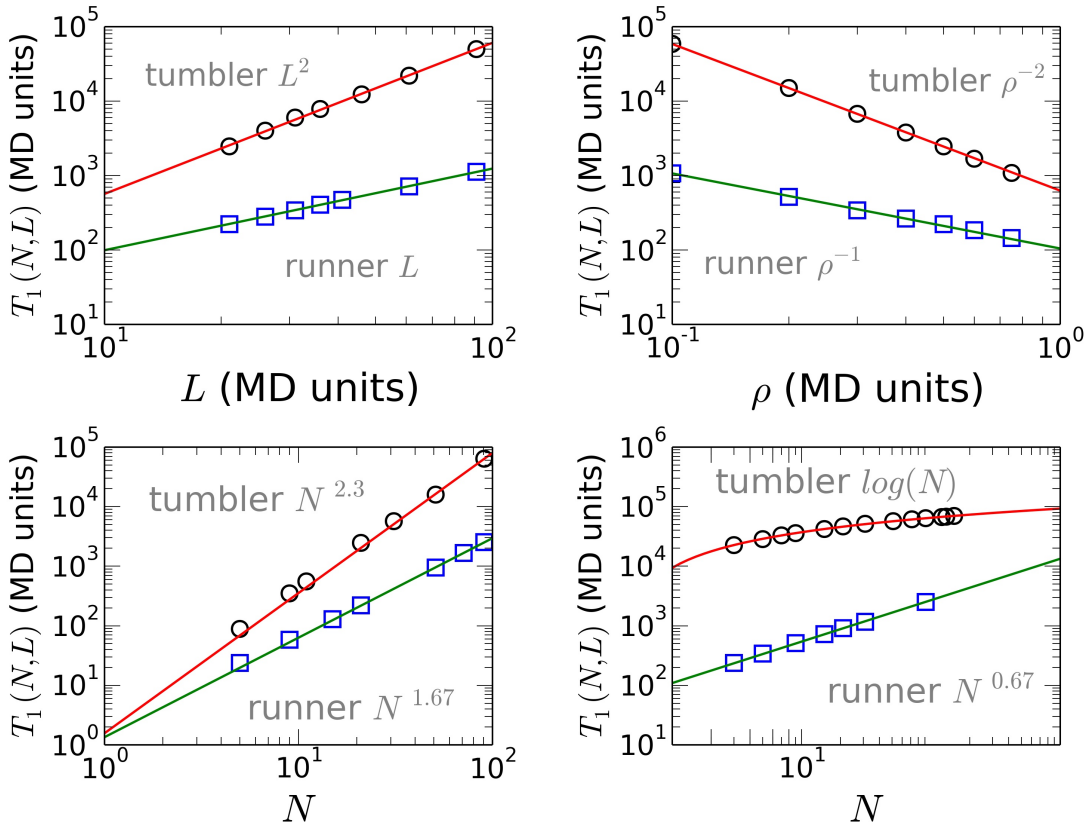

Figure 5.7: Mean emptying times for ASF systems, distinguishing between ASF of *runners* (Pe=100, Tu=0.75) or *tumblers* (Pe=100, Tu=200). In each panel, axis are in the logarithmic scale, symbols are data from numerical simulations, lines are best fits. Top left panel: MET as a function of the system size L for ASF systems of N=21 particles, ρ=0.5; best fit with a power law L^2 for tumblers, L for runners. Top right panel: MET as a function of the density ρ for ASF systems of N=21 particles, $L = L_0$; best fit with a power law ${\rho_0}^{-2}$ for tumblers, ${\rho_0}^{-1}$ for runners. Bottom left panel: MET as a function of the particles number N for ASF systems with ρ=0.75, $L = L_0$; best fit with a power law $N^{2.2}$ for tumblers, $N^{1.7}$ for runners. Bottom right panel: MET as a function of the particles number N for ASF systems of fixed L =60.66 (MD units); best fit with a logarithmic function for tumblers, with a power law $N^{0.7}$ for runners.

5.3.1 Emptying process in presence of an external force

As further characterization of the ASF dynamical properties and in analogy with Chapter 3, we study the emptying process for ASF systems in presence of an external force. We start again by validating the theoretical solution with Brownian Dynamics simulations (see Appendix A for details). Results are reported in Fig. 5.8: the theoretical lines are in a very well agreement with numerical data. Again, we study the behaviour of the MET, by limiting ourselves to its dependence on the external force. Numerical results are visible in the top panel

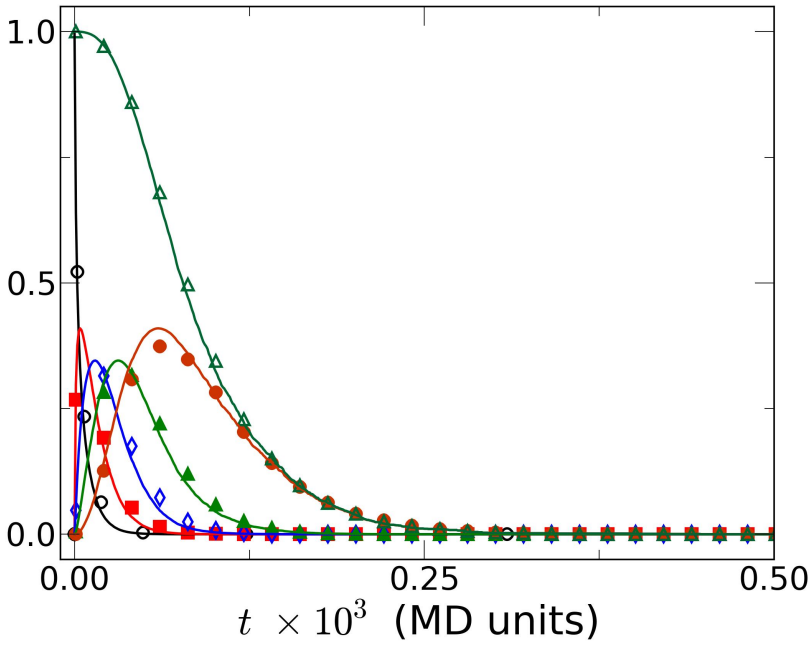

Figure 5.8: Example of emptying process for *tumblers* SPPs in presence of an external force: $p_n(t|N,L)$ (n=0 open circles, n=1 full squares, n=2 open diamonds, n=3 full triangles, n=4 full circles) and $S_1(t|N,L)$ (open triangles) for a system of N=5 particles, initially distributed with uniform probability in [-$L_0/2$,$L_0/2$], with number density ρ_0=0.5, absorbing boundaries at $L = L_0$, F_e=0.5, Pe=100, Tu=200 (MD units). Symbols are data from numerical simulations, while lines are Eq. (3.4) or Eq. (3.1).

of Fig. 5.9: METs remain fairly constant up to a certain threshold of the external force, whose value depends on the value of Tu, then show a power-law, $F_e^{-1.1}$ for *tumblers* and $F_e^{-1.7}$ for *runners*. *Tumblers* scale very much alike passive particles and are more sensitive to the external bias than *runners*.

Finally, we look for the explicit dependence of the MET from Pe and Tu. Results are reported in bottom panels of Fig. 5.9. Both plots show a region in which the MET remain constant, followed by a power-law behaviour, Tu $^{0.8}$ and Pe $^{-1.7}$ respectively.

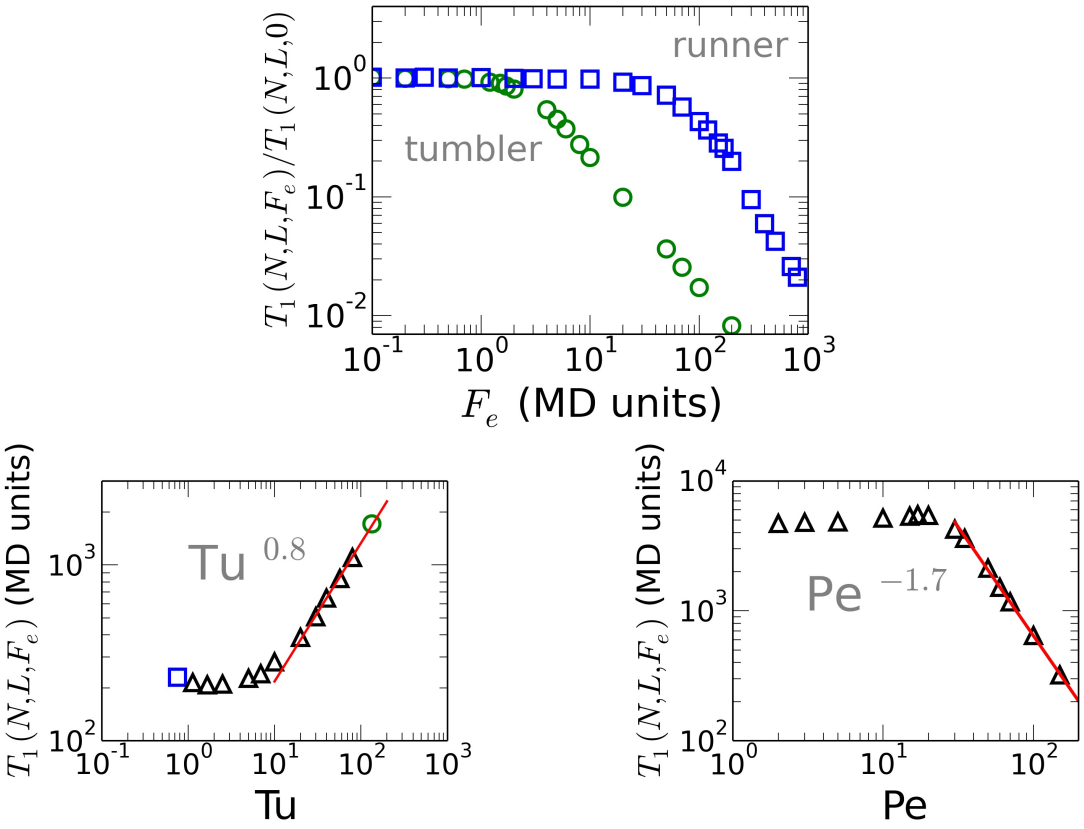

Figure 5.9: Log-log plot of $T_1(N, L, F_e)$ for ASF systems of N=21 particles, initially distributed with uniform probability in [-L_0/2,L_0/2], with number density ρ_0=0.5, absorbing boundaries at $L = L_0$ (MD units). Symbols are data from numerical simulations, lines are best fits. Top panel: $T_1(N, L, F_e)$ normalized over $T_1(N, L, F_e = 0)$, as function of the external force F_e, open circles Pe=100, Tu=200 (*tumblers*), open squares Pe=100, Tu=0.75 (*runners*); power-law trend $F_e^{-1.1}$ for *tumblers*, $F_e^{-1.7}$ for *runners*. Bottom left panel: $T_1(N, L, F_e)$ as function of Tu, Pe=100 fixed; power-law trend $\mathrm{Tu}^{0.8}$. The empty circle and square recall the top panel and refer to the *runner* (open square) or to the *tumbler* (open circle). Bottom right panel: $T_1(N, L, F_e)$ as function of Pe, Tu=40 fixed; power-law trend $\mathrm{Pe}^{-1.7}$.

5.4 Survival probability of an active Tagged Particle

We now investigate the survival probability of a Tagged Particle (the central one) for ASF systems. We start by validating the reconstruction method for *tumblers*: the theoretical approach is the same followed in section 3.3, we again use numerical data obtained from dedicated Brownian Dynamics simulations as input for the calculations. We limit to the case of random initial conditions on both spatial and angular coordinates. An example is reported in Fig. 5.10: as one can see,

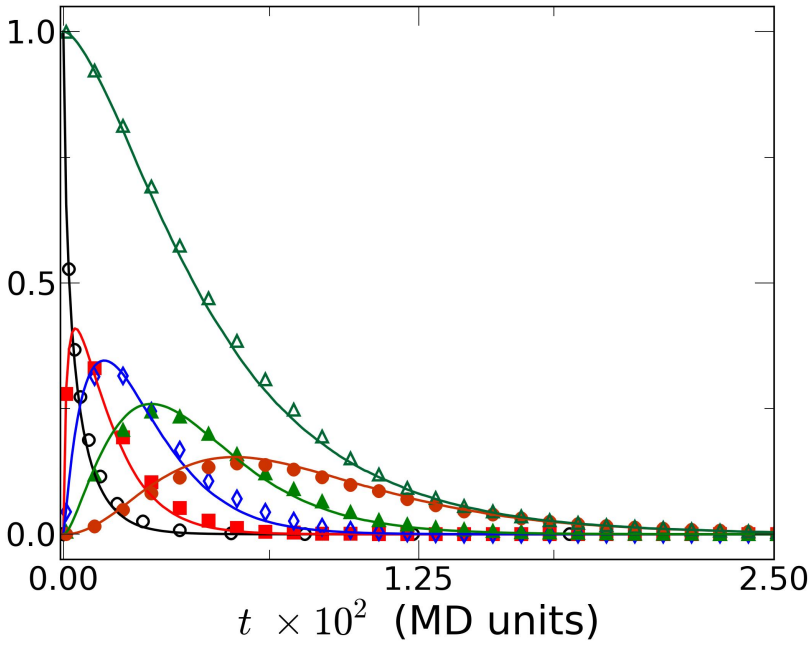

Figure 5.10: Example of Tagged Particle survival probability: $p_n(t|N, L, \mathrm{Pe}, \mathrm{Tu}, x_c \in [-L/2, L/2])$ (n=0 open circles, n=1 full squares, n=2 open diamonds, n=3 full triangles, n=4 full circles) and $S_{x_c}(t|N, L, \mathrm{Pe}, \mathrm{Tu})$ (open triangles) for a system of N=5 particles, initially distributed with uniform probability in [-L_0,L_0], with number density ρ_0=0.5, absorbing boundaries at $L = L_0$, Pe=100, Tu=200 (MD units). Symbols are data from numerical simulations, while lines are Eq. (3.12) or Eq. (3.13).

the theoretical lines are in a very well agreement with numerical data.

In analogy with the previous sections, study the dependence of the MFPT from the L and N, choosing the same two representative of section 5.3: for *tumblers* Pe=100, Tu=200, for *runners* Pe=100, Tu=0.75. We performed again the same measurements of section 3.2 and we report the results in Fig. 5.11. In each case *tumblers* scale exactly as passive particles; on the contrary, but coherently with the emptying process, *runners* show different trends.

We conclude this section with a digression on the survival probability of a tagged active particle in presence of a constant external force. In this case, the equilibrium assumption introduced in section 3.3.1 is no longer valid, as we have an additional force term in the system. We briefly discuss, in the spirit of the previous section, the dependence of the MFPT on the external force, for both *tumblers* and *runners*. Results of numerical simulations are visible in top panel of Fig. 5.12; many common features between METs and MFPTs are present also in this case. For example, the Mean First Passage Time, normalized over

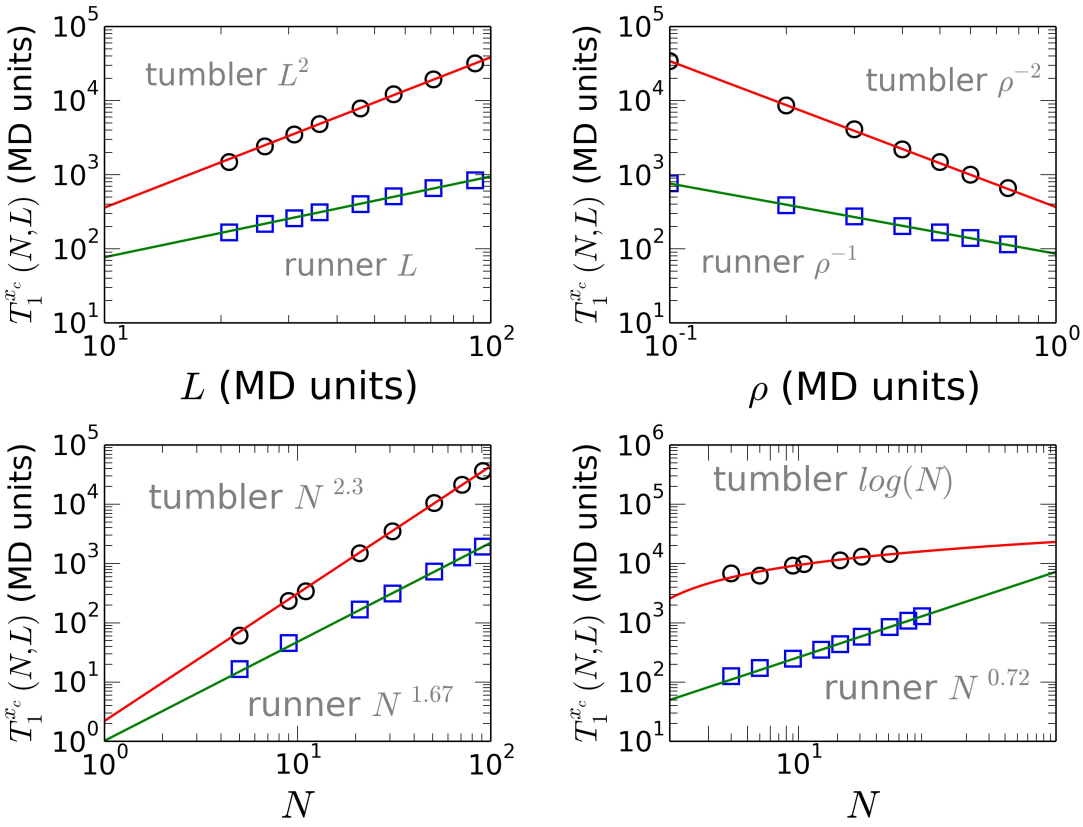

Figure 5.11: Mean first passage times for the central particle in a ASF systems, distinguishing between ASF of *runners* (Pe=100, Tu=0.75) or *tumblers* (Pe=100, Tu=200). In each panel, axis are in the logarithmic scale, symbols are data from numerical simulations, lines are best fits. Top left panel: MFPT as a function of the system size L for ASF systems of N=21 particles, ρ=0.5; best fit with a power law, L^2 for tumblers, L for runners. Top right panel: MFPT as a function of the density ρ for ASF systems of N=21 particles, $L = L_0$; best fit with a power law, ${\rho_0}^{-2}$ for *tumblers*, ${\rho_0}^{-1}$ for runners. Bottom left panel: MFPT as a function of the particles number N for ASF systems with ρ=0.75, $L = L_0$; best fit with a power law, $N^{2.3}$ for tumblers, $N^{1.7}$ for runners. Bottom right panel: MFPT as a function of the particles number N for ASF systems of fixed L =60.66 (MD units); best fit with a logarithmic function for tumblers, with a power law $N^{0.72}$ for runners.

$T_1^{x_c}(N, L, F_e = 0)$, remains fairly constant up to a certain threshold of the external force, whose value depends on the value of Tu, then show a power-law, $F_e^{-0.9}$ for *tumblers* and $F_e^{-1.3}$ for *runners*, which are similar to the ones observed for the Mean Emptying time.

We conclude by looking at the explicit dependence of the MFPT from Pe and Tu (see bottom panels of Fig. 5.12). Both plots show a region in which the MFPT remain constant, followed by a power-law behaviour, Tu $^{0.8}$ and Pe $^{-1.7}$ respectively. Both the trend exponents and the crossover values are remarkably

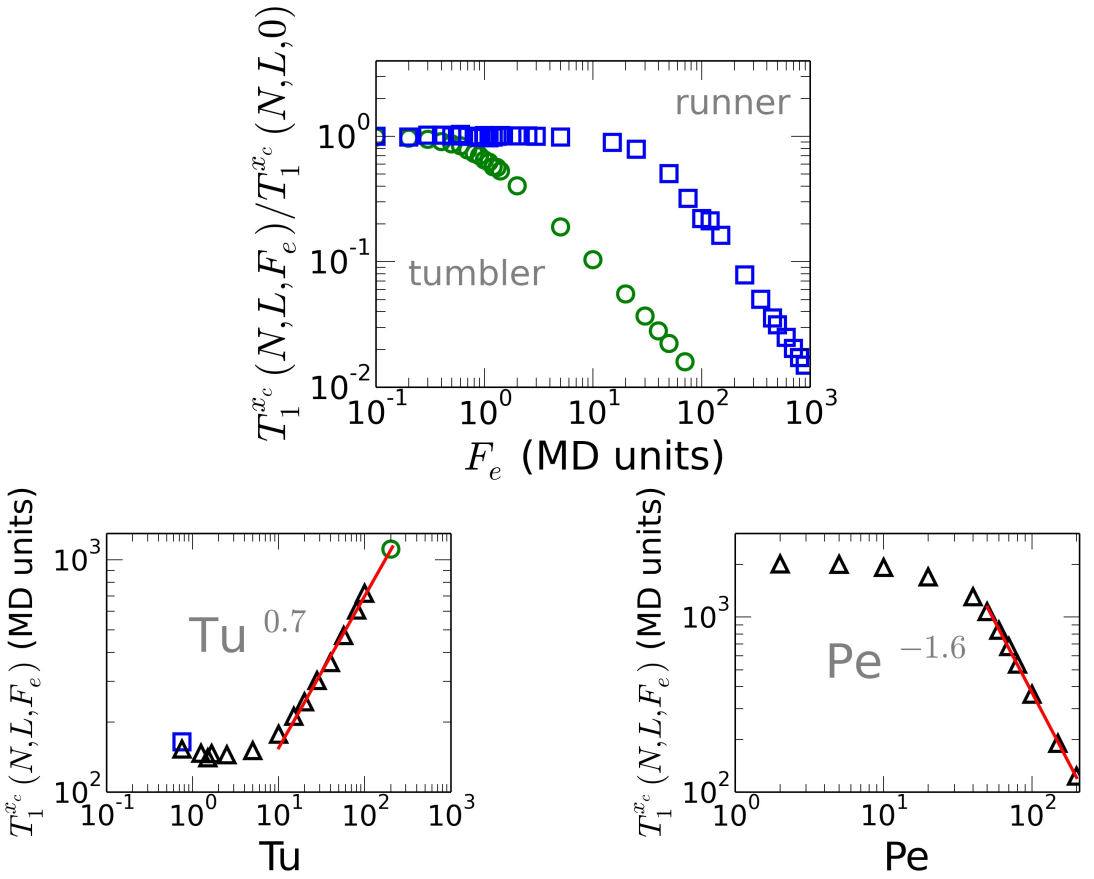

Figure 5.12: Log-log plot of $T_1^{x_c}(N, L, F_e)$, for an ASF system of N=21 particles, initially distributed with uniform probability in [-L_0/2,L_0/2], with number density ρ_0=0.5, absorbing boundaries at $L = L_0$ (MD units). Symbols are data from numerical simulations, lines are best fits. Top panel: normalized over $T_1^{x_c}(N, L, F_e = 0)$, as function of the external force F_e, open circles Pe=100, Tu=200 (*tumblers*), open squares Pe=100, Tu=0.75 (*runners*); power-law trend $F_e^{-0.9}$ for *tumblers*, $F_e^{-1.3}$ for *runners*. Bottom left panels: $T_1^{x_c}(N, L, F_e)$ as function of Tu; power-law trend $\mathrm{Tu}^{0.7}$. The empty circle and square recall the top panel and refer to the *runner* (open square) or to the *tumbler* (open circle). Bottom right panel: $T_1^{x_c}(N, L, F_e)$ as function of Pe, Tu=40 fixed; power-law trend $\mathrm{Pe}^{-1.6}$.

similar to those observed for the Mean Emptying Time.

5.5 Exit-side probabilities

We conclude this Chapter by studying numerically the exit-side probability for our model of ABPs in presence of a constant external force. As for passive particles, the exit-side probability for SPP is an experimentally accessible quantity, that can give many insights on the dynamical properties of the system. We start by

looking at the single particle case. We limit ourselves to random initial conditions in the angular variable; otherwise, if the system is small enough, particles with high angular decorrelation times (small Tu) will always exit from the same side. We will focus on the fraction of upstreamers ϕ_{F_e}, defined in section 3.4, that we recall here

$$\phi_{F_e} = 2\frac{\sum_k P_L(k)}{N} = 2\frac{\langle N_{F_e}\rangle}{N}$$

For particles dominated by F_e, $\phi_{F_e} \simeq 0$, i.e. the particle will almost certainly exit on the right side, whereas for small biases $\phi_{F_e} \simeq 1$, thus the particle effectively opposes to the external bias, ending on the left side with probability one half.

In the left panel of Fig. 5.13, ϕ_{F_e} is reported as function of Tu for different values

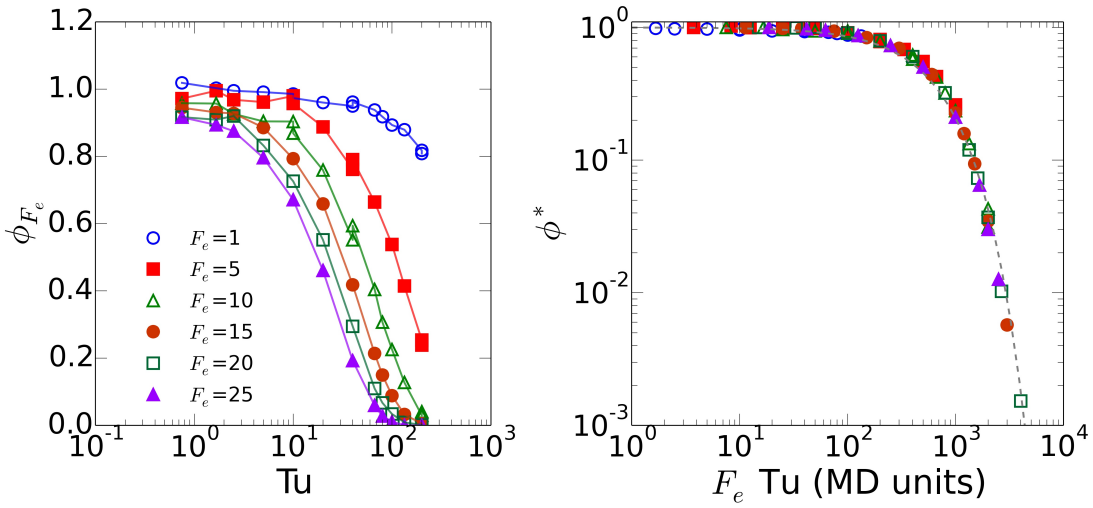

Figure 5.13: Left panel: single particle fraction of 'upstreamers' as function of Tu, for different values of F_e; Pe = 100 is fixed. Full lines are guide to the eye. Right panel: rescaled curves ϕ^* as function of F_e Tu collapse on a master curve. Dashed line is a best fit with an exponential function.

of the external force; Pe=100 is fixed. Whereas *tumblers* (large Tu) cannot leave the channel from its left end, we see that *runners* (small Tu) retain a remarkable capability of moving against the external bias. This is highlighted by an abrupt increase of ϕ_{F_e} as Tu decreases. Clearly, if the external bias is increased, the fraction $\phi^r_{F_e}$ of *runners* able to overcame the bias decreases accordingly, as shown in the left panel of Fig. 5.13. The fraction $\phi^* = \phi_{F_e}/\phi^r_{F_e}$ of total 'upstreamers' with respect to the fraction of *runners* collapses on a master curve when plotted against the product F_eTu. This master curve can be nicely fitted by an exponential function, reported as a dashed line in Fig. 5.13.

We now switch to several particles in Single File conditions, by studying the exit

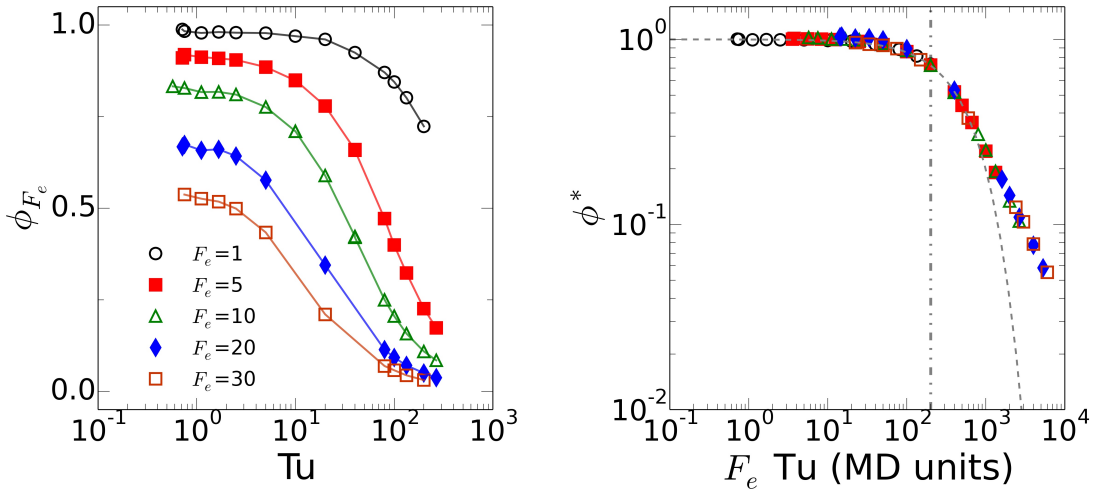

Figure 5.14: Left panel: fraction of 'upstreamers' of $N = 21$ ASF particles for different values of F_e at Pe=100 (MD units are used). Full lines are guide for the eyes. Right panel: same data of the left graph rescaled with respect to the initial amplitude (at zero Tu) and plotted against (F_e Tu). Dashed line is the (exponential) decay of a single particle emptying the channel in the presence of the same biases F_e. Dash-dotted vertical line is the active force of SPP.

probability with the same philosophy. In the left panel of Fig. 5.14 we report again ϕ_{F_e} as function of Tu for different values of the external force; Pe=100 is fixed. The behaviour observed is similar to the single particle case. At small Tu the system is still insensitive to F_e, although the fraction of upstreamers in the interacting system is systematically lower, compared to ϕ_{F_e} for a single particle at the same F_e. For this model, thus, the inability to overpass the preceding swimmer seems to decrease particles' capability to overcome external biases. Anyway, by normalizing again the fraction of upstreamers with respect to the fraction of runners as function of F_eTu, data collapse on a master curve, shown in the right panel of Fig. 5.14. This time the master curve exhibits two characteristic decays depending on the value of the effective force (F_e Tu) with respect to the typical active force $F_a = \mathrm{Pe}\, k_B T/R$ (see the vertical dash-dotted line in Fig. 5.14): if (F_e Tu) >> F_a the bias is too strong for the active particles and the fraction of 'upstreamers' decreases as a power law of (F_e Tu). If, on the other hand (F_e Tu) < F_a the master curve displays an exponential decay that equals the one observed for the single particle in presence of the same bias F_e. This can be explained as follows: as shown in section 5.1, *runners* tends to form clusters more likely than *tumblers* do. These clusters act as dynamically correlated

segments, thus behaving as a single active particle (of bigger size) during the emptying process.

This picture is confirmed by the analysis of the radial distribution function,

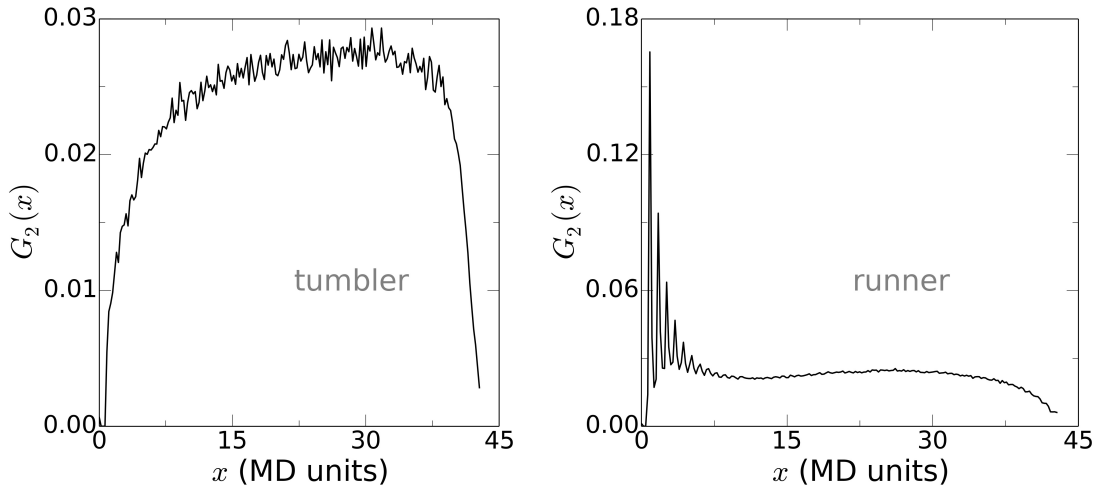

Figure 5.15: Radial distribution function $G_2(x)$, measured at the exit event of a particle at the left boundary for systems of N=21 particles with absorbing boundary conditions, system size L=43 (MD units), Pe=100 and different values of the tumbling number. Left panel: Tu=200 (*tumbler*). Right panel: Tu=0.75 (*runner*).

measured at the exit event of a particle at the left boundary. As visible in Fig. 5.15, *tumblers* leave the system one by one, as the probability to find a particle in the proximity of the boundary is very small. Conversely, $G_2(x)$ for *runners* display the presence of peaks even at the exit event, corresponding again to several aggregated particles exiting together.

We have studied the size of these dynamical clusters again by looking at the number of the peaks of the radial distribution function, for ASF systems of N=21 particles with Pe=100 fixed and different values of Tu and F_e. In the range $1< F_e <30$ considered, the number of peaks measured is fairly constant, and has been averaged to obtain the number of peaks as function of Tu only; results are shown in Fig. 5.16 (full symbols). The size of the dynamical clusters decays as a power law, following an initial plateau: remarkably, this plateau corresponds to the initial plateau observed in the left panel of Fig. 5.16. The decay of the cluster size does not appear to be affected by the presence of the external bias, as it is observed for the same system even in the absence of the external bias (open symbols in the inset of Fig. 5.14). Summarizing, although disadvantaged by the

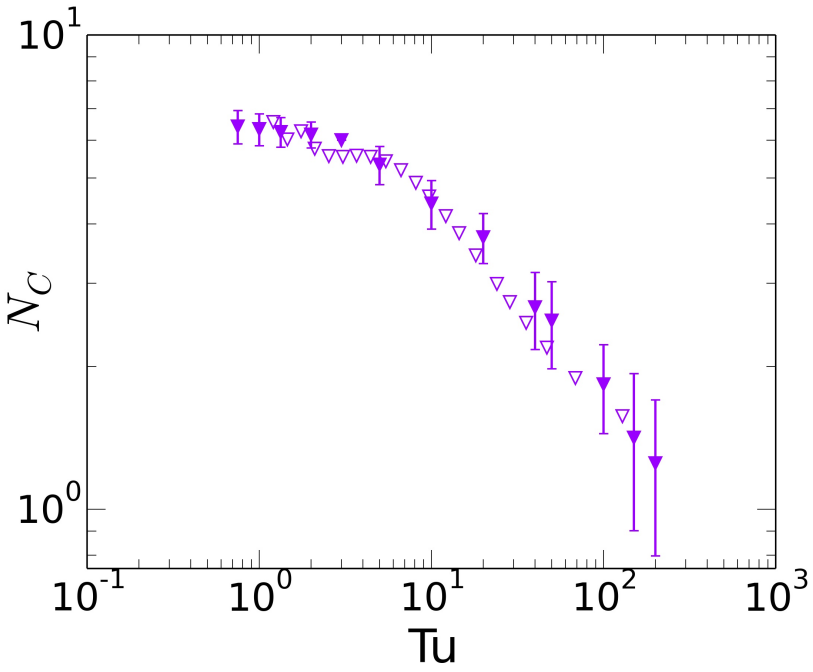

Figure 5.16: Size of the dynamical clusters as a function of Tu, averaged over the same values of F_e (filled triangles) and in the absence of external bias (open triangles).

Single File condition, particles with low Tu are anyway remarkably more capable to overcome an external bias with respect to high-Tu particles. The presence of clusters helps the system to maintain this capability, and when the cluster size begin to decrease, we observe a sudden drop in ϕ_{F_e}.

Conclusions

In this thesis, we have investigated the properties of Single File systems of active and passive particles, devoting particular attention on their behaviours in the presence of absorbing boundaries. In the last years Single File Diffusion has attracted increasing attention, inspired both by its scientific and technological relevance and by the emergence of pioneering experimental investigations, made possible by progresses on micro- and nano-scale fabrication and manipulation. Although relevant advances have shed light on the anomalous character of diffusion in Single File, many basic questions remained open, notably about the role of the boundary conditions.

Motivated by those open challenging problems, we have first studied the dynamical properties of passive Single File systems of point-like particles in presence of two absorbing boundaries. We have introduced the concept of emptying process and we have found the exact solution to this problem using the Reflection Principle method, either in the presence or in the absence of a constant external force. We have also found a solution for the survival probability of a Tagged Particle within the File, based on the (equilibrium) assumption that all the possible exit sequences are equiprobable. This method has then been adapted to calculate the survival probability in the presence of an external constant force. In all cases, we also exploited the trends of the Mean Emptying Times and of the Mean First Passage Times as function of the system size L, the initial number of particles N and the external force, finding the same trend as the single particle MFPT, with respect to L and F_e. The N dependence was observed to be very small: if the system size is fixed, only grows logarithmically.
We have compared numerical simulations of particles of size σ with experimental data of diffusing colloids in microfluidic channels, finding that the SFD model,

although neglecting hydrodynamic interactions, is in very good agreement with experimental findings. Finally, in the case in which the central particle is the only particle absorbed at the boundaries, the numerical study of the survival probability shows that $S(t)$ decay exponentially in time, even when its motion is severely hindered by the other particles. The comparison between the exponential decay constant and the mean first passage time supports this result.

Concerning Active Single File systems, to introduce activity we choose a model of Active Brownian Particles (ABP). In this model activity is due to a constant force, which acts on a direction performing Brownian motion. We studied in details the properties of a single ABP: three relevant timescales emerged, the rotational τ_r, the diffusive τ_D and the active τ_a. From these timescales it is possible to define a dimensionless parameter, the tumbling number Tu=τ_D/τ_r which, together with the well known Péclet number Pe, are sufficient to describe all the properties of the ABP. We devised an analytical relation between Pe and Tu that defines two classes of ABP: *runners* and *tumblers*, characterized by their tendency to perform straight runs or changes of direction, respectively.

This distinction, under Single File condition, leads to profound differences in the collective behaviour of the system. The transition 'runners-to-tumblers' is accompanied by the emergence of (dynamical) clustering, and has been studied numerically, counting the number of peaks of the radial distribution function. Collisions between *runners* are the 'nucleation points' for these aggregates, and are inelastic, while they remain elastic for *tumblers*. This dynamical crossover was tested by checking the validity of the Reflection Principle: we compared the theoretical and the numerical Mean Emptying Times and computed their relative difference, δ. Remarkably, the number of peaks, as function of Pe and Tu, has the same qualitative trend as δ, confirming that clusters formation and size are related to the anomalous collisional dynamics.

Finally, by means of Brownian Dynamics simulations, we studied the fraction of upstreaming particles ϕ_{F_e} as function of Tu (at fixed Pe); we found that *runners* show a remarkable capacity to oppose to the action of an external force. Data for different values of F_e can be rescaled on a master curve, that exhibits two characteristic decays: exponential if $F_e\,\mathrm{Tu} < F_a$ or power law, at least in the range where $F_e\mathrm{Tu}$ is slightly greater than F_a. The interpretation of the capacity to overcome external biases is very intriguing since it may be regarded

as a strategical advantage for *runners* microorganisms moving in confined environments, leading to better chances in food search, exploration or even infections.

Concluding, we have done an extensive and systematic work to establish a coherent and comprehensive theoretical framework on the dynamical properties of passive and active Single File systems, necessary also for comparing analytical results with numerical simulations and experimental data. We also elucidated the role played by the absorbing boundary condition producing, for the first time in this context, a direct comparison between simulations and experiments.
As future perspectives, it would be highly desirable to compare these findings on Active Single File with experimental data on bacteria and algae confined in microfluidic channels. In particular, cluster formation should be checked and the effect of an external bias should be investigated. Even if the realization of such microfluidic chips is within the range of the actual microfabrication techniques, biological factors, such as lack of nutrients, oxygen or light, could make the experimental validation of ASF a troublesome task. Also the anisotropic shape of most of bacteria could be relevant, as inside a very tight channel they would not be able to freely change their direction of motion. Anyhow, we think that the analytical and numerical work presented in this thesis can be profitably exploited as a valid starting point for the comparison of the experimental data with a theoretical model.
It would be also very interesting to study mixtures of passive and active particles, or even of bi- or poly-disperse active suspension, in Single File conditions, which is a totally unexplored topic: even in the case of mixtures of purely passive particles, not much is known. Mixtures of passive and active particles in bulk has been used to investigate the microrheology of active suspensions: it would be useful to check the effects of confinement on such properties. We finally believe that the route traced by the approach used in this thesis can lead to consistent advances in the knowledge of these systems.

Appendix A

Numerical simulations details

In this Appendix we briefly describe the numerical schemes used in our simulations. We used Brownian Dynamics or Molecular Dynamics simulations, which essential are two similar ways to provide a numerical integration of the equation of motion. A first scheme is built for point-like particles. In this case we could not use an interaction potential, which has a characteristic lengthscale, and we had to find another way to guarantee the order preservation. Between the collisions, we used a simple Brownian Dynamics scheme

$$x(t+\Delta t) = (k_B T)^{-1} D_t \left(F_e + \mu(t)\right) \Delta t \qquad x(0) = x_0$$

where D_t=0.1 is the diffusion coefficient, T=1 is the temperature of the heath bath, m=1 is the particle mass and $\Delta t = 10^{-3}$ is the elementary time-step; all the quantities are in MD reduced units. The random noise $\mu(t)$ is a normal pseudorandom number, obeying the fluctuation-dissipation theorem.

$$\langle \mu(t)\mu(t') \rangle = \sqrt{2D_t}\delta(t-t')$$

After a single time step, we check the order between each couple of particles, eventually restoring it switching the positions, as if an elastic collision had occurred; we repeat the check until the global order is restored.
We have also realized simulations of particle with a certain size σ, using a second simulation scheme, in which the exclusion is provided through a truncated-shifted

Lennard-Jones interaction potential [61]

$$U_{ij} = \begin{cases} 4\epsilon \left[\left(\frac{\sigma}{r_{ij}} \right)^{12} - \left(\frac{\sigma}{r_{ij}} \right)^{6} \right] + \epsilon & r_{ij} < \sigma \cdot 2^{1/6} \\ 0 & r_{ij} \geq \sigma \cdot 2^{1/6} \end{cases} \tag{A.1}$$

with σ=1 and ϵ=1 (MD units), while maintaining the Brownian Dynamics between the collisions.

We implement equivalent simulation schemes for self propelled particles, integrating the following equations of motion

$$\begin{cases} x(t+\Delta t) = (k_B T)^{-1} D_t \left(F_a \cos(\theta(t)) + F_e + \mu(t) \right) \Delta t & x(0) = x_0 \\ \theta(t+\Delta t) = (k_B T)^{-1} D_r \mu_R(t) \Delta t & \theta(0) = \theta_0 \end{cases}$$

where D_t=0.01 and D_R are the translational and rotational diffusion coefficients, T=1 is the temperature of the heath bath, m=1 is the particle mass and $\Delta t = 10^{-3} - 10^{-4}$ is the elementary time-step; all the quantities are in MD reduced units. The random noises $\mu(t)$ and $\mu_R(t)$ are normal independent pseudorandom numbers, each of them satisfying the fluctuation-dissipation theorem.

$$\langle \mu(t)\mu(t') \rangle = \sqrt{2D_t}\delta(t-t')$$

$$\langle \mu_R(t)\mu_R(t') \rangle = \sqrt{2D_r}\delta(t-t')$$

Between collision, usually Brownian Dynamics integration is used, but for high values of F_a a more accurate MD Velocity-Verlet scheme has also been implemented.

For point-like particles, collisions are treated following the same procedure described above, while to investigate the structural properties of the system we employed the second simulation method.

This two simulation methods give the same results in the dilute limit, as showed in Fig. A.1: the dilute limit can be achieved letting $\sigma \to 0$ (left panel) or using of a very large survival region $L \to \infty$ (right panel).

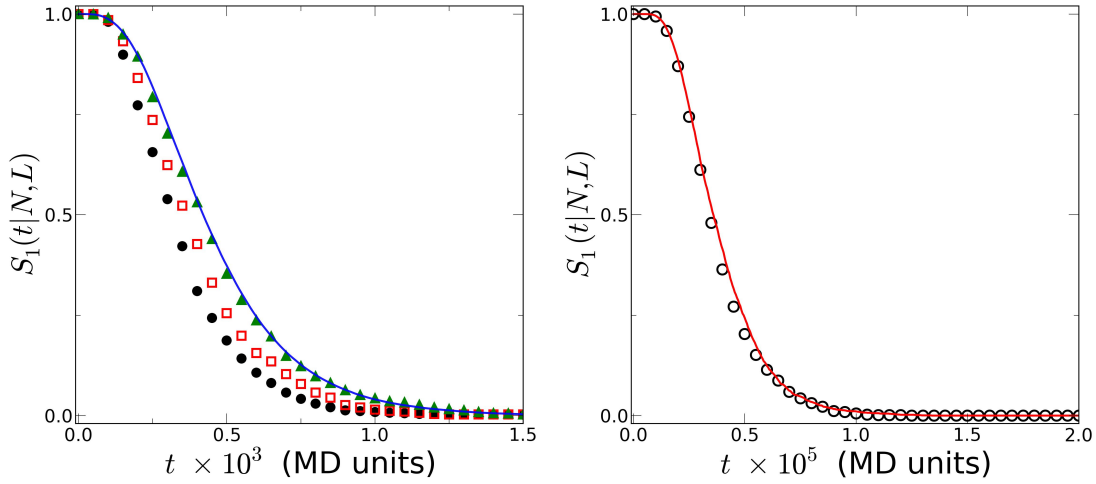

Figure A.1: Comparison between the two simulation methods described above in the dilute limit, checking the emptying probability $S_1(t|N,L)$. Left panel: dilute limit for $\sigma \to 0$, N=5 particles, L=12 (MD units), Pe=50 and Tu=200. The full line is the result of the first scheme, while the symbols are the result of the second, for different values of σ: full dots for σ=1, open squares for σ=0.5, full triangles for σ=0.1. Right panel: dilute limit for $L \to \infty$, N=5 particles, L=100 (MD units), Pe=100 and Tu=200. The full line is the result of the first scheme, while the symbols are the result of the second for σ=1.

Appendix B

Experimental details

In this Appendix we briefly describe the details of the experimental setup and of the data analysis used to obtain results reported in section 3.6. The microfluidic chip and the rest of experimental setup were realized at the Cavendish Laboratory, the Department of Physics of the University of Cambridge, in collaboration with Dr. Stefano Pagliara, a research fellow in the group of Prof. Keyser; data acquisition was also taken there. The chip is based on a novel approach to fabricate arrays of polydimethylsiloxane (PDMS) sub-micrometric channels of different height by using platinum wires deposited via Focused Ion Beam (FIB) as molds for soft lithography. An array of eight Platinum parallel wires, with different cross section, were deposited on a Silicon substrate via FIB; then, conventional photolithography is carried out to realize the rest of the chip. A PDMS replica of the resulting device was realized by standard replica molding. The resulting chip [161,162] is made of two inlet and outlet 16 μm thick reservoirs separated via a PDMS barrier and connected by the sub-micrometric channels (length 5 μm), obtained as negative replica of the Platinum wire, plus two lateral channels of 100 μm width and 16 μm thickness, to facilitate hydrostatic pressure equilibration between the two reservoirs. PDMS is bonded to a glass slide by exposing both surfaces to oxygen plasma treatment (8.5 s exposure to 2.5 W plasma power, Plasma etcher, Diener), thus improving adhesion quality and hydrophilicity.
Colloidal suspensions of 500 nm polystyrene particles (Polyscience) are made in a 5 mM KCl solution. Ultrapure water (Synergy System, Millipore Corp.) is used in the buffer preparation and the buffer is filtered twice through mixed cellulose esters (Medical Millex-GS Filter, 0.22 μm, Millipore Corp.). Finally, a dilution of

colloidal suspension in buffer is realized with a volume/volume ratio of 1:100. To manipulate colloids, holographic optical tweezers were used. An Ytterbium laser fiber (YLM-5-1064-LP, IPG Photonics) was passed through a beam expander and directed towards a phase-only spatial light modulator (SLM, LCOS X10468, Hamamatsu); the beam was then coupled to a 100x oil immersion objective (1.4 N.A., UPLSAPO, Olympus). Illumination was provided from above by a LED light (Thorlabs MWLED); the transmitted light was collected by the objective and reflected towards a CCD camera (The Imaging Source DMK 31BF03) by a dichroic mirror. A detailed scheme of the whole setup is reported in Fig. B.1.

The optical trap is generated and controlled using a custom-made program,

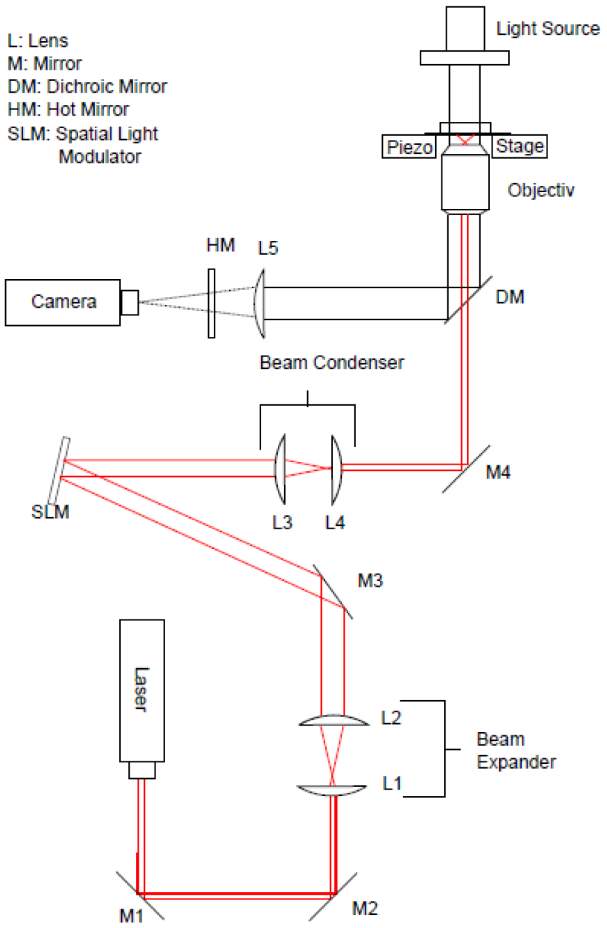

Figure B.1: Scheme of the experimental setup, from [183].

based on Labview; actually the whole measure, from positioning to laser control to image acquisition, was controlled and automated using a Labview program.

Particle tracking has been carried out offline through a specific custom-made program realized in IDL (Interactive Data Language), rooted on a reliable and well known tracking procedure [163]. Each single frame was processed by using a high pass filter in the frequency domain, to enhance the contrast between particles in the focal plane and the background. Particle location was identified as the local brightness maximum, then the trajectories were reconstructed by using a minimization algorithm, based on the probability distribution of a system of non-interacting Brownian particles. Although far from the ideal non-interacting case, the tracking algorithm works really well also in this case, and trajectories reconstructed from the image sequences are reliable. We recorded and analyzed 285 different realizations of the emptying process of N=3-6 particles, calculating each time the emptying time and the Mean Square Displacement, within the time window in which the last particle is alone. Specifically, the MSD was measured as

$$MSD(n\Delta t) = \frac{1}{N_f}\sum_{i}^{N_f}\left(x(t_i + n\Delta t) - x(t_i)\right)^2$$

where Δt=33 ms is the time interval between two consecutive frames (set by the acquisition frame rate), N_f is the number of frames which have a time difference $n\Delta t$, fixed for each n to be half the length of the available trajectory. Within the same channel, an average MSD was then computed to extract the diffusion coefficient. The estimated diffusion coefficients are in the range 0.07-0.25 μm^2, compatible with independent measurement [184]. These estimates are fundamental to compare the emptying times τ between each channel, through the rescalement

$$t \to t' = \frac{D_k\, t}{R^2}$$

Due to limited statistics the D_k estimates are quite rough; thus an alternative method was devised. As already mentioned in section 3.6, the second rescaling method

$$t \to t'' = \frac{T_1{}^{(num)}}{T_1^k}\, t$$

is more reliable, because $T_1{}^{(num)}$ can be calculated with very high accuracy, as the limit is set only by the machine precision, and a good estimate of T_1^k can be obtained from a limited set of data. Surprisingly, the two rescalement procedure gives compatible results, both in the calculation of the emptying probability and

of the central particle survival probability, calculated as

$$S(t|L) = \mathrm{Prob}\Big\{\tau > t|L\Big\} \tag{B.1}$$

where τ is the (properly rescaled) emptying time, i.e. the minimum time at which the channel of length L is empty. This property is thus quite robust. Finally, errors estimation in these measures is a complicated task, as we have many sources of uncertainty, arising from limits in the acquisition setup, in the tracking algorithm and in the estimation of the diffusion coefficients. We limited, for now, to give a rough estimate of the error, considering $S(t)$ as the result of a counting process. For each time t we effectively count how many emptying times are bigger than t, say N_t. Thus, we assign the square root of that number as error estimation, normalized on the total number of measurements $\sqrt{N_t}/N$.

Appendix C

Spatial correlations in Single File Diffusion

In this Appendix we briefly report a short numerical study on spatial correlations in a SFD system. We want to characterize the following quantity for a Single File system of N passive particle with natural boundary conditions:

$$C(x_C - x_L, x_C) = \frac{\langle (x_C - x_L - (x_C^0 - x_L^0) \cdot (x_C - x_C^0) \rangle}{\sqrt{\langle (x_C - x_L - x_C^0 - x_L^0)^2 \rangle} \cdot \sqrt{\langle (x_C - x_C^0)^2 \rangle}} \tag{C.1}$$

where x_C, x_L are the coordinate of the central and leftmost (i.e. the first) particles, respectively. This quantity can provide a different characterization of the SF dynamics, as showed also in [137]. We have first performed Brownian Dynamics simulations for systems of N=75 particles with size $\sigma = 1$, equispaced initial conditions and different initial densities ρ_0; results are shown in Fig. C.1. We have observed that the different regimes (diffusive, subdiffusive and collective diffusive) correspond to different behaviours of this correlation function (see Fig. 3.19 for comparison): particularly

- in the initial diffusive regime we observe $C(x_C - x_L, x_C) = C_0$
- in the subdiffusive regime we observe a decay of $C(x_C - x_L, x_C)$
- in the collective diffusion regime we reach again a constant value $C(x_C - x_L, x_C) = C_1$

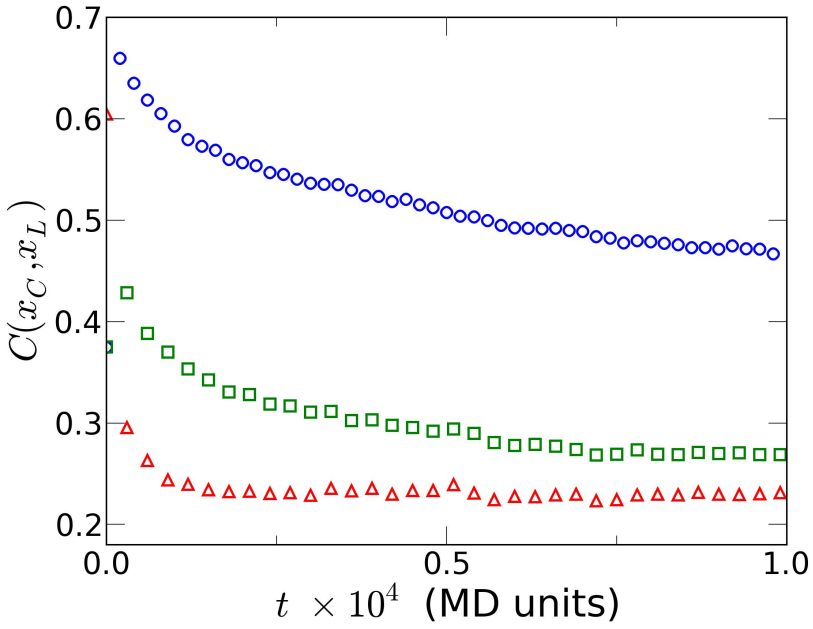

Figure C.1: $C(x_C - x_L, x_C)$ from numerical simulations, for a system of N=75 particles with different initial densities: circles ρ_0=0.1, squares ρ_0=0.3, triangles ρ_0=0.75.

The expression C.1 can be simplified to:

$$C(x_C - x_L, x_C) = \frac{MSD(x_C) - \langle (x_C - x_C^0) \cdot (x_L - x_L^0) \rangle}{\sqrt{MSD(x_C) + MSD(x_L) - 2\langle (x_C - x_C^0) \cdot (x_L - x_L^0) \rangle} \sqrt{MSD(x_C)}}$$

We want to give prediction of the constant values observed in the two diffusive regimes. First, we focus on the initial diffusion, when there is still no interaction between particles. Using $MSD(x_C) = MSD(X_L) = 2Dt$ and the absence of correlation between the particles, we obtain

$$C(x_C - x_L, x_C) = \frac{2Dt}{\sqrt{4Dt}\sqrt{2Dt}} = \frac{2}{\sqrt{8}} \tag{C.2}$$

which is good agreement with numerical results.

To estimate the plateau value in the collective diffusion regime, we calculate the averages with the Reflection Principle Method [145] (see section 2.2.1 for details). The total probability density $P(\mathbf{x}, t|\mathbf{x}^0)$ is given by Eq. (2.2). The correlation $\langle (x_C - x_C^0) \cdot (x_L - x_L^0) \rangle$ will be given by

$$\langle (x_C - x_C^0) \cdot (x_L - x_L^0) \rangle = \int_A (x_C - x_C^0) \cdot (x_L - x_L^0)\, P(\mathbf{x}, t|\mathbf{x}^0) d\mathbf{x} \tag{C.3}$$

where A is the section of the configurational space available for integration. Unlike the emptying process (see section 3.2), in this case we cannot permute the integration domains, as we have lost the symmetry of the integrand. The above integral becomes very complicated even in the case of three particles. We can avoid the analytical complexity by performing numerical integration, which unfortunately limits the applicability of this method to N=3.

In Fig. C.2, we show a comparison between numerical simulations (symbols) and

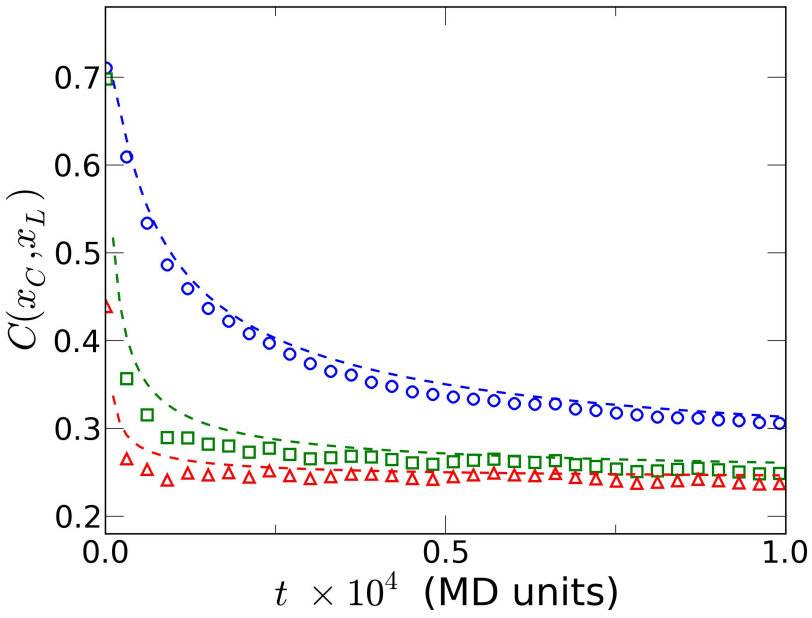

Figure C.2: Comparison between numerical simulations (symbols) and the numerical integration of the averages in Eq. (C.1) (dashed lines), for a system of N=3 particles with different initial densities: circles ρ_0=0.1, squares ρ_0=0.3, triangles ρ_0=0.75.

the numerical integration of the averages in Eq. (C.1) (dashed lines). As visible, lines slightly overestimate this correlations with respect to numerical data, but the overall accordance is quite good.

Recently, in [185] experimental measures of correlations of silica particles in microfluidic channels were performed; correlations were motivated as effect of hydrodynamic interactions. Here we have presented a first partial proof that this kind of behaviour can be motivated simply by order preservation; an experimental measure of this quantity will certainly bring a more concrete evidence of the correctness of this argument.

Appendix D

Survival probability of single Brownian particle

In this Appendix we list some technical details about the survival probability $S(t|x_0, L)$ of a single Brownian particle; in particular, we report the detailed calculation for $S(t|x_0, L)$ of a Brownian particle in the presence of two absorbing boundary conditions and of a constant external force.
The 'emptying process' we have introduced in Chapter 3 is the N-particle generalization of the usual survival probability

$$S(t|x_0) = \int_{b_1}^{b_2} p_1(x, t|x_0) \tag{D.1}$$

as they are both the probability that the system (a particle or an ensemble of particles) is in a particular region of the configurational space from the initial time t_0 to time t. Since we are interested in the exit event of a particle, it is useful to recall that the *first passage time density* of a Brownian particle is defined as

$$f(t|L, x_0) = Prob(t \leq t^* \leq t + dt|L, x_0) = -\frac{dS}{dt}(t|x_0) \tag{D.2}$$

that is the probability distribution functions of exit times t^*; it has a very simple relation with $S(t|x_0)$ given by

$$S(t|x_{i,0}) = P(t^* > t) = \int_t^\infty -\frac{dS}{dt'}(t'|x_0)dt' \tag{D.3}$$

On the other hand, it is also related in a very simple way to the *exit probability*, which is the probability that the system is out of the selected region of the configurational space

$$1 - S(t|x_{i,0}) = Prob(t^* < t) = \int_0^t -\frac{dS}{dt'}(t'|x_0)dt' \tag{D.4}$$

The relations we have listed so far are general. In the absence of any external force, the probability distribution function of a single Brownian particle in the presence of two absorbing boundaries at $x = b_1$ and $x = b_2$ is

$$p_1(x,t|x_0) = \frac{2}{(b_2 - b_1)} \sum_{n=0}^{\infty} \sin\left(\frac{n\pi(x - b_1)}{b_2 - b_1}\right) \sin\left(\frac{n\pi(x_0 - b_1)}{b_2 - b_1}\right) e^{-\frac{D_t n^2 \pi^2 t}{(b_2 - b_1)^2}} \tag{D.5}$$

By using the definition, the survival probability inside [-$L/2$, $L/2$] reads

$$S(t|x_{i,0}, L) = \frac{4}{\pi} \sum_{n=0}^{\infty} \frac{\sin\left(\frac{(2n+1)\pi(x_{i,0}+L/2)}{L}\right)}{(2n+1)} e^{-\frac{D_t(2n+1)^2\pi^2 t}{L^2}} \tag{D.6}$$

In the case of random initial conditions between [-$L/2$,$L/2$], Eq. D.6 simplify to

$$S(t|L) = \frac{8}{\pi^2} \sum_{n=0}^{\infty} \frac{1}{(2n+1)^2} e^{-\frac{D_t(2n+1)^2\pi^2 t}{L^2}} \tag{D.7}$$

more generally, if the initial condition is chosen at random in a region [-$L_0/2$, $L_0/2$], with $L_0 \leq L$, the survival probability reads

$$S(t|L, L_0) = \frac{4}{\pi^2} \frac{L}{L_0} \sum_{n=0}^{\infty} \frac{\sin\left(\frac{\pi \frac{L_0}{2}(2n+1)+\pi n L}{L}\right) + \cos\left(\frac{\pi(2n+1)\frac{L_0 - L}{2}}{L}\right)}{(2n+1)^2} e^{-\frac{D_t(2n+1)^2\pi^2 t}{L^2}} \tag{D.8}$$

which reduces to D.7 for $L_0 = L$.

We consider now the case of a point particle in contact with a thermal bath subjected to a constant force F_e; in the overdamped limit, the Langevin equation is given by

$$\frac{dx}{dt}(t) = \frac{F_e}{m\gamma_t} + \mu(t) \tag{D.9}$$

$\mu(t)$ is a Gaussian white noise satisfying fluctuation-dissipation $\langle \mu(t) \rangle = 0$, $\langle \mu(t)\mu(t') \rangle = \sqrt{2D_t}\delta(t - t')$. Using the standard method, we switch to the Fokker-Planck equa-

tion

$$\frac{\partial}{\partial t}p_1(x,t|x_0) = -\frac{F_e}{m\gamma_t}\frac{\partial}{\partial x}p_1(x,t|x_0) + D_t\frac{\partial^2}{\partial x^2}p_1(x,t|x_0) \tag{D.10}$$

As in the free case, we can solve the equation using the method of the separation of variables $p_1(x,t|x_0) = X(x)\cdot T(t)$; dividing both sides for $X(x)\cdot T(t)$ we obtain

$$D_t^{-1}\frac{T'(t)}{T} = -2\Gamma\frac{X'(x)}{X} + \frac{X''(x)}{X} = -\lambda^2 \tag{D.11}$$

where $\Gamma = F_e/2m\gamma_t D_t$. The two equation must be solved separately: the time equation has solution

$$T(t) = T_\lambda e^{-\lambda^2 D_t t} \tag{D.12}$$

We imposed the separation constant to be positive such that the time equation is not divergent in the long time limit. The spatial equation is

$$X''(x) - 2\Gamma X'(x) + \lambda^2 X(x) = 0 \tag{D.13}$$

this is a second order linear differential equation with constant coefficient: the solution depends from the solution of the characteristic equation

$$y^2 - 2\Gamma y + \lambda^2 = 0 \qquad\qquad y_{1/2} = \Gamma \pm \frac{1}{2}\sqrt{4\Gamma^2 - 4\lambda^2} \tag{D.14}$$

The general solution is

$$X(x) = c_1 \exp(\Gamma\, x)\, \exp\left(\frac{1}{2}\sqrt{4\Gamma^2 - 4\lambda^2}\, x\right) + c_2 \exp(\Gamma\, x)\, \exp\left(-\frac{1}{2}\sqrt{4\Gamma^2 - 4\lambda^2}\right) \tag{D.15}$$

We choose Γ such that the discriminant is always negative

$$\lambda_{min} > \Gamma \tag{D.16}$$

The solution (D.15) becomes

$$X(x) = A_\lambda \exp(\Gamma\, x) \cos\left(\frac{1}{2}\sqrt{4\lambda^2 - 4\Gamma^2}\, x\right) + B_\lambda \exp(\Gamma\, x) \sin\left(\frac{1}{2}\sqrt{4\lambda^2 - 4\Gamma^2}\, x\right) \quad \text{(D.17)}$$

We have now to impose the absorbing boundary conditions at the point b_1 and b_2: we switch to the variables

$$z = x - b_1$$

$$L^* = b_2 - b_1$$

In this way, $z \in [0, L]$ and the BC turn out to be the same of the free case: in particular

$$\sin\left(\frac{1}{2}\sqrt{4\lambda^2 - 4\Gamma^2}\, L^*\right) = 0 \quad \text{(D.18)}$$

that gives

$$\lambda = \sqrt{\left(\frac{n\pi}{L^*}\right)^2 + \Gamma^2} \quad \text{(D.19)}$$

This tells us that we can choose any Γ, and the condition (D.16) remains valid. Following the free case we obtain

$$P(z, t|z_0) = \sum_n A_n \exp(\Gamma\, z) \sin\left(\frac{n\pi}{L^*} z\right) \exp\left(-D_t \left[\left(\frac{n\pi}{L^*}\right)^2 + \Gamma^2\right] t\right) \quad \text{(D.20)}$$

We have now to impose the initial conditions:

$$P(x, t \to 0|x_0) = \sum_n A_n \exp(\Gamma\, x) \sin\left(\frac{n\pi}{L^*} x\right) = \delta(x - x_0) \quad \text{(D.21)}$$

To find A_n, we have to invert the Fourier series, using the correct orthonormal base

$$\begin{aligned} A_n &= \frac{2}{L^*} \int_0^{L^*} \exp(-\Gamma\, z) \sin\left(\frac{n\pi}{L^*} z\right) \delta(z - z_0) dz \\ &= \frac{2}{L^*} \exp(-\Gamma\, z_0) \sin\left(\frac{n\pi}{L^*} z_0\right) \end{aligned} \quad \text{(D.22)}$$

The solution is now

$$P(z,t|z_0) = \frac{2}{L^*}\sum_n \exp(\Gamma\, z)\exp(-\Gamma\, z_0)\sin\left(\frac{n\pi}{L^*}z\right) \sin\left(\frac{n\pi}{L^*}z_0\right)\exp\left(-D_t\left[\left(\frac{n\pi}{L^*}\right)^2+\Gamma^2\right]\,t\right) \quad \text{(D.23)}$$

Coming back to the original case

$$P(x,t|x_0) = \frac{2}{b_2-b_1}\sum_n \exp(\Gamma\,(x-b_1))\exp(-\Gamma\,(x_0-b_1))\sin\left(\frac{n\pi}{b_2-b_1}(x-b_1)\right) \sin\left(\frac{n\pi}{b_2-b_1}(x_0-b_1)\right)\exp\left(-D_t\left[\left(\frac{n\pi}{b_2-b_1}\right)^2+\Gamma^2\right]\,t\right) \quad \text{(D.24)}$$

In the case of our interest, $b_1 = -L/2$, $b_2 = L/2$

$$P(x,t|x_0) = \frac{2}{L}\sum_n \exp(\Gamma\,(x+L/2))\exp(-\Gamma\,(x_0+L/2))\sin\left(\frac{n\pi}{L}(x+L/2)\right) \sin\left(\frac{n\pi}{L}(x_0+L/2)\right)\exp\left(-D_t\left[\left(\frac{n\pi}{L}\right)^2+\Gamma^2\right]\,t\right) \quad \text{(D.25)}$$

We now simply use the definition to calculate $S(t|x_0)$: we integrate between -$L/2$ and $L/2$

$$\int_{-L/2}^{L/2}\exp(\Gamma\,(x+L/2))\sin\left(\frac{n\pi}{L}(x+L/2)\right)dx = \frac{n\pi\,(1-\exp(\Gamma L)\cos(n\pi))}{(\Gamma L)^2+(n\pi)^2} \quad \text{(D.26)}$$

and we obtain

$$S(t|x_0) = \frac{2}{L}\sum_n \frac{n\pi\,(1-\exp(\Gamma L)\cos(n\pi))}{(\Gamma L)^2+(n\pi)^2}\exp(-\Gamma\,(x_0+L/2)) \sin\left(\frac{n\pi}{L}(x_0+L/2)\right)\exp\left(-D_t\left[\left(\frac{n\pi}{L}\right)^2+\Gamma^2\right]\,t\right) \quad \text{(D.27)}$$

If we choose random uniform initial position inside [-$L/2$, $L/2$]

$$S(t|L,\Gamma) = 2\sum_n (n\pi)^2\frac{\left(1-e^{\Gamma L}\cos(\pi n)\right)\left(1-e^{-\Gamma L}\cos(\pi n)\right)}{\left[(\Gamma L)^2+(n\pi)^2\right]^2}\,e^{\left(-D_t\left[\left(\frac{n\pi}{L}\right)^2+\Gamma^2\right]t\right)} \quad \text{(D.28)}$$

more generally, if the initial condition is chosen at random in a region [-$L_0/2$, $L_0/2$], with $L_0 \leq L$, the survival probability reads

$$S(t|L,L_0,\Gamma) = \frac{2L}{L_0}\sum_n (n\pi)^2 \frac{\left(1-e^{\Gamma L}\cos(\pi n)\right)}{\left[(\Gamma L)^2+(n\pi)^2\right]^2}\left[e^{-\Gamma(L-L_0)}\left(2L\Gamma\sin\left(\tfrac{n\pi(L-L_0)}{L}\right)n\pi\cos\left(\tfrac{n\pi(L-L_0)}{L}\right)\right)+\right.$$
$$\left.-e^{-\Gamma(L+L_0)}\left(-2L\Gamma\sin\left(\tfrac{n\pi(L+L_0)}{L}\right)+n\pi\cos\left(\tfrac{n\pi(L+L_0)}{L}\right)\right)\right]e^{\left(-D_t\left[\left(\frac{n\pi}{L}\right)^2+\Gamma^2\right]t\right)} \quad \text{(D.29)}$$

which reduces to D.28 for $L_0 = L$. A straightforward integration of the survival probability over time leads to the analytical form of the MFPT: we report the simplest case of $L = L_0$

$$T_1(L,\Gamma) = 2\frac{4L^2}{D_t}\sum_n (n\pi)^2 \frac{\left(1-e^{\Gamma L}\cos(\pi n)\right)\left(1-e^{-\Gamma L}\cos(\pi n)\right)}{\left[(\Gamma L)^2+(n\pi)^2\right]^3} \quad \text{(D.30)}$$

Although this solution is exact and analytical is rather formal, and one cannot tell how of this quantity behaves varying L or Γ at first sight. In Fig. D.1, we

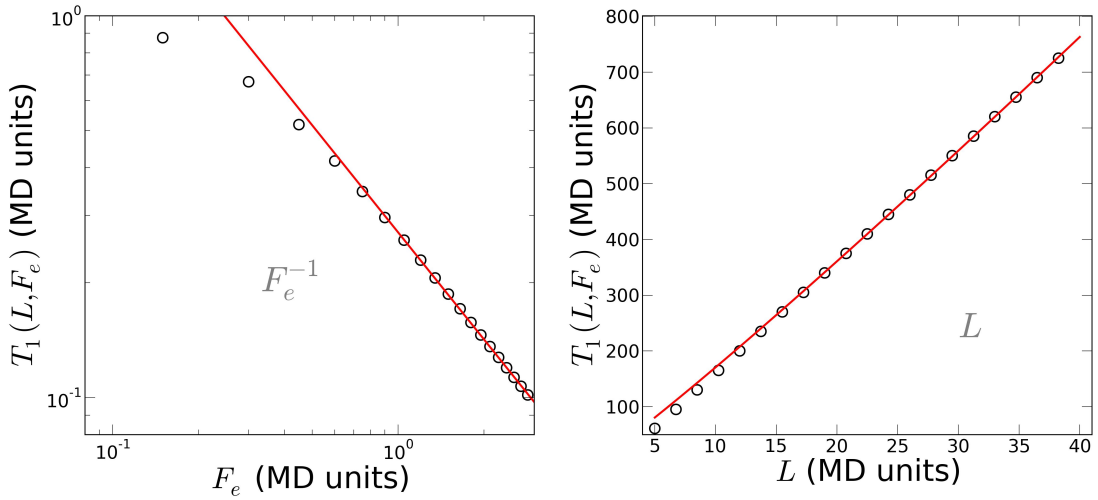

Figure D.1: MFPT of a Brownian particle in presence of a constant external force, Eq. (D.30) Left panel: Log-log plot of the MFPT, normalized over $T_1(N,L,F_e=0)$, as function of F_e, absorbing boundaries at L=10 (MD units): open circles are data from numerical simulations, the line is the best fit with a power law, $F_e^{\bar{\zeta}}$, $\bar{\zeta}$=-1. Right panel: MFPT as function of L, for a fixed F_e=0.5 (MD units): open circles are data from numerical simulations, the line is the best fit with a power law, $L^{\bar{\alpha}}$, $\bar{\alpha}$=1.

plot Eq. (D.30) as function of F_e (left panel) and L (right panel). As function of the external force, $T_1(L,\Gamma)$ show a power-law behaviour F_e^{-1} for sufficiently high F_e; a good approximation of this threshold can be $F_e R > k_B T$, i.e Brownian

motion cannot oppose to the bias. As function of L, the MFPT show a linear behaviour, in contrast with the L^2 behaviour of a Brownian particle.
Finally, we calculate the exit-side probability for a single Brownian particle in the absence or in the presence of a constant external force. Given a Brownian particle in one dimension, we ask what is the probability to exit from one side of the channel. We can answer this quite easily by calculating the *hitting probability*

$$H(x^*|x_0) = \int_0^\infty j(x,t|x_0)|_{x=x^*}\, dt = \int_0^\infty -D_t \left.\frac{\partial p(x,t|x_0)}{\partial x}\right|_{x=x^*} dt \qquad \text{(D.31)}$$

at the end of the channel x^* =-$L/2$,$L/2$. We apply (D.31) using the the probability function D.5 and we obtain

$$H(-L/2|x_0) = \frac{2}{\pi}\sum_{n=1}^{\infty} \frac{\sin\left(\frac{n\pi(x_0+L/2)}{L}\right)}{n} \qquad \text{(D.32)}$$

Choosing for example $x_0 = 0$, we obtain $H(-L/2|x_0) = 1/2$, as expected. Clearly, $H(L/2|x_0) = 1 - H(-L/2|x_0)$.
In the presence of a constant external force, we apply again (D.31) using the this probability function and we obtain

$$H(-L/2|x_0) = \frac{2}{L}\sum_{n=1}^{\infty} n\pi \exp\left(-\Gamma\left(x_0 + L/2\right)\right) \sin\left(\frac{n\pi}{L}(x_0 + L/2)\right) \frac{1}{(n\pi)^2 + \Gamma^2} \qquad \text{(D.33)}$$

Bibliography

[1] J.B. Perrin. *Atoms.* Constable & Company Ltd London, 1916.

[2] http://www.rowland.harvard.edu/labs/bacteria/index.php.

[3] E. Frey and K. Kroy. Brownian motion: a paradigm of soft matter and biological physics. *Ann. Phys. (Leipzig)*, 14:20–50, 2005.

[4] J.P. Bouchaud and A. Georges. Anomalous diffusion in disordered media: statistical mechanisms, models and physical applications. *Phys. Rep.*, 195:127–293, 1990.

[5] J. Kärger and M. Ruthven. *Diffusion in Zeolites and in Other Microporous Solids.* Wiley, New York, 1992.

[6] J. Caro and M. Noack. Zeolite membranes – recent developments and progress. *Microporous and Mesoporous Materials*, 115:215–233, 2008.

[7] M. C. Daniel and D. Astruc. Gold nanoparticles: assembly, supramolecular chemistry, quantum-size-related properties, and applications toward biology, catalysis, and nanotechnology. *Chem. Rev.*, 104:293–346, 2004.

[8] A. Corma. From microporous to mesoporous molecular sieve materials and their use in catalysis. *Chem. Rev.*, 97:2373–2419, 1997.

[9] J. J. Kasianowicz, E. Brandin, D. Branton, and D. W. Deamer. Characterization of individual polynucleotide molecules using a membrane channel. *Proc. Natl. Acad. Sci.*, 93:13770, 1996.

[10] A. Meller, L. Nivon, and D. Branton. Voltage-driven DNA translocations through a nanopore. *Phys. Rev. Lett.*, 86:3435, 2001.

[11] C. Dekker. Solid-state nanopores. *Nature nanotechnology*, 2:209, 2007.

[12] P.C. Bressloff and J.M. Newby. Stochastic model of intracellular transport. *Rev. Mod. Phys.*, 85:135–196, 2013.

[13] V. Schaller, C. Weber, C. Semmrich, E. Frey, and A. R. Bausch. Polar patterns of driven filaments. *Nature*, 467:73–77, 2010.

[14] L. Angelani, R. Di Leonardo, and G. Ruocco. Self-starting micromotors in a bacterial bath. *Phys. Rev. Lett.*, 102:048104, 2009.

[15] T. Vicsek and A. Zafeiris. Collective motion. *Phys. Rep.*, 517:71–140, 2012.

[16] A. Puglisi, V. Loreto, U. M. B. Marconi, and A. Vulpiani. Kinetic approach to granular gases. *Phys. Rev. E.*, 59:5582, 1999.

[17] J. Toner and Y. Tu. Long-Range Order in a Two-Dimensional Dynamical XY Model: How Birds Fly Together. *Phys. Rev. Lett.*, 75:4326, 1995.

[18] R. Voituriez, J. F. Joanny, and J. Prost. Spontaneous flow transition in active polar gels. *Europhys. Lett.*, 70:404, 2005.

[19] A.P. Berke, L. Turner, H. C. Berg, and E. Lauga. Hydrodynamic attraction of swimming microorganisms by surfaces. *Phys. Rev. Lett.*, 101:038102, 2008.

[20] J. Männik, R. Driessen, P. Galajda, J. E. Keymer, and C. Dekker. Bacterial growth and motility in sub-micron constrictions. *Proc. Nat. Acad. Sci.*, 106:14861–14866, 2009.

[21] A. Hodgkin and R. Keynes. The potassium permeability of a giant nerve fibre. *J. Physiol.*, 128:61, 1955.

[22] E. J. A. Lea. Permeation through long narrow pores. *J. Theor. Biol.*, 5:102, 1963.

[23] P.A. Rosenberg and A. Finkelstein. Water permeability of gramicidin a-treated lipid bilayer membranes. *J. Gen. Physiol.*, 72:341, 1978.

[24] M. O. Jensen, D. W. Borhani, K. Lindorff-Larsen, P. Maragakis, V. Jogini, M. P. Eastwood, R. O. Dror, and D. E. Shaw. Principles of conduction and hydrophobic gating in K^+ channels. *Proc. Natl. Acad. Sci*, 107:5833–5838, 2010.

[25] K. Hahn, J. Kärger, and V. Kukla. Single-file diffusion observation. *Phys. Rev. Lett.*, 76:2762, 1996.

[26] Q. H. Wei, C. Bechinger, and P. Leiderer. Single file diffusion of colloids in one-dimensional channel. *Science*, 287:625–627, 2000.

[27] B. Lin, M. Meron, B. Cui, S.A. Rice, and H. Diamant. From random walk to single file diffusion. *Phys. Rev. Lett.*, 94:216001, 2005.

[28] B. Lin, B. Cui, J.H. Lee, and J. Yu. Hydrodinamic couplig in diffusion of quasi-one-dimensional brownian particles. *Europhys. Lett.*, 57:724, 2002.

[29] C.Y. Chou, B.C. Eng, and M. Robert. One-dimensional diffusion of colloids in polymer solutions. *J. Chem. Phys.*, 124:044902, 2006.

[30] C. Lutz, M. Kollmann, P. Leiderer, and C. Bechinger. Diffusion of colloids in one-dimensional light channels. *J. Phys. Cond. Matt.*, 16:026001, 2004.

[31] G. Coupier, M. Saint Jean, and C. Guthmann. Single file diffusion in macroscopic wigner rings. *Phys. Rev. E*, 73:031112, 2006.

[32] J.B. Delfau, C. Coste, and M. Saint Jean. Single file diffusion of macroscopic charged particles. *Phys. Rev. E*, 81:051201, 2010.

[33] S.Y. Yang, J. Yang, E.-S. Kim, G. Jeon, E.J. Oh, K.Y. Choi, S.K. Hahn, and J.K. Kim. Single-file diffusion of protein drugs through cylindrical nanochannels. *ACS Nano*, 4:3817–3822, 2010.

[34] A. Striolo. The mechanism of water diffusion in narrow carbon nanotubes. *Nano Lett.*, 6:633–639, 2006.

[35] A. Melbinger, L. Reese, and E. Frey. Microtubule length regulation by molecular motors. *Phys. Rev. Lett.*, 108:258104, 2012.

[36] C. Loverdo, O. Bénichou, M. Moreau, and R. Voituriez. Enhanced reaction kinetics in biological cells. *Nat. Phys.*, 4:134–137, 2008.

[37] T. Chou, K. Mallick, and R. K. P. Zia. Non-equilibrium statistical mechanics: from a paradigmatic model to biological transport. *Rep. Prog. Phys.*, 74:116601, 2011.

[38] P. S. Burada, P. Hänggi, F. Marchesoni, G. Schmid, and P. Talkner. Diffusion in confined geometries. *ChemPhysChem*, 10:45, 2009.

[39] A. Ryabov and P. Chvosta. Survival of interacting brownian particles in crowded one-dimensional environment. *J. Chem. Phys.*, 136:064114, 2012.

[40] A. Ryabov. Single-file diffusion in an interval: First passage properties. *J. Chem. Phys.*, 138:154104, 2013.

[41] L.P. Sanders and T. Ambjörnsson. First Passage Times for a tracer particle in single file diffusion and Fractional Brownian Motion. *J. Chem. Phys.*, 136:175103, 2012.

[42] R. Brown. A brief account of microscopical observations made in the months of june, july, and august 1827, on the particles contained in the pollen of plants; and on the general existence of active molecules in organic and inorganic bodies. *Edinb. New Philos. J.*, 5:358–371, 1828.

[43] L. Bachelier. Théorie de la spéculation. *Annales Scientifiques de l' École Normale Supérieure*, 17:21, 1900.

[44] A. Einstein. Über die von der molekularkinetischen theorie der wärme geforderte bewegung von in ruhenden flüssigkeiten suspendierten teilchen. *Ann. Phys. (Leipzig)*, 17:549–560, 1905.

[45] J.B. Perrin. Mouvement brownien et réalité moléculaire. *Ann. de Chimie et de Physique (VIII)*, 18:5–114, 1909.

[46] P. Langevin. Sur la théorie du mouvement brownien. *C.R. Acad. Sci. Paris*, 146:530, 1908.

[47] H. Risken. *The Fokker-Planck Equation: Methods of Solution and Applications*. Springer, 1996.

[48] W. Moerner. A dozen years of single-molecule spectroscopy in physics, chemistry, and biophysics. *J. Phys. Chem. B*, 106:910–927, 2002.

[49] S. Nie and R. Zare. Optical detection of single molecules. *Ann. Rev. Biophys. Biomol. Struct.*, 26:567–596, 1997.

[50] S. Weiss. Measuring conformational dynamics of biomolecules by single molecule fluorescence spectroscopy. *Nature Struct. Biol.*, 7:724–729, 2000.

[51] S.C. Kou. Stochastic modeling in nanoscale biophysics: subdiffusion with protein. *Ann. Appl. Stat.*, 2:501–535, 2008.

[52] H. Scher and E.W. Montroll. Anomalous transit-time dispersion in amorphous solids. *Phys. Rev. B*, 12:2455–2477, 1975.

[53] R Metzler and J. Klafter. The random walk's guide to anomalous diffusion: a fractional dynamics approach. *Phys. Rep.*, 339:1–77, 2000.

[54] M.J. Saxton. Anomalous diffusion due to obstacles: a Monte Carlo study. *Biophys. J.*, 66:394–401, 1994.

[55] B.B. Mandelbrot and J.W. Van Ness. Fractional Brownian Motions, Fractional Noises and Applications. *SIAM Rev.*, 10:422–437, 1968.

[56] C. Baerlocher, L.B. McCusker, and D.H. Olson. *Atlas of zeolites framework types*. Elsevier, 2007.

[57] J. Chuang, Y. Kantor, and M. Kardar. Anomalous dynamics of translocation. *Phys. Rev. E*, 65:011802, 2001.

[58] C. Chatelain, Y. Kantor, and M. Kardar. Probability distributions for polymer translocation. *Phys. Rev. E*, 78:021129, 2008.

[59] D. Panja and G. Barkema. Simulations of two-dimensional unbiased polymer translocation using the bond fluctuation model. *J. Chem. Phys.*, 132:014902, 2010.

[60] K. Kremer and K. Binder. Monte carlo simulation of lattice models for macromolecules. *Computer Phys. Rep.*, 7:259–310, 1988.

[61] K. Grest and G.S. Kremer. Molecular dynamics simulation for polymers in the presence of heath bath. *Phys. Rev. A*, 33, 1986.

[62] I. Carmesin and K. Kermer. The bond fluctuation method: a new effective algorithm for the dynamics of polymers in all spatial dimensions. *Macromolecules*, 21:2819–2823, 1988.

[63] B. Alberts, A. Johnson, J. Lewis, M. Raff, K. Roberts, and P. Walter. *Molecular Biology of the Cell.* Garland, New York, 2008.

[64] G.M. Cooper and R.E. Hausman. *The cell: a molecular approach.* ASM Press, Washington D.C., 2007.

[65] A.B. Fulton. How crowded is the cytoplasm? *Cell*, 30:345–347, 1982.

[66] K. Luby-Phelps. Cytoarchitecture and physical properties of cytoplasm: Volume, viscosity, diffusion, intracellular surface area. *International Review of Cytology*, 192:189–221, 1999.

[67] J.A. Dix and A.S. Verkman. Crowding effects on diffusion in solutions and cells. *Annu. Rev. Biophys.*, 37:247–263, 2008.

[68] O.G. Berg, R.B. Winter, and P.H. Von Hippel. Diffusion-driven mechanisms pf protein translocation on nucleic acid I: Models and theory. *Biochemistry*, 20:6929–6948, 1981.

[69] L. Mirny, M. Slutsky, Z. Wunderlich, A. Tafvizi, J. Leith, and A. Kosmrlj. How a protein searches for its site on dna: the mechanism of facilitated diffusion. *J. Phys. A: Math. Theor.*, 42:434013, 2009.

[70] F. Santamaria, S. Wils, E. de Schutter, and G. J. Augustine. Anomalous diffusion in Purkinje cell dendrites caused by spines. *Neuron*, 52:635, 2006.

[71] A. Kusumi, C. Nakada, K. Ritchie, K. Murase, K. Suzuki, H. Murakoshi, R. S. Kasai, J. Kondo, and T. Fujiwara. Paradigm shift of the plasma membrane concept from the two dimensional continuum fluid to the partitioned fluid: High-speed single-molecule tracking of membrane molecules. *Annu. Rev. Biophys. Biomol. Struct*, 34:351–378, 2005.

[72] A. Kusumi, Y.M. Shirai, I. Koyama-Honda, K.G.N. Suzuki, and T.K. Fujiwara. Hierarchical organization of the plasma membrane: Investigations by single-molecule tracking vs. fluorescence correlation spectroscopy. *FEBS Lett.*, 584:1814, 2010.

[73] E.J. Tran and S.R. Wente. Dynamic nuclear pore complexes: Life on the edge. *Cell*, 125:1041–1053, 2006.

[74] K. Ribbeck and D. Görlich. The permeability barrier of nuclear pore complexes appears to operate via hydrophobic exclusion. *EMBO J.*, 21:2664–2671, 2002.

[75] F. Schweitzer. *Brownian Agents and Active Particles: Collective Dynamics in the Natural and Social Sciences*. Springer, Berlin, 2003.

[76] M.C. Marchetti, J.F. Joanny, S. Ramaswamy, T.B. Liverpool, J. Prost, M. Rao, and R. Aditi Simha. Hydrodynamics of soft active matter. *Rev. Mod. Phys.*, 85:1143–1189, 2013.

[77] T. Surrey, F. Nédélec, S. Leibler, and E. Karsenti. Physical properties determining self-organization of motors and microtubules. *Science*, 292:1167–1171, 2001.

[78] F. Jülicher, K. Kruse, J. Prost, and J.F. Joanny. Active behavior of the cytoskeleton. *Phys. Rep.*, 449:3–28, 2007.

[79] C. Dombrowski, L. Cisneros, S. Chatkaew, R. E. Goldstein, and J. O. Kessler. Self-concentration and large-scale coherence in bacterial dynamics. *Phys. Rev. Lett.*, 93:098103, 2004.

[80] R. Kemkemer, D. Kling, D. Kaufmann, and H. Gruler. Elastic properties of nematoid arrangements formed by amoeboid cells. *Eur. Phys. J. E.*, 1:215, 2000.

[81] I.R. Fischhoff, S.R. Sundaresan, J. Cordingley, H.M. Larkin, M.-J. Sellier, and D.I. Rubenstein. Social relationships and reproductive state influence leadership roles in movements of plains zebra, equus burchellii. *Animal Behaviour*, 73:825–831, 2007.

[82] J. Buhl, D.J.T. Sumpter, I.D. Couzin, J.J. Hale, E. Despland, E.R. Miller, and S.J. Simpson. From disorder to order in marching locust. *Science*, 312:1402–1406, 2006.

[83] M. Moussaid, D. Helbing, and G. Theraulaz. How simple rules determine pedestrian behavior and crowd disasters. *Proc. Nat.Acad. Sci.*, 108:6884–6888, 2011.

[84] C.K. Hemelrijk and H. Kunz. Density distribution and size sorting in fish schools: an individual-based model. *Behavioral Ecology*, 16:178–187, 2005.

[85] A.J.W. Ward, D.T.J. Sumpter, I.D. Couzin, P.J.B. Hart, and J. Krause. Quorum decision-making facilitates information transfer in fish shoals. *Proc. Nat.Acad. Sci.*, 105:6948, 2008.

[86] M. Ballerini, N. Cabibbo, R. Candelier, A. Cavagna, E. Cisbani, I. Giardina, V. Lecomte, A. Orlandi, G. Parisi, A. Procaccini, M. Viale, and V. Zdravkovic. Interaction ruling animal collective behavior depends on topological rather than metric distance: Evidence from a field study. *Proc. Nat.Acad. Sci.*, 105:1232, 2008.

[87] A. Kudrolli, G. Lumay, D. Volfson, and L.S. Tsimring. Swarming and swirling in self-propelled polar granular rods. *Phys. Rev. Lett.*, 100:058001, 2008.

[88] V. Narayan, N. Menon, and S. Ramaswamy. Nonequilibrium steady states in a vibrated-rod monolayer: tetratic, nematic and smectic correlations. *J. Stat. Mech.: Theory and Experiment*, page 01005, 2006.

[89] V. Narayan, S. Ramaswamy, and N. Menon. Long-lived giant number fluctuations in a swarming granular nematic. *Science*, 317:105–108, 2007.

[90] W. F. Paxton, K. C. Kistler, C. C. Olmeda, A. Sen, S. K. S. Angelo, Y. Cao, T. E. Mallouk, P. E. Lammert, and V. H. Crespi. Catalytic nanomotors: Autonomous movement of striped nanorods. *J. Am. Chem. Soc.*, 126:13424–13431, 2004.

[91] J. Palacci, C. Cottin-Bizonne, C. Ybert, and L. Bocquet. Sedimentation and effective temperature of active colloidal suspensions. *Phys. Rev. Lett.*, 105:088304, 2010.

[92] M. Ibele, T.E. Mallouk, and A. Sen. Schooling behavior of light-powered autonomous micromotors in water. *Angewandte Chemie International Edition*, 48:3308–3312, 2009.

[93] N.J. Suematsu, S. Nakata, A. Awazu, and H. Nishimori. Collective behavior of inanimate boats. *Phys. Rev. E*, 81:056210, 2010.

[94] G. Baglietto and E. V. Albano. Nature of the order-disorder transition in the Vicsek model for the collective motion of self-propelled particles. *Phys. Rev. E*, 80:050103, 2009.

[95] M. Aldana, V. Dossetti, C. Huepe, V. M. Kenkre, and H. Larralde. Phase transitions in systems of self-propelled agents and related network models. *Phys. Rev. Lett.*, 98:095702, 2007.

[96] F. D. C. Farrel, M. C. Marchetti, D. Marenduzzo, and J. Tailleur. Pattern formation in self-propelled particles with density-dependent motility. *Phys. Rev. Lett.*, 108:248101, 2012.

[97] S. Mishra, A. Baskaran, and M. C. Marchetti. Fluctuations and pattern formation in self-propelled particles. *Phys. Rev. E*, 81:061916, 2010.

[98] H. H. Wensink, J. Dunkel, S. Heidenreich, K. Drescher, R.E. Goldstein, H. Löwen, and J. M. Yeomans. Meso-scale turbulence in living fluids. *Proc. Nat. Acad. Sci.*, 109:14308–14313, 2012.

[99] S. Rafaï, L. Jibuti, and P. Peyla. Effective viscosity of microswimmer suspensions. *Phys. Rev. Lett.*, 104:098102, 2010.

[100] G. P. Saracco, G. Gonnella, D. Marenduzzo, and E. Orlandini. Equilibrium and dynamical behavior in the Vicsek model for self-propelled particles under shear. *Centr. Europ. J. Phys.*, 10:1109–1115, 2012.

[101] Y. Hatwalne, S. Ramaswamy, Madan Rao, and R. Aditi Simha. Rheology of active-particle suspensions. *Phys. Rev. Lett.*, 92:118101, 2004.

[102] T.B. Liverpool and M.C. Marchetti. Rheology of active filament solutions. *Phys. Rev. Lett.*, 97:268101, 2006.

[103] B.M. Haines, A. Sokolov, I.S. Aranson, L. Berlyand, and D.A. Karpeev. Three-dimensional model for the effective viscosity of bacterial suspensions. *Phys. Rev. E*, 80:0491922, 2009.

[104] L. Giomi, T.B. Liverpool, and M.C. Marchetti. Sheared active fluids: Thickening, thinning, and vanishing viscosity. *Phys. Rev. E*, 81:051908, 2010.

[105] M. E. Cates. Diffusive transport without detailed balance in motile bacteria: does microbiology need statistical physics? *Rep. Prog. Phys.*, 75:042601, 2012.

[106] H.C. Berg. E coli *in Motion*. Springer-Verlag, New York, 2003.

[107] F. Julicher, A. Ajdari, and J. Prost. Modeling molecular motors. *Rev. Mod. Phys.*, 69:1269–1282, 1997.

[108] E. Karsenti, F. Nédélec, and T. Surrey. Modelling microtubule patterns. *Nat. Cell. Biol.*, 8:1204, 2006.

[109] J. Howard. *Mechanics of Motor Proteins and the Cytoskeleton*. Sinauer, Sunderland, MA, 2001.

[110] P.W. Baas and F.J. Ahmad. Force generation by cytoskeletal motor proteins as a regulator of axonal elongation and retraction. *Trends Cell Biol.*, 11:244–249, 2001.

[111] T. Mitchison and M. Kirschner. Cytoskeletal dynamics and nerve growth. *Neuron*, 1:761–772, 1988.

[112] R. Wedlich-Soldner, S.C. Wai, T. Schmidt, , and R. Li. Robust cell polarity is a dynamic state established by coupling transport and GTPase signaling. *J. Cell. Biol.*, 166:889, 2004.

[113] B. Brandenburg and X. Zhuang. Virus trafficking : learning from single-virus tracking. *Nat. Rev. Microbiol.*, 5:197–208, 2007.

[114] O. Bénichou, C. Loverdo, M. Moreau, and R. Voituriez. Intermittent search strategies. *Rev. Mod. Phys.*, 83:81–129, 2011.

[115] T. Antal and P.L. Krapivsky. "burnt-bridge" mechanism of molecular motor motion. *Phys. Rev. E*, 72:046104, 2005.

[116] C.T. MacDonald, J.H. Gibbs, and A.C. Pipkin. Kinetics of biopolymerization on nucleic acid templates. *Biopolymers*, 6:1–25, 1968.

[117] G. Miño, T. E. Mallouk, T. Darnige, M. Hoyos, J. Dauchet, J. Dunstan, R. Soto, Y. Wang, A. Rousselet, and E. Clement. Enhanced diffusion due to active swimmers at a solid surface. *Phys. Rev. Lett.*, 106:048102, 2011.

[118] G. Li, J. Bensson, L. Nisimova, D. Munger, P. Mahautmr, J.X. Tang, M.R. Maxey, and Y. V. Brun. Accumulation of swimming bacteria near a solid surface. *Phys. Rev. E*, 84:041932, 2011.

[119] H. H. Wensink and H. Löwen. Aggregation of self-propelled colloidal rods near confining walls. *Phys. Rev. E*, 78:031409, 2008.

[120] J. Elgeti and G. Gompper. Self-propelled rods near surfaces. *Europhys. Lett.*, 85:38002, 2009.

[121] J. Elgeti and G. Gompper. Wall accumulation of self-propelled spheres. *Europhys. Lett.*, 101:48003, 2013.

[122] A. Kaiser, H.H. Wensink, and H. Löwen. How to capture active particles. *Phys. Rev. Lett.*, 108:268307, 2012.

[123] R. Di Leonardo, L. Angelani, D. Dell'Arciprete, G. Ruocco, V. Iebba, S. Schippa, M. P. Conte, F. Mecarini, F. De Angelis, and E. Di Fabrizio. Bacterial ratchet motors. *Proc. Nat. Acad. Sci.*, 107:9541–9545, 2010.

[124] S.E. Hulme, W.R. DiLuzio, S.S. Shevkoplyas, L. Turner, M. Mayer, H.C. Berg, and G.M. Whitesides. Using ratchets and sorters to fractionate motile cells of escherichia coli by length. *Lab on a Chip*, 8:1888–1895, 2008.

[125] G. Lambert, D. Liao, and R.H. Austin. Collective escape of chemotactic swimmers through microscopic ratchets. *Phys. Rev. Lett.*, 104:168102, 2010.

[126] P. Galajda, J. Keymer, P. Chaikin, and R. Austin. A wall of funnels concentrates swimming bacteria. *J. Bacteriol.*, 189:8704–8707, 2007.

[127] A. Sokolov, M.M. Apodaca, B.A. Grzybowski, and I.S. Aranson. Swimming bacteria power microscopic gears. *Proc. Nat. Acad. Sci.*, 107:969–974, 2010.

[128] D. Volfson, S. Cookson, J. Hasty, and L.S. Tsimring. Biomechanical ordering of dense cell populations. *Proc. Nat. Acad. Sci.*, 105:15346–15351, 2008.

[129] H. Wioland, F.G. Woodhouse, J. Dunkel, J.O. Kessler, and R.E. Goldstein. Confinement stabilizes a bacterial suspension into a spiral vortex. *Phys. Rev. Lett.*, 110:268102, 2013.

[130] A. Czirók, E. Ben-Jacob, I. Cohen, and T. Vicsek. Formation of complex bacterial colonies via self-generated vortices. *Phys. Rev. E*, 54:1791, 1996.

[131] F.G. Woodhouse and R.E. Goldstein. Spontaneous circulation of confined active suspensions. *Phys. Rev. Lett.*, 109:168105, 2012.

[132] F.G. Woodhouse and R.E. Goldstein. Cytoplasmic streaming in plant cells emerges naturally by microfilament self-organization. *Proc. Nat. Acad. Sci.*, 110:14132–14137, 2013.

[133] A. Kumar, A. Maitra, M. Sumit, G.V. Shivashankar, and S. Ramaswamy. Actomyosin contractility rotates the cell nucleus. *arXiv*, page 1302.6052., 2013.

[134] L. Lizana, T. Ambjörnsson, A. Taloni, E. Barkai, and M. Lomholt. Harmonization of many-body system. *Phys. Rev. E.*, 81:051118, 2010.

[135] J.B. Delfau, C. Coste, and M. Saint-Jean. Single file diffusion of particles with long range interactions: damping and finite size effects. *Phys. Rev. E*, 84:011101, 2011.

[136] O. Flomenbom and A. Taloni. On single-file and less dense processes. *Europhys. Lett.*, 83:20004, 2008.

[137] N. Leibovich and E. Barkai. Everlasting effect of initial conditions on single-file diffusion. *Phys. Rev. E*, 88:032107, 2013.

[138] L. Lizana, M.A. Lomholt, and T. Ambjörnsson. Single-file diffusion with non-thermal initial conditions. *arXiv*, 1304.1635, 2013.

[139] S.J. Manzi, J.J. Torrez Herrera, and V.D. Pereyra. Single-file diffusion in a box: Effect of the initial configuration. *Phys. Rev. E*, 86:021129, 2012.

[140] E. J. Harris. Diffusion with 'collision' between particles. *J. Appl. Prob.*, 2:323–338, 1965.

[141] D. W. Jepsen. Dynamics of a simple many body system of hard rods. *J. Math. Phys*, 6:405, 1965.

[142] D. G. Levitt. Dynamics of a single-file pore: Non-fickian behavior. *Phys. Rev. A*, 8:3050, 1973.

[143] M. Kollmann. Single-file diffusion of atomic and colloidal systems: asymptotic laws. *Phys Rev Lett.*, 18:90, 2003.

[144] A. Taloni and M. Lomholt. Langevin formulation for single file diffusion. *Phys. Rev. E*, 78:51116, 2008.

[145] C. Rödenbeck, J. Kärger, and K. Hahn. Calculating exact propagators in single-file systems via the Reflection Principle. *Phys. Rev. E*, 57:4382, 1998.

[146] E. Barkai and R. Silbey. Theory of single file diffusion in a force field. *Phys. Rev. Lett.*, 102:050602, 2009.

[147] E. Barkai and R. Silbey. Diffusion of tagged particle in an exclusion process. *Phys. Rev. E*, 81:041129, 2009.

[148] L. Lizana and T. Ambjörnsson. Single-file diffusion in a box. *Phys. Rev. Lett.*, 100:200601, 2008.

[149] S. Alexander and P. Pincus. Diffusion of labeled particles on one-dimensional chains. *Phys. Rev. B*, 18:2011, 1978.

[150] J. Percus. Anomalous self-diffusion for one-dimensional hard cores. *Phys. Rev. A*, 9:557, 1974.

[151] S. F. Burlatsky, G. Oshanin, M. Moreau, and W.P. Reinhardt. Motion of a driven tracer particle in a one-dimensional symmetric lattice gas. *Phys. Rev. E*, 54:3165, 1996.

[152] R. Adler, R. Feldman, and M. Taqqu. *A Practical Guide to Heavy tails: Statistical Techniques for Analyzing Heavy-Tailed Distributions.* Birkhäuser, Boston, 1998.

[153] T. Konstantopoulos and S.J. Lin. Fractional brownian approximations of queueing networks. In *Stochastic Networks. Lecture Notes in Statist.*, page 257–273. Springer, New York, 1996.

[154] B. Mandelbrot. *Fractals and Scaling in Finance*. Springer, New York, 1997.

[155] T. Mikosch, S. Resnick, H. Rootzén, and A. Stegman. Is network traffic approximated by stable Lévy motion or Fractional Brownian Motion? *Ann. Appl. Probab.*, 12:23–68, 2002.

[156] G. Samorodnitsky and M. Taqqu. *Stable Non-Gaussian Random Processes*. Chapman and Hall, New York, 1994.

[157] R. Zwanzig. *Nonequilibrium Statistical Mechanics*. Oxford Univ. Press, New York, 2001.

[158] G. Coupier, M. Saint-Jean, and C. Guthmann. Single file diffusion enhancement in a fluctuating modulated quasi-1d channel. *Europhys. Lett.*, 77:60001, 2007.

[159] S. Redner. *A guide to first passage processes*. Cambridge University Press, 2001.

[160] J-H. Jeon, A.V. Chechkin, and R. Metzler. First passage behaviour of multi-dimensional fractional brownian motion and application to reaction phenomena. *arXiv*, page 1306.1667, 2013.

[161] S. Pagliara, C. Chimerel, R. Langford, D.G.A.L. Aarts, and U.F. Keyser. Parallel sub-micrometre channels with different dimensions for laser scattering detection. *Lab Chip*, 11:3365, 2011.

[162] S. Pagliara, C. Schwall, and U.F. Keyser. Optimizing diffusive transport through a syntetic membrane channel. *Adv. Mater.*, 25:844–849, 2013.

[163] J. C. Crocker and D.G. Grier. Methods of digital video microscopy for colloidal studies. *J. Colloid Interface Sci.*, 179:198, 1996.

[164] K. Kruse and F. Jülicher. Actively contracting bundles of polar filaments. *Phys. Rev. Lett.*, 85:1778, 2000.

[165] P. Kraikivski, R. Lipowsky, and J. Kierfeld. Enhanced ordering of interacting filaments by molecular motors. *Phys. Rev. Lett.*, 96:258103, 2006.

[166] T. B. Liverpool, A. C. Maggs, and A. Ajdari. Viscoelasticity of solutions of motile polymers. *Phys. Rev. Lett.*, 86:4171, 2001.

[167] A. Baskaran and M.C. Marchetti. Enhanced diffusion and ordering of self-propelled rods. *Phys. Rev. Lett*, 101:268101, 2008.

[168] H.P. Zhang, A. Be'er, E.-L. Florin, and H.L. Swinney. Collective motion and density fluctuations in bacterial colonies. *Proc. Natl. Acad. Sci.*, 107:626, 2010.

[169] V. Narayan, S. Ramaswamy, and N. Menon. Long-lived giant number fluctuations in a swarming granular nematic. *Science*, 317:105, 2007.

[170] B. ten Hagen, S. van Teeffelen, and H. Löwen. Brownian motion of a self propelled particle. *J. Phys.: Condens. Matter*, 23, 2011.

[171] H. Bruus. *Theoretical Microfluidics*. Oxford University Press, 2008.

[172] P. Romanczuk, M. Bär, W. Ebeling, B. Lindner, and L. Schimansky-Geier. Active brownian particles from individual to collective stochastic dynamics. *Eur. Phys. J. Special Topics*, 202:1–162, 2012.

[173] E. Lauga and R.E. Goldstein. Dance of the microswimmers. *Phys. Today*, 65:30, 2012.

[174] E. Lauga and T. R. Powers. The hydrodynamics of swimming microorganisms. *Rep. Prog. Phys.*, 72:096601, 2009.

[175] J.P. Hernandez-Ortiz, P.T. Underhill, and M.D. Graham. Dynamics of confined suspensions of swimming particles. *J. Phys.: Condens. Matter*, 21:204107, 2009.

[176] D. Marenduzzo, E. Orlandini, and J.M. Yeomans. Hydrodynamics and rheology of active liquid crystals: A numerical investigation. *Phys. Rev. Lett*, 98:118102, 2007.

[177] L. Xie, T. Altindal, S. Chattopadhyay, and X.-L. Wu. Bacterial flagellum as a propeller and as a rudder for efficient chemotaxis. *Proc. Nat. Acad. Sci.*, 108:2246–2251, 2011.

[178] K.J. Duffy and R.M. Ford. Turn angle and run time distributions characterize swimming behavior for *Pseudomonas putida*. *J. Bacteriol.*, 179:1428–1430, 1997.

[179] J. Saragosti, P. Silberzan, and A. Buguin. Modeling *E. coli* tumbles by rotational diffusion. implications for chemotaxis. *PLOSOne*, 7:e35412, 2012.

[180] G. Rosser, A.G. Fletcher, D.A. Wilkinson, J.A. de Beyer, C.A. Yates, J.P. Armitage, P.K. Maini, and R.E. Baker. Novel methods for analysing bacterial tracks reveal persistence in *Rhodobacter sphaeroides*. *PLOS Comp. Biol.*, 9:1003276, 2013.

[181] K. Drescher, K.C. Leptos, and R.E. Goldstein. How to track protists in three dimensions. *Rev. Sci. Instruments*, 80:014301, 2009.

[182] J.R. Howse, R.A.L. Jones, A.J. Ryan, T. Gough, R. Vafabakhsh, and R. Golestanian. Self-motile colloidal particles: From directed propulsion to random walk. *Phys. Rev. Lett.*, 99:048102, 2007.

[183] C. Schwall. Mimicking protein channels in a chip. Master thesis, Ludwig-Maximilians-Universitat Munchen Fakultat fur Physik, 2013.

[184] S. Pagliara and U.F. Keyser. in preparation.

[185] E. Kosheleva, B. Leahy, H. Diamant, B. Lin, and S. A. Rice. Long-range hydrodynamic correlations in quasi-one-dimensional circular and straight geometries. *Phys. Rev. E*, 86:041402, 2012.